The Quantum Interference Effect of Electron Waves in Semiconductor Quantum Wires Fabricated by Focused Ion Beam Implantation

（集束イオンビーム注入により作製した
半導体量子細線における電子波の量子干渉効果）

A Thesis Presented to
the Graduate School of the University of Tokyo
in Partial Fulfillment of the Requirements
for the Degree of Doctor of Philosophy
in Electronic Engineering

by

Toshiro Hiramoto

December 23, 1988

Dissertation Supervisor

Professor Toshiaki Ikoma

To My Parents

Preface

This thesis describes a part of the research work carried out at the Institute of Industrial Science, University of Tokyo, under the direction of Professor Toshiaki Ikoma while the author was a graduate student at the Department of Electronic Engineering, University of Tokyo, from 1984 to 1989.

For many years, there was an argument among theoretical physicists as to whether or not the quantum interference of electron waves could be observed in disordered condensed matters. Since the observation of the periodic oscillation in magnetoresistance of metal cylinders in 1981, the quantum interference effect has attracted much attention and opened a new "mesoscopic" regime in the solid state physics. Now, the quantum interference in the mesoscopic regime is one of the issues of greatest interest not only in physics but also in electronics.

In this thesis, the quantum interference effect of electron waves in semiconductor quantum wires fabricated by focused ion beam implantation is described from the technological point of view.

Chapter 1 is the background of the research work on the quantum interference effect in semiconductor quantum wires. The purpose of the present study is also described.

Chapter 2 is on the microfabrication of III-V semiconductors by the focused ion beam implantation. The fabrication process of the very narrow GaAs quantum wires is described.

Chapter 3 is focused on the study of the phase coherence length of electron waves in GaAs quantum wires. The phase breaking mechanisms of electron waves at low temperatures are discussed.

Chapter 4 describes the conductance fluctuations in GaAs quantum wires. The correlation energy and the energy averaging effect in GaAs quantum wires at the finite temperatures are discussed.

Chapter 5 deals with the performance of GaAs quantum wire transistors at low temperatures. The effect of the localization on the device characteristics is clarified.

Chapter 6 is the summary of the present study.

Roppongi, Tokyo
December 1988

Toshiro Hiramoto

Acknowledgements

This thesis describes a part of the research work carried out at the Institute of Industrial Science, University of Tokyo, while the author was a graduate student at the Department of Electronic Engineering, University of Tokyo, from 1984 to 1989.

The author wishes to express his sincere gratitude to Professor Toshiaki Ikoma, Institute of Industrial Science, University of Tokyo, the dissertation supervisor, for continuous encouragement and guidance. His suggestions are always full of insight. The work could not be accomplished without them.

Dr. Kazuhiko Hirakawa, Institute of Industrial Science, University of Tokyo, is gratefully acknowledged for daily discussions, which are very fruitful and exciting, in Ikoma Laboratory.

Special Thanks are given to Professor Hiroyuki Sakaki, Institute of Industrial Science, University of Tokyo, for kindly supplying the AlGaAs/GaAs heterostructures and for fruitful discussions. Thanks are also due to Professor Yasuhiro Iye, Institute for Solid State Physics, University of Tokyo, for arranging the electrical measurements at very low temperatures and at high magnetic field, and for stimulating discussions. The author also thanks Dr. T. Tamegai, Institute for Solid State Physics, for performing the electrical measurements at low temperatures.

The author is grateful to Professors T. Nishinaga and Y. Arakawa, University of Tokyo, for useful discussions and constant encouragements. The author thanks Professor J. Frey, University of Maryland, and Professor C. M. Penchina, University of Massachusetts, for fruitful discussions and critical reading of the manuscripts of the published papers. The author also thank Prof. T. Okumura, Tokyo metropolitan University, and Prof. T. Kimura, University of Electro-Communications, for fruitful discussions at the weekly meetings in Ikoma laboratory. Dr. K. Ishibashi, RIKEN, and Y. Takagaki, Osaka University, are acknowledged for fruitful discussions on the quantum interference effect.

The author would like to express his sincere gratitude to Ms. Y. Kurihara for constant encouragement. The author owes much to her for all the office work she has done for him and for the comfortable arrangement of the laboratory. Her conversation is full of wit and always relaxes him.

The author would like to express his sincere thanks to his colleagues; Dr. T. Saito, Dr. H. Noge, Dr. Y. Mochizuki, Dr. D. M. Hofmann, Dr. P. Oldiges, Dr. X. Zhao, T. Makimoto, T. Odagiri, Y. Hagihara, Y. Hashimoto, M. Noguchi, and S. Lee for fruitful discussions and kind assistance extended to the author. Drs. Noge and Mochizuki showed the author what the "research" in the university was. Dr. Oldiges and Odagiri helped the author develop the focused-ion-beam technology. The author would like to thank J. Motohisa for kindly supplying the automatic measurement programs. The author also thanks the

secretaries in Ikoma Laboratory; N. Naito, E. Sakamoto, J. Hirayama, and J. Saito, for their assistance of office work in the laboratory.

The author would like to thank the undergraduate students from the Shibaura Institute of Technology, M. Koyama, T. Tahara, Y. Mizukawa, H. Kuroda, H. Mori, H. Ouchi, Y. Suzuki, and A. Momose, who helped him perform the experiments. Without their assistance, the work would not been completed.

Scholarship support was generously supplied by the Japan Society for the Promotion of Science.

Finally, the author would like to thank his parents for their constant encouragements.

Abstract

We have established qualitative and quantitative understanding of the quantum interference effect of electron waves in semiconductor quantum wires. We have addressed the following four problems which are very important in the quantum interference effect from the technological point of view:

(1) Fabrication process of semiconductor quantum wires.
(2) Phase coherence length and phase breaking mechanisms of electron waves in GaAs quantum wires.
(3) Correlation energy of electron wavefunctions in GaAs quantum wires.
(4) Effect of localization on characteristics of GaAs quantum wire transistors.

We have clarified these important points in the quantum interference effect and have shown the possibility of the quantum interference devices in semiconductors.

Contents

Chapter 1

Introduction

Abstract

The background of the study on the quantum interference effect of electron waves is reviewed from the technological point of view and the unsolved issues for its device applications are pointed out. The purpose of the present study is described.

§ 1.1 Background of the study

Recently, the size of semiconductor electron devices has been becoming smaller and smaller. The design rule of the large scale integrated circuits (LSIs) has broken the wall of 1 μm. The reduction of the device size leads to high integration of devices in a chip, high speed in the device operation, and high cost performance of the integrated circuits. These are the key features of the present semiconductor microdevices. The device size will be reduced even more, as long as these three features are improved and, more importantly, the fabrication technology is advanced as well to make the reduction possible.

It can be said, therefore, that the semiconductor industry is supported by the highly-developed microfabrication-technology. The submicron lithography is one of the most important techniques. At present, the optical lithography is widely employed to transfer the submicron patterns on the masks to the semiconductor wafer. It is difficult to make structures less than 0.5 μm in this technique. In order to fabricate finer structures, the optical lithography should be replaced by the electron beam (EB) or focused ion beam (FIB) lithography. These techniques enable us to fabricate very fine semiconductors with dimensions less than 0.1 μm.

What happens when the size of the conventional electron devices is scaled down to less than 0.1 μm? Although the small devices are often designed on the basis of the proportional scaling rule, this rule does not always apply. Because of the short gate length, for example, the

electric field is focused on the channel, especially near the drain electrode, and the hot electrons are generated in Si metal-oxide-semiconductor field effect transistors (MOSFETs), causing the shift of the threshold voltage. In GaAs metal-semiconductor FETs (MESFETs), the current through the semi-insulating (SI) substrates also causes the shift of the threshold voltage. In order to suppress these effects, the small devices are designed in a sophisticated way and accordingly their fabrication process becomes still more complicated and difficult. It would be these two factors, i. e., the degradation of the performance in the very small devices of the conventional type and the technological difficulty in fabricating them, that gives a limit to the reduction of the device size. The device size would reach the limit in the near feature. It is, therefore, strongly desirable to develop a new type of devices that would operate on the basis of a new physical principle.

On the other hand, it is expected that completely new physical phenomena will arise when the size of the semiconductor structures is reduced. One of the best examples is the size quantization effect in semiconductor superlattices and quantum wells.[1] When the electrons are confined into a very thin semiconductor film of the order of the de Bloglie wavelength, the electron wavefunction is quantized. The state density in the two-dimensional (2D) electrons is quite different from that in the ordinary three-dimensional (3D) electrons, leading to a remarkable change in electrical and optical properties. The recent progress in the thin-film growth technique has made it possible to form 2D electrons easily in heterostructures and has demonstrated great advantage in applying such structures to electrical and optical

devices, such as high electron mobility transistors (HEMTs)[2] and multi-quantum well (MQW) lasers.[3]

Further confinement of carriers, i. e. confinement into one-dimension (1D) of freedom, will also lead to new physical phenomena. Sakaki[4] calculated the probability of the ionized-impurity scattering of electrons at low temperatures in the ultrafine semiconductor quantum wires where the electron momentum is quantized in two directions and the electrons populate only the ground level. He found that the scattering probability is drastically suppressed in the ideal quantum wire, because the allowed scattering in the 1D wire is only backscattering whose probability is very small, resulting in the enhancement of the electron mobility. This enhanced mobility has not been confirmed experimentally, because it is still difficult to fabricate the ideal 1D quantum wires with dimension comparable to the de Bloglie wavelength.

Even when the sample size is much larger than the de Bloglie length and the electron motion is not quantized, a quantum effect will appear. For example, a negative magnetoresistance was observed in Si-MOSFET at low temperatures,[5] and random fluctuations of magnetoconductance were observed in narrow Au wires.[6] It turned out that these phenomena were due to the interference between electron waves. This is the quantum interference effect of electron waves. The quantum interference has manifested itself in various ways in electron transport in condensed matters, especially of very small structures, and has been of great interest in physics. Recently, it

has attracted much attention from the technological point of view as well.

§ 1.2 Quantum interference effect

The wavefunction of each electron consists of two parts: amplitude $C(r)$ and phase ϕ; $\Psi = C(r) \exp(i\phi)$. The phase ϕ plays an important role in the quantum interference effect, while ϕ is neglected in the classical transport theories. The interference gives rise to various phenomena in electron transport in condensed matters, such as the localization, conductance fluctuations, and the Aharonov-Bohm effect.

1.2.1 Historical review of the quantum interference effect

The possibility of the localization of the electron wavefunctions in disordered materials was first discussed by Anderson in 1958.[7] In 1979, Abrahams *et al.*[8] proposed the scaling theory and concluded that at the zero-temperature and with no inelastic scattering, the electron wavefunctions in 2D and 1D would always localize, irrespective of the degree of the disorder. This means 2D and 1D systems are always insulators at $T = 0$. At finite temperatures and with inelastic scattering, the localization effect is suppressed and the conductivity becomes sensitive to the temperature and the magnetic field. This region is called weak localization regime. The weak localization effect has been extensively studied theoretically and experimentally, especially in 2D, and it has clarified that this is the result of the interference between electron waves.

On the other hand, the direct interference of electron waves in condensed matters has been independently investigated. It is well

known that when an electron beam splits into two and recombines in vacuum, the beam intensity is modified by the interference of the electron wave and oscillates as a function of the magnetic field with a period of h/e, where h is the Planck constant and e the electron change. This is the Aharonov-Bohm (AB) effect.[9,10] It is noted that there is essentially no scattering and the phase information is always maintained in vacuum. Then, how does the electron wave interfere in condensed matters? The electron transport in metals or semiconductors is diffusive; the electrons are frequently scattered by lattice defects, impurities, boundaries, and so on. It was argued for years by solid state physicists whether or not such elastic (momentum) scattering would destroy the phase information of electron waves and prevent the AB oscillation.

In 1981, Sharvin and Sharvin[11] observed the $h/2e$ oscillation in magnetoresistance in a very small Mg cylinder. This was the first demonstration that the electron can interfere in metals and that the electron wave retains its phase memory even if the electron is subjected to the frequent elastic scattering. In 1985, Webb *et al.*[12] observed the h/e oscillation due to the AB effect in resistance of a small Au loop. It was suggested from these experiments that it was not the elastic scattering but the inelastic scattering that breaks the phase information of the electron waves.

Random oscillations in magnetoresistance of the Au ring were also observed superposed on the AB oscillation.[6] This random conductance fluctuations were observed even in a single Au wire.[6] It turned out that this was the superposition of the AB oscillation in local loops in the

wire. The theoretical work was developed after the observation of this random conductance oscillations, and an important conclusion was derived: the amplitude of the conductance fluctuations is of the order of e^2/h at the zero-temperature in completely coherent samples (i. e. no inelastic scattering), irrespective of the sample size and the degree of the disorder.[13,14] This is called the "universal conductance fluctuations".

1.2.2 Phase coherence length

As described above, the condition for the quantum interference effect to be observed is that the phase information of the electron waves should be preserved during the sequence in which the electron splits into two, travels in different paths, and recombines. The distance over which the electron wavefunction retains its phase memory is called phase coherence length, L_ϕ, which is one of the most important parameters in the quantum interference effect. Therefore, the size of the loop which the interfering electron forms should be smaller than L_ϕ.

Some of the quantum interference effects such as weak localization are observable in macroscopic samples (ex. thin films), because the effect is not smeared out by the ensemble averaging. On the contrary, the interference effects such as the AB effect and conductance fluctuations are smeared out and is never observed in the macroscopic samples. This kind of interference can be observed only in samples comparable to or smaller than L_ϕ.

Table I shows the characteristic lengths which are important in the quantum effect. While the de Bloglie wavelength (and thus the Fermi wavelength λ_F in degenerated semiconductors) is about 10 nm in normal semiconductors, L_ϕ is of the order of 0.1 ~ 1 μm; much longer than λ_F. It should be noted that this length is comparable to the size L of the semiconductor microstructures which are now available by the state-of-the-art technology mentioned above. This is why the quantum interference effect is observed even in the present quantum wires, in which the electron motion is not quantized in two direction because of the larger width than λ_F. On the other hand, the mean free path l is 0.01 ~ 10 μm in semiconductors. When the sample size L is larger than l, the electron transport in semiconductors is diffusive as in metals, rather than ballistic.

1.2.3 Mesoscopic region

In the study of the quantum interference effect, the relationship of these length scales is, in most cases, $\lambda_F << l < L_\phi \sim L$. This regime of the sample size is much larger than the microscopic region, but much smaller than the macroscopic region. Therefore, the conventional theories for the microscopic or macroscopic regions do not always apply in this regime. This regime is a completely new field in the solid state physics and recently called a "mesoscopic region". The quantum interference effects such as the AB effect and conductance fluctuations are characteristic phenomena in the mesoscopic region.

1.2.4 Quantum interference devices

The quantum interference effect results from the wave nature of the electron. If this effect is applied to an electron device, it will be a completely new type of device because in all the conventional electron devices the electron acts as a particle, and it is expected to have excellent performances such as ultrafast speed, high integration, low-power dissipation, and multifunction. Several quantum interference devices have been proposed so far. Datta *et al.* proposed to utilize the electric-field AB effect in double-layered GaAs channels between the AlGaAs layers controlled by the gate electrodes on them.[15,16] They also proposed a wave-guide like quantum transistor which is controlled by a remote gate.[16] Yamamoto and Hokawa analyzed the AB effect device in a GaAs ring.[17] The interference in these devices is smeared out if the devices are large. Therefore, the size of the devices should be smaller than L_ϕ.

1.2.5 Phase breaking mechanisms of electron waves

It is very important to evaluate the values of L_ϕ and to make L_ϕ longer from the viewpoint of the device applications of the interference as well as of the physical interest. It is also very important to investigate the phase breaking mechanisms of electron waves, because they determine L_ϕ. As described before, the phase is not broken by the elastic scattering but by the inelastic scattering. At room temperature, the main inelastic scattering is the phonon scattering, by which L_ϕ is very short. L_ϕ becomes longer at low temperatures. It is believed that the main phase breaking mechanism (inelastic

scattering) in semiconductors is the electron-electron scattering at low temperatures,[18] but the mechanism is still unclear. It is essential to clarify the phase breaking mechanisms for the practical application of the quantum interference.

1.2.6 Correlation energy

When the temperature increases, L_ϕ becomes shorter by the electron-electron scattering and the electron-phonon scattering, and the quantum interference effect is reduced. Another issue which is important at the finite temperatures is the energy averaging effect. The energy bandwidth within which the electron wavefunctions are correlated is called the correlation energy, E_c. When E_c is smaller than the energy broadening due to the finite temperature, the energy averaging takes place, causing the reduction of the quantum interference.[19]

In metals, E_c is very small and it is hard to observe, for example, the AB oscillation even in 4.2 K due to the energy averaging. In semiconductors, E_c is considered to be much larger than that in metals. Therefore, semiconductors seem more suitable for the quantum interference devices than metals. However, there are very few experimental reports on E_c in semiconductors. It is very important to investigate E_c and to obtain the value of E_c in order to clarify at how high temperature the quantum interference devices can operate.

Table I Typical length scales, which are important in quantum effects, in semiconductors at low temperatures.

de Bloglie wavelength		5 nm	~	50 nm
Fermi wavelength	λ_F	5 nm	~	50 nm
Phase coherence length	L_ϕ	0.1 μm	~	1 μm
Thermal diffusion length	L_T	0.1 μm	~	1 μm
Mean free path	l	10 nm	~	10 μm
Sample size	L			

§ 1.3 Focused ion beam technology

The quantum interference effect, especially the weak localization effect, has been studied mainly in 2D systems for years. On the other hand, the study of the interference in the 1D quantum wires did not begin until several years ago mainly because of the difficulty in fabricating very narrow wire structures. The optical lithography does not apply as mentioned in § 1.1. The charged beam lithography or the holographic lithography are often employed for the fabrication process. The focused ion beam (FIB) technology is one of the most promising techniques to fabricate the quantum wires.[20-22]

The FIB process is a very versatile process; it can be employed not only for the FIB lithography,[23] but also for direct implantation of various impurities,[24,25] maskless submicron etching,[26] submicron deposition,[27] mask repairing,[28] and microscopy.[29] Particularly, the direct FIB implantation into semiconductors has various applications, such as maskless doping of n- and p-type impurities into very small regions in a wafer,[24] the selective formation of the high-resistive regions in a conducting semiconductor film,[30,31] and the compositional disordering of superlattices.[32] Since the diameter of FIB is about 0.1 μm, this process is very suitable to fabricate the quantum wires in the mesoscopic region.

§ 1.4 Purpose of the present study

The quantum interference effect has been a matter of physical interest for years. However, the technological importance of the quantum interference in the mesoscopic region has been recognized only recently and, as mentioned in the previous sections, a lot of problems remain unsolved for the practical applications of this effect to new electron devices.

The purpose of the present study is to establish qualitative and quantitative understanding of the quantum interference effect of electron waves in semiconductor quantum wires from the technological point of view.

To achieve this purpose, one has to answer the following questions:
1) How can we fabricate semiconductor quantum wires in the mesoscopic region?
2) How long is the phase coherence length, L_{ϕ}, of electron waves in semiconductors, how can we make L_{ϕ} longer, and what phase breaking mechanism determines L_{ϕ}?
3) How large is the correlation energy in semiconductors and at what kind of temperature does the quantum interference effect appear?
4) How does the quantum wire transistors in the mesoscopic region operate?

The focused ion beam (FIB) technology is chosen for the microfabrication technique, because of its versatile applications.

GaAs is chosen as a material to investigate the above questions. This is because:

1) The process technology of semiconductors is most developed in GaAs, except for in Si. Therefore, this material is suitable for the microfabrication.

2) The electron mobility in GaAs can be changed in a large range; from 1000 cm^2/Vs in bulk GaAs to more than 100000 cm^2/Vs in selectively doped heterostructures. Therefore, this material is very suitable to investigate the effect of the electron mobility and thus, of the elastic scattering on the quantum interference. Moreover, the high mobility gives a very long mean free path and a very long coherence length, which are suitable for the quantum interference devices.

Chapter 2 deals with the first question. The feasibility of the FIB implantation technique for the fabrication of very fine semiconductor structures is demonstrated. It is shown that the GaAs quantum wires of as narrow as 20-nm wide can be fabricated by this technique.

Chapter 3 is focused on the phase coherence length, L_ϕ, and the phase breaking mechanisms of electron waves. The values of L_ϕ are estimated by the weak localization effect. A suitable material to obtain long L_ϕ is clarified. The temperature dependence of L_ϕ and the unknown phase-breaking mechanism at low temperatures are also discussed.

Chapter 4 describes the conductance fluctuations and correlation energy in GaAs quantum wires. It is shown that the conductance

fluctuates with the Fermi energy as well as with the magnetic field. The correlation energy is estimated and the advantages of semiconductors for the quantum interference devices are discussed.

Chapter 5 is allotted to the performances of the GaAs quantum wire transistors. It is shown that the localization effect strongly affects the device characteristics near the threshold.

Chapter 2

Microfabrication of III-V Semiconductors by Focused Ion Beam Implantation

Abstract

Microfabrication processes of GaAs and AlGaAs by the focused ion beam (FIB) implantation are demonstrated. Focused Si and Be ions are implanted into semi-insulating GaAs substrates and activated by rapid thermal annealing (RTA). It is shown that the electrical properties in FIB-implanted GaAs is comparable to those in GaAs implanted by the conventional unfocused ion beam (UIB). The profiles of Be ions which are doped by FIB in GaAs are observed experimentally and are in good agreement with a calculation. Anomalous diffusion of implanted Be is observed during the long time annealing, indicating that the RTA process is essential for the FIB implantation. Microstructures with submicron dimensions, such as surface nipi-structures with a 1.0 μm period and GaAs gratings with a 0.37 μm period, are successfully fabricated by the FIB implantation. Quasi-one-dimensional GaAs conducting wires are also fabricated by two method. One utilizes the gap spacing between two high-resistive regions formed by the FIB implantation and the other makes use of the expansion of depletion regions in pn-junctions. The minimum width of the fabricated wires is as small as 20 nm. These results demonstrate the feasibility of the FIB implantation technique for the microfabrication of III-V semiconductors.

§ 2.1 Introduction

Recently, the dimensions of the semiconductor devices are becoming smaller and smaller. The optical lithography process is widely employed, but the resolution of this process is limited by the wavelength of the used ultraviolet light and it is difficult to fabricate microstructures with dimensions of less than 0.5 μm.

To attain better resolution of the order of ~0.1 μm, the electron-beam (EB) lithography has been applied. EB can be focused into ~1 nm diameter by the state-of-the-art technology. Because of very light mass of the electron, however, EB has some disadvantages: EB requires a very high dose to expose the resist, causing a charge-up effect of electrons on the surface of the resist. In addition, some electrons are backscattered from the semiconductor to the resist, and the resolution of the exposed patterns is much worse than the diameter of EB.

Focused ion beam (FIB) technology is another technique that makes it possible to fabricate very fine patterns with ~0.1 μm dimensions. Since ions have much heavier mass than the electron, FIB is free from the problems described above. Moreover, FIB can be applied to manifold purposes; direct implantation of various impurities into semiconductors without any masks,[24,25,30-32] maskless submicron etching of semiconductors,[26] submicron deposition of metals on semiconductors,[27] mask repairing,[28] FIB lithography,[23] and scanning ion microscopy.[29] FIB technology has recently attracted much attention due to these advantages.

In this study, the FIB technology is employed as a tool for direct implantation of ions into semiconductors among aforementioned various applications. The reasons are as follows.

1) The direct FIB implantation is a versatile process and can be applied to various purposes in combination with other processes. It is usually applied to a doping of both n- and p-type impurities into very small area of semiconductors with successive rapid thermal annealing (RTA).[24] It is also applied to the selective formation of high-resistive regions in conductive semiconductor films without the annealing process[20,21] and to submicron etching of semiconductors in combination with an enhanced etching of damaged regions.[24]

2) The direct implantation by FIB is the simplest process among the submicron processes to which FIB can be applied. This process requires no resist and no ambient gas, which are required in the FIB lithography and the FIB-assisted etching and deposition, respectively.

In this chapter, the feasibility of the FIB implantation for the microfabrication of III-V semiconductors is demonstrated.

The feature of the FIB implantation system is summarized in § 2.2.

In § 2.3, rapid thermal annealing (RTA) of FIB-implanted GaAs is investigated. The RTA process is essential in the impurity doping into very small area by the FIB implantation, because the diffusion of implanted ions during the annealing should be suppressed. It is shown that electrical properties of FIB-implanted GaAs which is subjected to RTA are quite similar to those of UIB-implanted GaAs,

although the FIB implantation requires higher annealing temperatures.

In § 2.4, the profiles of FIB implanted ions in GaAs are studied experimentally and theoretically. It is shown that the implanted Be ions spread laterally to the width of ~ 1 μm even if the ion beam is focused into 0.1 μm diameter. The calculated profiles are in good agreement with the observation for short time annealing, although anomalous diffusion of Be is observed during annealing longer than 10 min.

§ 2.5 describes the fabrication of very fine semiconductor structures by the FIB implantation. Surface-nipi structures are fabricated by the focused Si- and Be-implantation and RTA. The minimum interval between the n- and p-type regions is 0.5 μm. A enhanced etching of damaged regions induced by the FIB implantation is applied to forming fine GaAs gratings with submicron periods. The minimum dimension of these microstructures is as small as 30 nm.

§ 2.6 is devoted to the fabrication of quasi-one-dimensional GaAs conducting wires by the FIB implantation. Two methods are developed. The first method utilizes the formation of the high-resistive regions in conducting GaAs layers by the FIB implantation. Very narrow GaAs wires are formed between the two high-resistive regions. In the other method, focused Si-ion-beam is line-implanted into p-GaAs to form an n-type GaAs wire in p-GaAs. Then the n-type wire is squeezed by reverse-biasing the pn-junction. The minimum width of the fabricated wires is as small as 20 nm.

§ 2.2 Focused ion beam implantation system

Figure 2.1 shows a schematic view of the FIB implantation system used in this study. The system is JIBL-100L from JEOL. The ion source is a liquid metal. A ternary alloy liquid-metal-ion-source of Au-Si-Be is used. This ion source has an advantage that it contains both an n-type dopant (Si) and a p-type dopant (Be). When a negative voltage is applied to the extractor, the ions are emitted from the tip of the needle of the ion source by field emission. The maximum accelerating voltage is 100 keV. The desired ion can be selected in the $E \times B$ mass separator. The ion beam is focused by the objective lens into ~0.1 μm diameter and scanned onto samples by the deflector. Since the deflector is controlled by a computer, any desired patterns can be drawn with an accuracy of ~0.1 μm.

For the position alignment, marks are formed in samples by a wet-etch in advance. Before the implantation into a sample, the ion beam is scanned onto the marks and their positions are precisely determined by monitoring the secondary electrons emitted from the mark edges by ion-bombardment. Then, the ion beam is implanted into the desired position on the sample on the basis of the mark position. The accuracy of the position alignment is about 0.1 μm. This value is small enough for the practical usage.

The FIB system is described in more detail in Refs. 33 and 34.

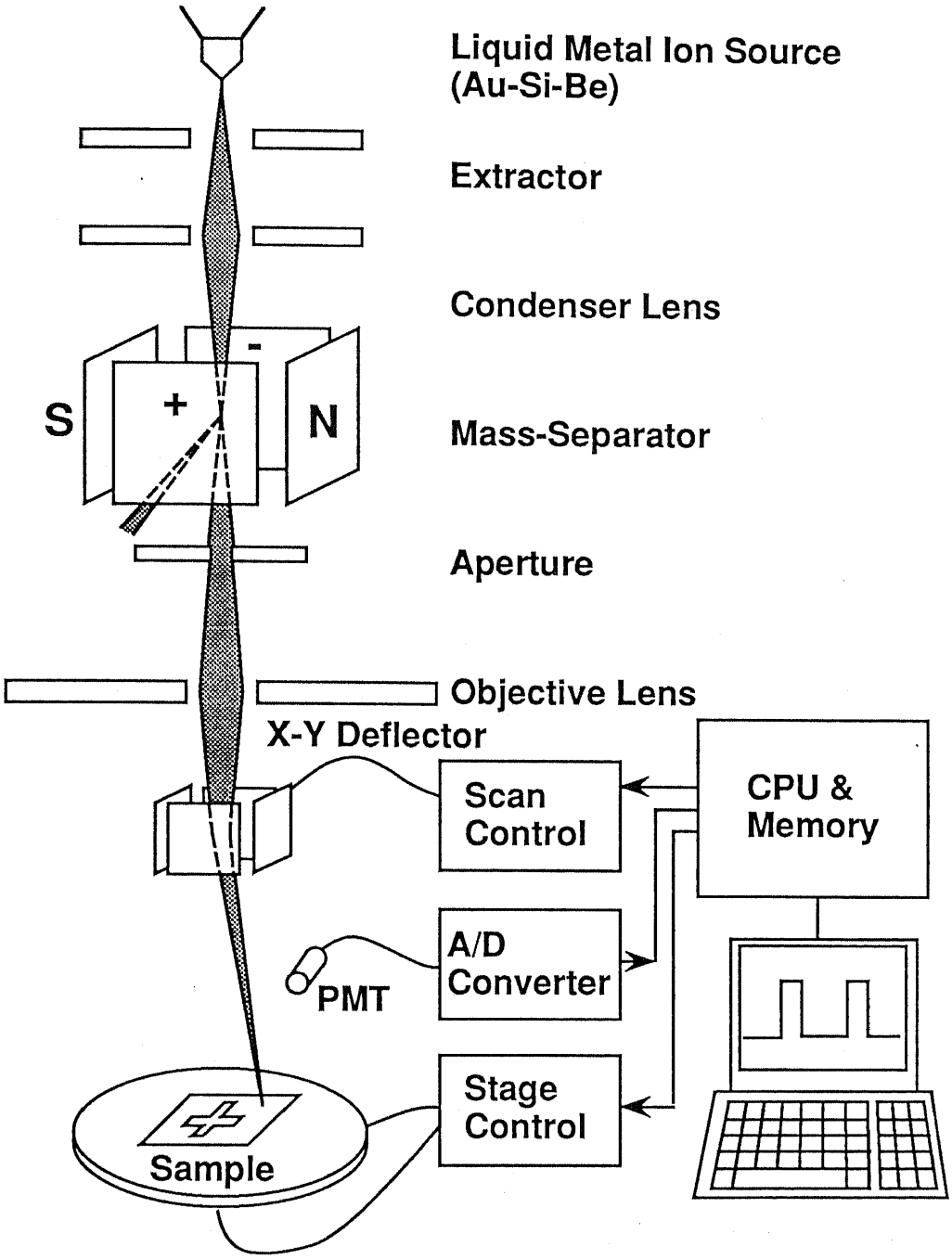

Fig. 2.1 A schematic view of the focused-ion-beam implantation system (JIBL-100L) used in the present study.

§ 2.3 Rapid thermal annealing of focused-ion-implanted GaAs

The focused ion beam (FIB) implantation is one of the most promising techniques for microfabrication of semiconductors. In this section, a special attention is paid to a selective doping of n- and p-type impurities into very small regions by the FIB implantation without any masks.

In the impurity doping process by implantation, a post-implantation annealing is necessary to recover the damage induced by the implantation and to activate the implanted ions. The current density of FIB is 0.1 ~ 1 A/cm^2, which is about 5 orders of magnitude higher than that of the conventional unfocused ion beam (UIB). This means that the damage induced by the FIB implantation may be different from those by the UIB implantation. In fact, it was reported that FIB-implanted GaAs was found to have less damage than UIB-implanted GaAs by Raman spectroscopy.[35,36] Therefore, it is important to investigate the electrical properties of FIB-implanted GaAs. Moreover, in the doping by the FIB implantation, the diffusion of implanted ions during the annealing should be suppressed in order to maintain the doped regions (and thus, the electrically active regions) very small. Therefore, FIB implanted GaAs should be annealed very quickly. Rapid thermal annealing (RTA) is very effective for the purpose.

The RTA process for unfocused Si-implanted GaAs has been studied in detail.[33,37-40] This section describes a study on RTA of focused Si- and Be-implanted GaAs. It is shown that the electrical properties of

FIB-implanted GaAs which is subjected to RTA are quite similar to those of UIB-implanted GaAs, except that a reduction of activation efficiency of FIB-implanted Si was observed in annealing temperature range from 800 to 1000 °C.

2.3.1 Rapid thermal annealing system

Although several methods are reported for very short time annealing, such as rapid heating by a graphite heater[41] and an Ar arc lamp,[42] RTA using halogen lamps is most widely employed for the semiconductor processing.[37,40] The advantages of RTA using halogen lamps are: the implanted ions undergo little diffusion during the brief annealing, there is no need to encapsulate an implanted layer because of very short annealing, and no contamination from a quartz tube is involved because only the sample is heated by the light from the halogen lamps.

Figure 2.2 (a) shows a schematic cross-section of the RTA system used in this study. It consists of a quartz tube and four halogen lamps. Each lamp has a gold-coated elliptical reflector that focuses the light onto a graphite boat with a lid, in which a GaAs susceptor is placed. A GaAs sample without a cap is placed on the susceptor with the face-to-face configuration. GaAs powder is placed on them to provide arsenic pressure. No light reaches the wafer with this configuration.

The sample temperature during annealing is monitored by a thermocouple whose tip is buried in the graphite boat. The maximum temperature and its hold time are controlled with a PID controller.

The graphite boat is blown by a cold Ar gas to cool the sample quickly. Figure 2.2 (b) shows the variation of the sample temperature with time. In this case, the maximum temperature, heating rate, and hold time are set to be 1000 °C, 100 °C/s and 1 s, respectively. The cooling rate from 1000 to 600 °C is about 30 °C/s.

2.3.2 Focused Si-implanted GaAs

Si is one of the most popular n-type dopants in GaAs. Si-implantation into GaAs and annealing are extensively studied and widely used for the fabrication of GaAs electron devices. The focused Si-implantation and annealing were also reported.[35] In this case, the annealing was the conventional furnace annealing, and it was found that the electrical and optical properties of focused Si-implanted GaAs are very similar to those of unfocused Si-implanted GaAs. However, there has been no report on RTA of focused Si-implanted GaAs. Here, RTA of focused Si-implanted GaAs is investigated and their electrical properties are compared with those of unfocused Si-implanted GaAs.

The starting materials are semi-insulating (SI) undoped GaAs substrates grown by the liquid encapsulated Czochralski (LEC) method. The focused Si-ion-beam (FIB) was implanted to small regions of 120×120 μm^2 squares of the GaAs substrates, as shown in the inset of Fig. 2.2 (b). The implantation dose was 5×10^{13} cm^{-2} and the implantation energy was 100 keV. Then RTA for 1 s was performed. The annealing temperature was changed from 750 to 1100 °C. The Ohmic electrodes were formed by a Au/Ge/Ni

evaporation. The electron density and mobility were measured at room temperature by the van der Pauw technique.

For comparison, the conventional unfocused Si-ions (UIB) were implanted into the LEC GaAs substrates. The dose was 5×10^{13} cm^{-2} and the energy was 100 keV, which were the same as those of the FIB implantation. However, in this case, the ions were implanted to the whole area of the wafers. Then, the wafers were cut to 4×4 mm^2 squares and subjected to RTA with the FIB-implanted samples at the same time. The Ohmic contacts were formed by In/Sn alloy. The electrical properties were also measure by the van der Pauw technique.

Figures 2.3 (a) and (b) show the sheet electron density and the electron mobility of Si-implanted GaAs by FIB and UIB as a function of the annealing temperature. As a whole, the electron density increases and the mobility decreases with increasing the annealing temperature. However, a significant difference between FIB and UIB is found in the temperature range from 800 to 1000 °C. The electron density (and thus, the activation efficiency) in FIB-implanted GaAs is much smaller than that in UIB-implanted GaAs, and remains almost constant in this temperature range. The mobility of FIB-implanted GaAs is reduced there. When the annealing temperature is more than 1000 °C, the electron density in FIB-implanted GaAs suddenly increases and reaches almost the same value as that in UIB-implanted GaAs.

The origin of this anomalous behavior of FIB implanted GaAs is discussed below. One possible cause is the damage, because the FIB-induced damage may be heavier than the UIB-induced one, causing a reduction of the activation efficiency, and may be recovered by annealing higher than 1000 °C. This is expected because FIB has much (about 5 times) higher current-density than UIB. In Fig. 2.3 (a), however, the electron density is the same for FIB and UIB at less than 800 °C, where the damage would not be recovered yet. Moreover, in the temperature range from 800 to 1000 °C, the mobility in FIB-implanted GaAs is reduced while the electron density is constant. These results are not explained by the FIB-induced damage. The results suggest that some acceptors are created in the temperature range. Possible acceptors are Si_{As}[38] and Cu_{Ga},[43] but the origin of the anomaly is not clear at present.

From the above results, the optimal temperature of RTA for focused Si-implanted GaAs is considered as 1000 ~ 1100 °C. By RTA in this temperature range, the activation efficiency of focused Si-implanted GaAs is almost the same as that of the unfocused Si-implanted GaAs and reaches about 40 %.

2.3.3 Focused Be-implanted GaAs

Be is also one of the best p-type dopants in GaAs. Be has a small diffusion coefficient in GaAs and is widely employed as a dopant in molecular beam epitaxy (MBE). Be-implantation into GaAs has been reported[44-46] and high activation efficiency more than 90 % has been attained. Experimental results on the focused Be-implantation and

rapid thermal annealing were also reported by Uematsu.[47] However, he reported that the activation efficiency of Be in GaAs depended on the implantation energy in the case of the FIB implantation and was as low as 15 % at 200 keV implantation. He attributed this phenomenon to the damage induced by the FIB implantation with high current density. Here, we describe our experimental results on the electrical properties of focused Be-implanted GaAs which are subjected to RTA.

The starting materials are undoped SI LEC GaAs substrates. The focused Be-ion-beam was implanted into the areas of 120×120 μm^2 on the substrates as well as focused Si-ion-beam described before. To examine the implantation-energy dependence of the electrical properties of the implanted layers, the ions were implanted at 100 and 200 keV. The implantation dose was 6.0×10^{13} cm^{-2} for 100 keV implantation and 5.0×10^{13} cm^{-2} for 200 keV. Then RTA was performed. The annealing temperature and the annealing time were varied as parameters: the isochronal annealing for 1 s from 700 to 1000 °C and the isothermal annealing at 800 °C from 1 to 1200 s. A Au/Zn alloy was evaporated on the samples and sintered to form the Ohmic contacts. The hole density and mobility were measured at room temperature by the van der Pauw technique.

Figure 2.4 (a) shows the temperature dependence of the activation efficiency and the hole mobility of Be-implanted GaAs for the 1 s isochronal annealing. The activation efficiency gradually increases with increasing the annealing temperature and reaches about 90 % at 1000 °C for both implantation energy. It is noted that in the

temperature range from 800 to 1000 °C there is no reduction of the activation efficiency as is observed in focused Si-implanted GaAs, and that there is no dependence of the activation efficiency on the implantation energy as was observed by Uematsu.[47]

The hole mobility remains almost constant in the temperature range from 700 to 900 °C. The mobility is about 210 cm^2/Vs and is higher for 200 keV implantation than that for 100 keV implantation. This is because the projected range of Be is larger and the net hole concentration in the unit volume is smaller for the 200 keV implantation than those for 100 keV when the sheet concentration of Be (and hole) is the same. The effect of the ionized-impurity scattering is thus smaller in the 200 keV implantation, leading to higher hole mobility.

Figure 2.4 (b) shows the annealing-time dependence of the activation efficiency and the hole mobility at the 800 °C isothermal annealing. The activation efficiency is only ~60 % for 1 s annealing but increases with increasing the annealing time, reaching 90 % for 60 s annealing. For longer annealing time, the activation efficiency remains almost constant. No difference is observed between the implantation energies of 100 keV and 200 keV. The hole mobility is kept constant and higher in the 200 keV implantation than that in 100 keV.

It was reported that the Be ions in GaAs which were implanted by conventional UIB were well activated by RTA with the annealing hold time set to 0 s.[46] The activation efficiency was about 90 % for the dose of 2×10^{13} cm^{-2} and was independent of the annealing

temperature from 700 to 1050 °C. The hole mobility was about 230 cm^2/Vs.

The low activation efficiency at low temperatures in Fig. 2.4 (a) suggests that the FIB-induced damage is still present in the implanted layers. This damage is annealed out by high-temperature (~1000 °C) or long-time annealing (~60 s), and the activation efficiency and the mobility become comparable to those of unfocused Be implanted GaAs, as shown in Figs. 2.4 (a) and (b). These results show that the electrical properties of focused Be-implanted GaAs is excellent as long as the annealing conditions of RTA is optimized.

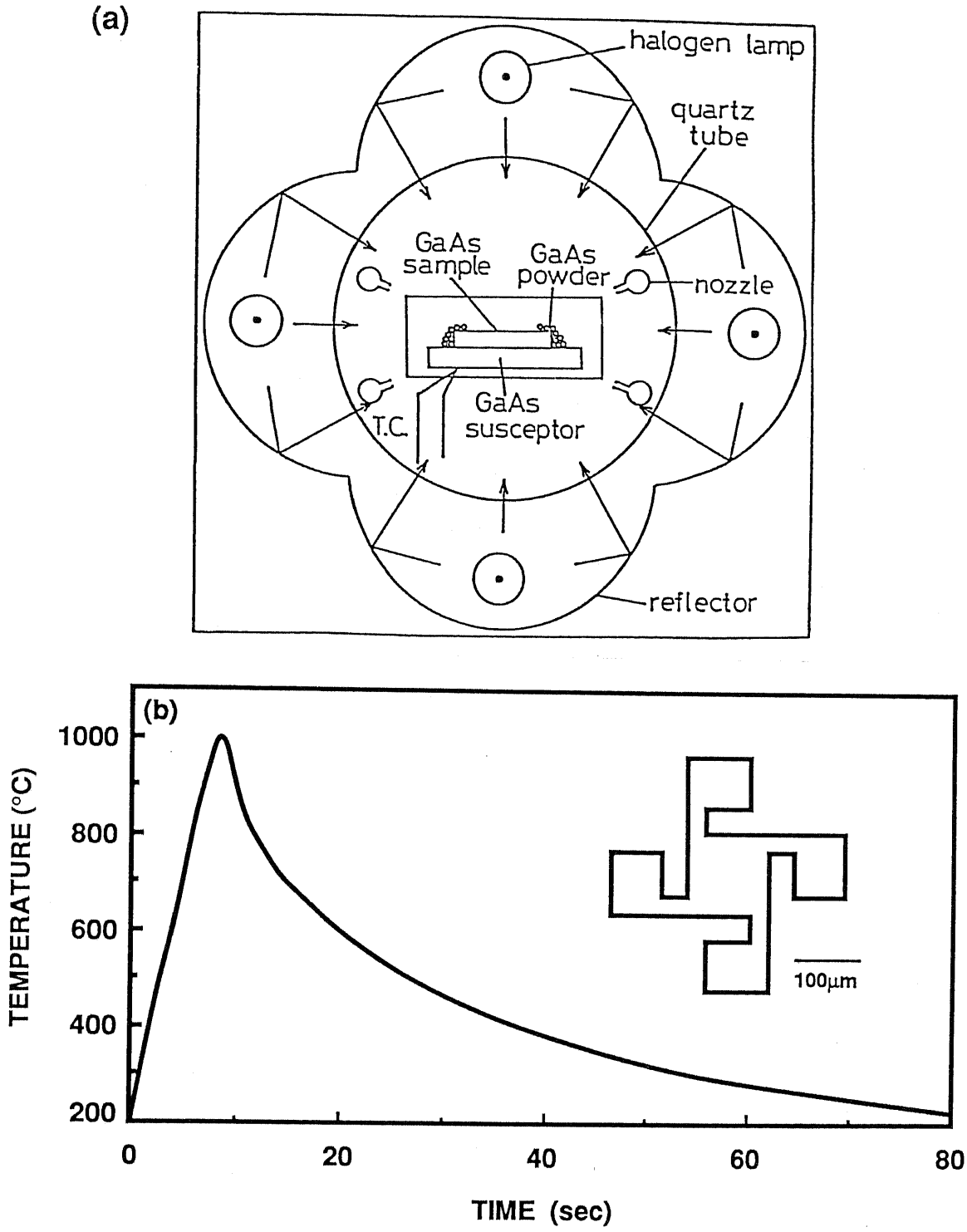

Fig. 2.2 (a) A schematic cross-sectional view of the rapid thermal annealing furnace used in the present study. (b) Variation of the sample temperature with time in the rapid thermal annealing. The inset shows the pattern of the focused-ion-beam implantation for the van der Pauw measurements.

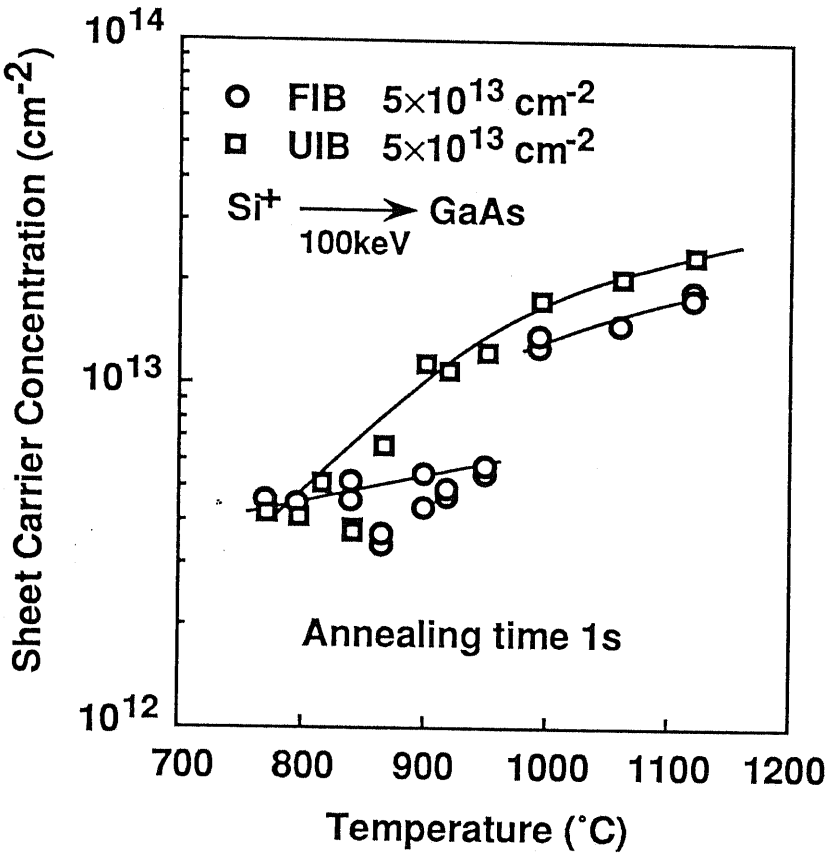

Fig. 2.3 (a) Sheet electron density of the Si-implanted GaAs as a function of the annealing temperature. The implantation was performed both by the focused-ion-beam (FIB) and the conventional unfocused-ion-beam (UIB). Rapid thermal annealing was carried out for 1 s.

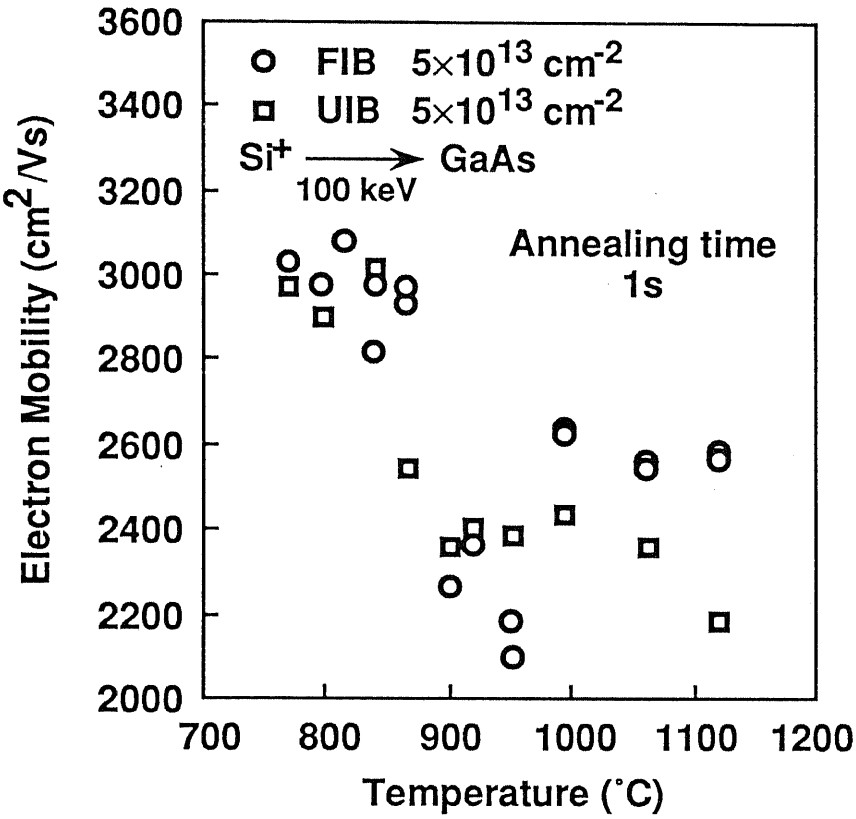

Fig. 2.3 (b) Electron mobility of the Si-implanted GaAs as a function of the annealing temperature. The implantation was performed both by the focused-ion-beam (FIB) and the conventional unfocused-ion-beam (UIB). Rapid thermal annealing was carried out for 1 s.

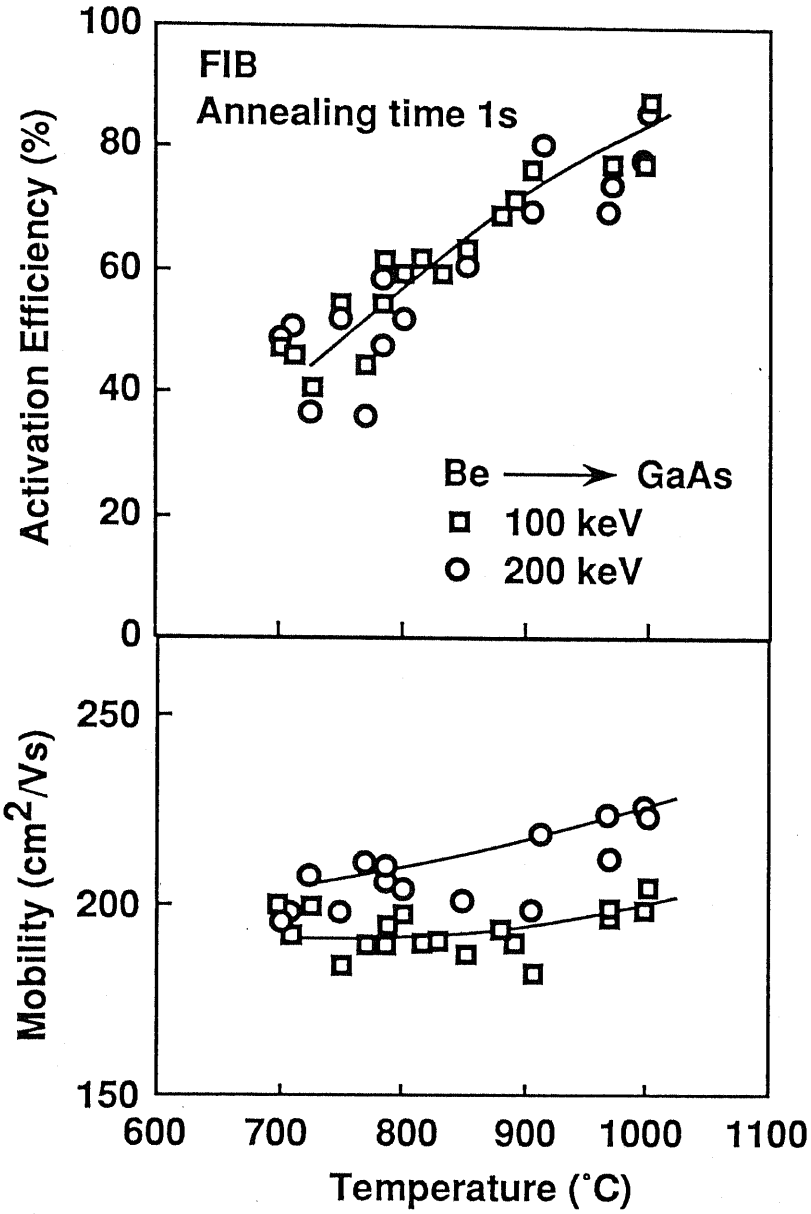

Fig. 2.4 (a) The annealing-temperature dependence of the activation efficiency and the hole mobility in focused Be-ion-implanted GaAs. The annealing hold time in RTA was 1 s.

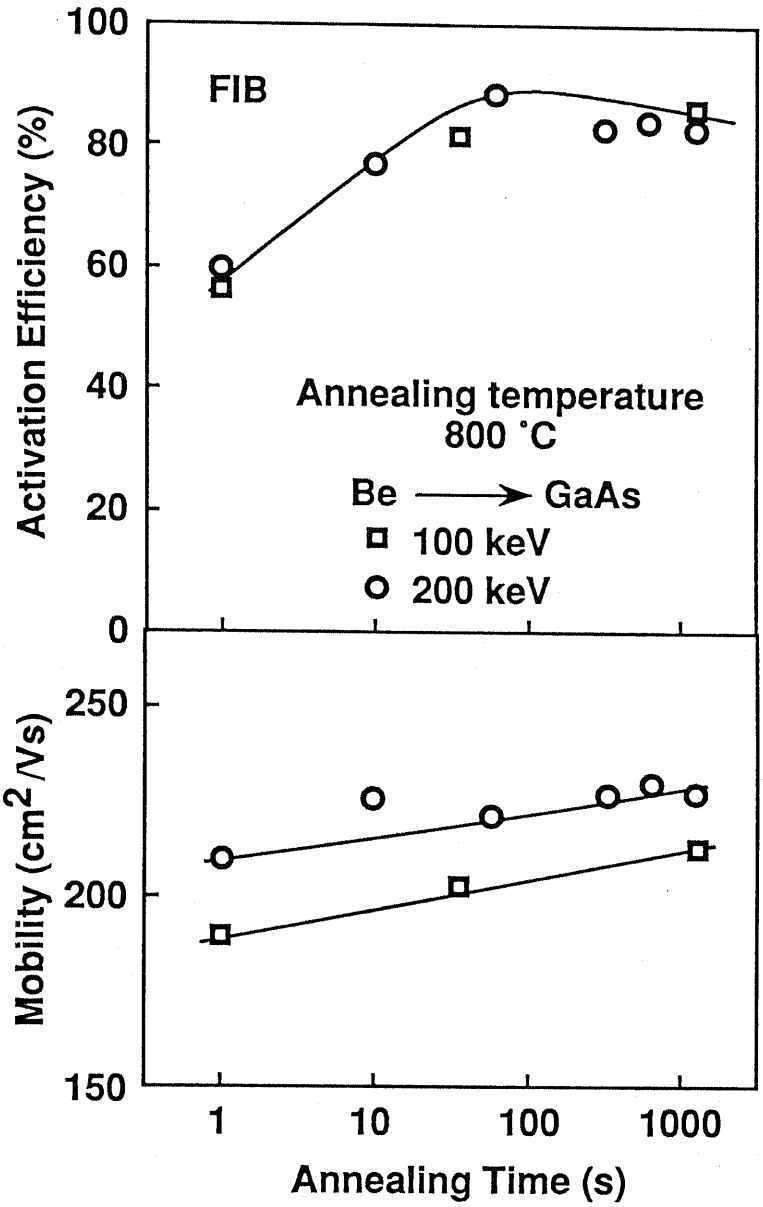

Fig. 2.4 (b) The annealing-time dependence of the activation efficiency and the hole mobility in focused Be-ion-implanted GaAs. The annealing temperature was 800 °C.

§ 2.4 Ion profiles of line-implanted Be in GaAs

Understanding of a carrier profile after ion-implantation and annealing is very important for the practical usage of the FIB implantation. In this section, the profiles of FIB-implanted ions in GaAs are studied experimentally and theoretically.[24] Although the beam diameter is about 0.1 μm, it is expected that the implanted species are scattered into a large volume by collision with atoms in semiconductors and also spread by diffusion during annealing.

In order to observe the profiles of implanted ions experimentally, focused Be-ions are line-implanted into n-GaAs, thus forming p-type regions in n-GaAs. In this case, the shape of the boundary between the p- and n-type regions is considered to correspond to the line where the Be density is the same as the electron density of the original n-GaAs substrate. Then, the samples are cleaved and the cleaved surfaces are stain-etched and observed by scanning electron microscopy (SEM). Accordingly, the profiles of the implanted Be can be obtained.

Samples used in this experiment are n-GaAs with different electron densities. They are Si-doped horizontal Bridgman (HB) GaAs and S-doped vapor phase epitaxial (VPE) GaAs. The carrier densities in HB and VPE GaAs are 5×10^{17} and 7×10^{16} cm^{-3}, respectively. Focused Be-ion-beam was implanted into n-GaAs. In this case, each implanted region was a single line (line-implantation). The implantation energy was 200 keV, the line-dose varied from 3×10^{9} to 1×10^{10} cm^{-1}, and the scanning speed 0.34 cm/s. The wafers were

annealed in the RTA furnace at 800 °C. The annealing (hold) time was varied from 1 to 1800 s.

For the observation of the pn-junction boundaries, the wafers were cleaved and stain-etched with $HF:H_2O_2:H_2O$ = 1:1:10 under white light illumination. Only the p-type regions are etched and the n-type regions remain unetched under this condition. The pn-boundary appeared with a clear contrast in SEM images.

Figure 2.5 shows SEM micrographs of the pn-boundaries formed in Si-doped HB GaAs after annealing for 1, 60, 600, and 1800 s. In this case, the line-dose is 1×10^{10} cm^{-1}. Even after the annealing for 1 s, the pn-boundary is spread laterally to 1.1 μm and in depth to 1.1 μm, as shown in Fig. 2.5 (a). For longer annealing, the lateral spreading is 1.7 μm (60 s), 2.3 μm (600 s), and 2.6 μm (1800 s). Correspondingly, the depth is 1.3 μm (60 s), 1.8 μm (600 s), and 1.7 μm (1800 s). Apparently, this behavior indicates anomalous diffusion of Be taking place.

From a simple theory, the expected profiles of Be in GaAs are calculated.[24,48] It takes into account the lateral spread of implanted ions based on the LSS theory and the diffusion during annealing. It is assumed that the focused ion beam has a Gaussian shape with the standard deviation of 0.05 μm (which corresponds to a diameter of 0.1 μm). A simple diffusion equation is also assumed with a temperature-dependent diffusivity of Be ($D = 7.3 \times 10^{-6} \exp(-1.2/kT)$ cm^2/s).[49]

Figure 2.6 shows the calculated pn-junction boundaries which are formed by focused-Be line-implantation into n-GaAs followed by 1 s and 60 s annealing. The conditions of substrate, implantation, and annealing are the same as the experiment shown in Figs. 2.5 (a) and (b). The calculation shows that after 1 s annealing the peak density of Be is 3.1×10^{18} cm^{-3}, and the lateral spreading and the depth of the pn-boundary are 1.2 μm and 0.82 μm, respectively. In this case, the calculation agrees well with the experiment. It is considered that the surface depletion region affected the stain-etching and an upper half of the oval shape was obscured in Fig. 2.5 (a) and (b). For 60 s annealing, however, the pn-boundary spreads more than the calculation shows.

These results show that very short time annealing is necessary for the post annealing of the FIB implantation. It is also shown that as long as RTA for very short time is employed, the profiles of the implanted ions (thus the carrier profiles) are predicted by the simple calculation. This is very important for the designs of electron devices which is fabricated by the FIB implantation.[48]

The calculation shows that for annealing longer than 600 s the peak concentration of Be should become lower than the background donor density, and hence a pn-junction should disappear. However, in the experiment, a pn-junction still remains after 600 s annealing and the pn-boundary is very different from the calculated shape. This suggests that more acceptors are created in the p-type region or the background donors are reduced. In order to examine the thermal conversion effect in the surface regions of n-GaAs during the long

time annealing, the electron density in the unimplanted regions were measured. The reduction of the electron density was not remarkable. It seems that the hole concentration increases only around the implanted regions. It should be also noted that the observation of a crystal facet of (111) orientation (Fig. 2.5 (c)) indicates preferential diffusion taking place.

Figure 2.7 shows SEM micrographs of the pn-junction boundaries formed in S-doped VPE GaAs. The spreading of the pn-boundary after long-time annealing is smaller than that in Si-doped HB GaAs. Figure 2.8 shows the calculated pn-boundaries. The calculation takes the slight reduction of the electron density during annealing into consideration. The calculation agrees well even after long time annealing.

The difference between Si-doped HB GaAs and S-doped VPE GaAs is the nature of the dopants. Si belongs to group IV while S to group VI. It is suggested that during long time annealing at 800 °C, Si might transfer from the Ga site to the As site to create more acceptors in the HB substrate which contains rather high density of Si. It is also anticipated that the anomalous diffusion is dependent on the crystal quality.

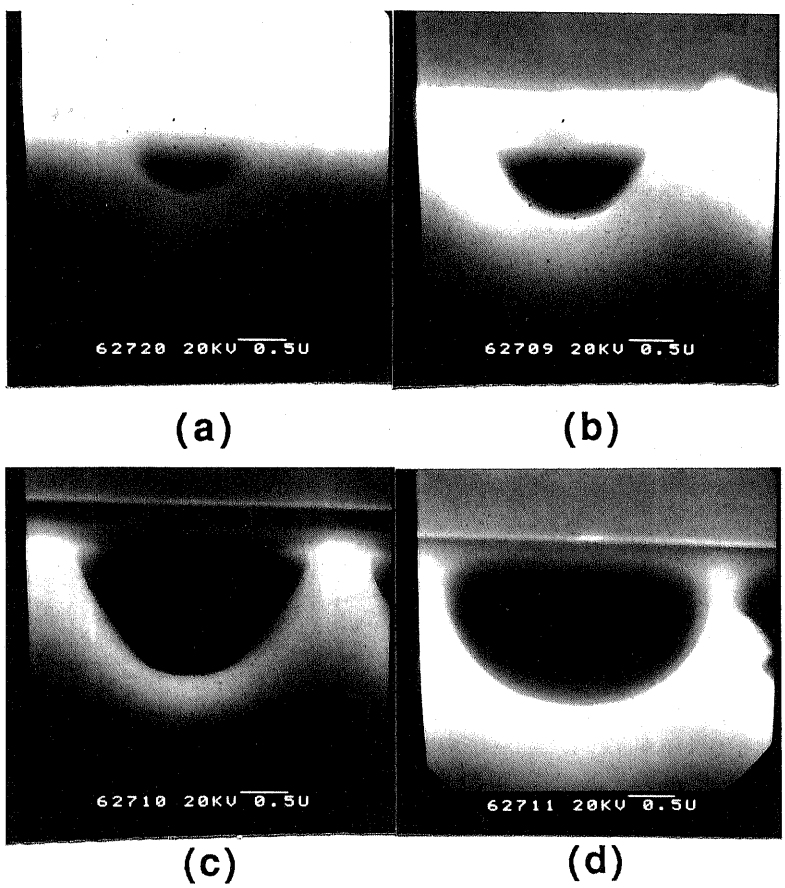

Fig. 2.5 SEM micrographs of the pn-boundary formed by the line-implantation of the focused Be-ions into Si-doped HB GaAs. The annealing was performed for (a) 1 s, (b) 60 s, (c) 600 s, and (d) 1800 s, respectively. The line-dose is 1×10^{10} cm^{-1}.

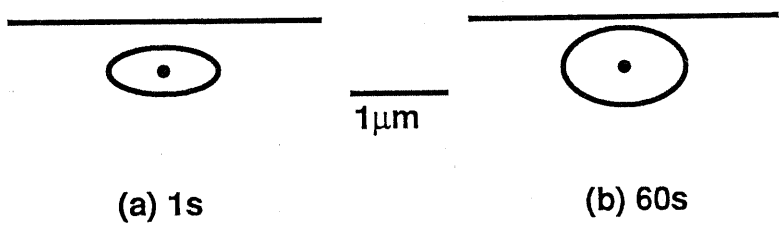

Fig. 2.6 Calculated pn-boundary after focused Be-implantation and annealing. The annealing time is (a) 1 s and (b) 60 s. The electron density of the substrate is assumed to be 4×10^{17} cm^{-3}, due to the slight thermal conversion. The assumed condition of the implantation and the annealing is the same as the experiments in Fig. 2.5 (a) and (b).

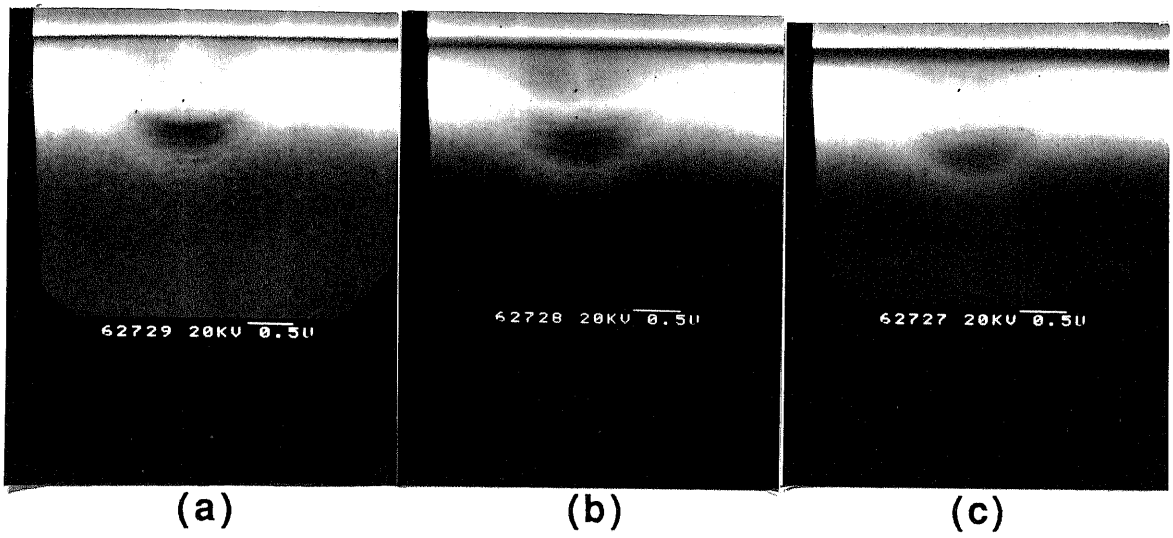

Fig. 2.7 SEM micrographs of the pn-boundary formed by the line-implantation of the focused Be-ions into S-doped VPE GaAs. The annealing was performed for (a) 60 s, (b) 600 s, and (c) 1800 s, respectively. The line-dose is 1×10^{10} cm^{-1}.

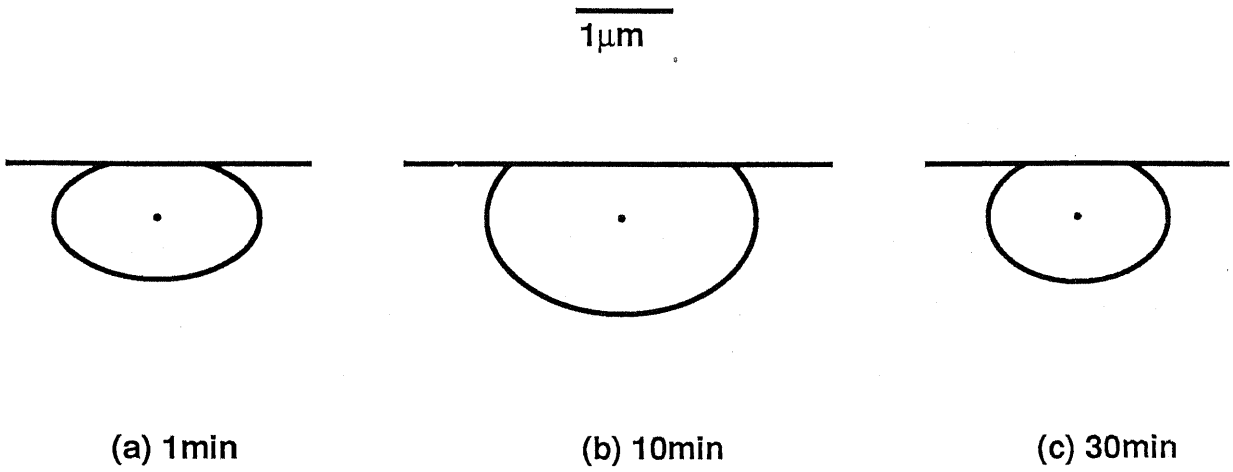

Fig. 2.8 Calculated pn-boundary after focused Be-implantation and annealing. The annealing time is (a) 60 s, (b) 600 s, and (c) 1800 s. The electron density of the substrate is assumed to be 5×10^{16} cm^{-3}, due to the slight thermal conversion. The assumed condition of the implantation and the annealing is the same as the experiments in Fig. 2.7 (a), (b), and (c).

§2.5 Fabrication of microstructures

In this section, the fabrication of very fine structures by the FIB implantation is demonstrated.[24] The doping technique of n- and p-type dopants into very small regions by FIB is applied to the formation of surface nipi-structures. The enhanced etching technique of the FIB-implanted regions is applied to the formation of GaAs gratings and very fine structures.

2.5.1 Surface nipi-structure

A "modulated" semiconductor structure has various properties that a normal bulk semiconductor does not have. Due to the recent progress of the semiconductor film growth techniques, many modulated semiconductor structures have been fabricated, such as selectively doped heterostructures,[50] quantum wells (QW), superlattices,[1] and nipi-structures (doping superlattices).[52] However, these structures are modulated only in the direction normal to the films. Here, a surface modulated structure, which is modulated in the direction parallel to the film, is successfully fabricated by the FIB implantation.[24]

The starting material was a semi-insulating LEC GaAs substrate. First, focused Si-ion-beam was line-implanted periodically into the substrate. Next, focused Be-ion-beam was also line-implanted periodically to just in the midst of the Si-implanted lines. The period was changed from 1 to 4 μm. Then the annealing was performed at 800 °C for 60 s, thus forming the surface nipi-structures. The

structures were observed by SEM in the secondary electron (SE) mode and the electron-beam-induced current (EBIC) mode.

Figure 2.9 (a) shows a SEM image in the SE mode of the nipi-structure with the period of 4 μm. In this case, a reverse-bias of 5 V is applied across the pn junction. The potential of the n-type region is then lowered and the efficiency of the SE emission is reduced. Therefore, the black region in the image corresponds to the n-type region and a white region to p-region. A clear contrast in the two regions is observed.

Figure 2.9 (b) shows an EBIC image and a line profile of the EBIC signal. When the electron beam is impinged to the depletion region between the n- and p-type regions where the electric field due to the built-in potential is applied, the electrons move toward the n-type region, thus making current. Therefore, the white region in the EBIC image represents the depletion region. In the line profile, the lowest and the second lowest currents correspond, respectively, to p- and n-regions. These images show that the perfect nipi-structure with 4 μm period is formed by the FIB implantation.

When the period of the nipi-structure is decreased to 1 μm, where the interval between the Si- and Be-implanted lines is 0.5 μm, a contrast of the EBIC image becomes unclear, as shown in Fig. 2.9 (c). This is considered to result from the resolution limit of the EBIC technique. We conclude that a nipi-structure with down to 1 μm period can be formed by the FIB implantation. To realize a quantum effect in a surface nipi-structure, the period must be made much smaller. It will

be possible to realize such structures by optimizing the implantation and annealing conditions.

2.5.2 GaAs gratings with submicron period

In order to realize very fine structures in GaAs and AlGaAs, the FIB implantation technique is combined with the stain-etching technique.[24]

First, preferential etching of p-type or n-type regions is tested. The starting material is an SI LEC GaAs substrate. Focused Si- and Be-ion-beam was line-implanted to the substrate. RTA was performed to activate the ions. The sample was immersed in the stain-etchants. Two etching conditions were employed.
Condition A: $HF:H_2O_2:H_2O = 10:1:1$ under the dark condition.
Condition B: $HF:H_2O_2:H_2O = 1:1:10$ under white light illumination.
The sample was cleaved and observed by SEM.

Figure 2.10 shows SEM images of the etched structures. Under the condition A, both Si-and Be-implanted regions are selectively etched as shown in Fig. 2.10 (a). Under the condition B, on the other hand, the Si-implanted regions remain unetched and only the unimplanted regions (semi-insulating) are selectively etched as shown in Fig. 2.10 (b). Consequently, submicron mesa structures are formed. However, the dimensions of the fabricated structures are from 0.3 to 1 μm, and not so small. This is because the implanted ions spread in semiconductors and the p- or n-type regions cannot be as small as the diameter of the ion-beam.

In order to realize smaller semiconductor structures, an enhanced etching of damaged regions induced by the FIB implantation was applied. Focused Si-ion-beam was employed to minimize the ion spread in semiconductors.

The starting materials are (100) oriented SI LEC GaAs and epitaxial $Al_xGa_{1-x}As$ (x = 0.1). The focused Si-ion-beam was line-implanted into the samples along $(0\bar{1}1)$ or $(0\bar{1}\bar{1})$ direction. The line-dose was changed from 2×10^9 to 5×10^{10} cm^{-1}, and scanning speed from 0.03 to 1.8 cm/s. When the line-dose is high enough the implanted regions become amorphous,[52] while such amorphous regions cannot be created by the conventional UIB Si-implantation.[53] This is because the current density of FIB is much higher than that of UIB. The amorphous regions were selectively etched with hot HCl (80 °C) and submicron patterns were fabricated.

Figure 2.11 shows fabricated GaAs gratings with a submicron period along the $(0\bar{1}1)$ direction. The period is 0.37 μm in Figs. 2.11 (a) and (b), and 0.5 μm in Fig. 2.11 (c). The critical dose for the formation of the amorphous region is about 3×10^9 cm^{-1}. When the line-dose is just above the critical dose, a width of the grooves was about 0.2 μm (Fig. 2.11 (a)). The width and shape of grooves can be varied by changing the line-dose as shown in Fig. 3 (b) and (c).

It is found that the critical dose depends on the scanning speed. Figure 2.12 shows the dependence of the critical dose on the scanning speed. The slower the scanning rate, the lower the critical dose. The width of the groove is also shown in the figure. The groove width

becomes wider with decreasing the scanning rate even when the line-dose is the same. This result indicates the high current-density effect of the FIB implantation, i. e., the damage induced by the FIB implantation is heavier when the FIB is scanned slower even if the implantation dose is constant, as was observed in focused B-ion-implantation into Si.[54]

When the focused Si-ion-beam is line-implanted along the $(0\bar{1}\bar{1})$ direction, the shape of the grooves changes. Figure 2.13 shows the grooves fabricated on AlGaAs along the $(0\bar{1}\bar{1})$ direction. The line-dose was 1×10^{10} cm^{-1} and the scanning speed was 0.08 cm/s. The width of groove becomes smaller near the surface than in the deeper region, due to the dependence of the amorphous formation and the etching rate on the crystal orientation. It should be noted that the narrowest structure of AlGaAs between grooves is about 30 nm. This technique can be applied to the fabrication of gratings for DFB lasers and ultrathin wires.

Since FIB is precisely controlled by a computer, a grating pattern with an arbitrary shape can be drawn on target materials. As an example, circular gratings were fabricated on a GaAs substrate as shown in Fig. 2.14. The fabrication process is the same as described above. Since the cleaved surface in Fig. 2.14 (b) is the $(0\bar{1}\bar{1})$ surface, the shape of the grooves is very similar to that in Fig. 2.13. With this technique, a Fresnel lens can be fabricated. This technique will find various applications in optoelectronics.

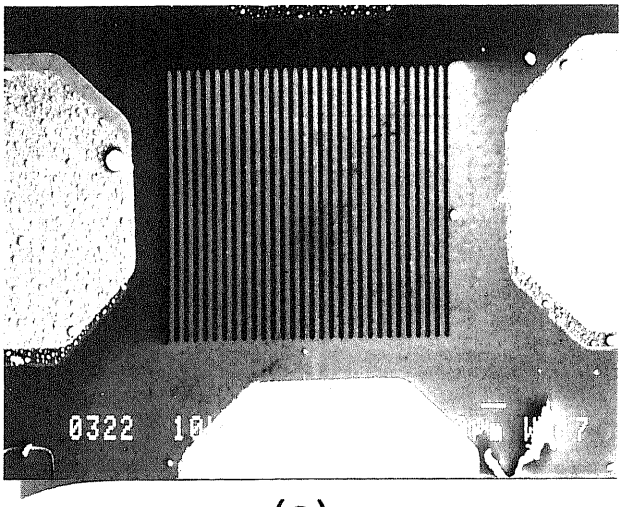

(a)

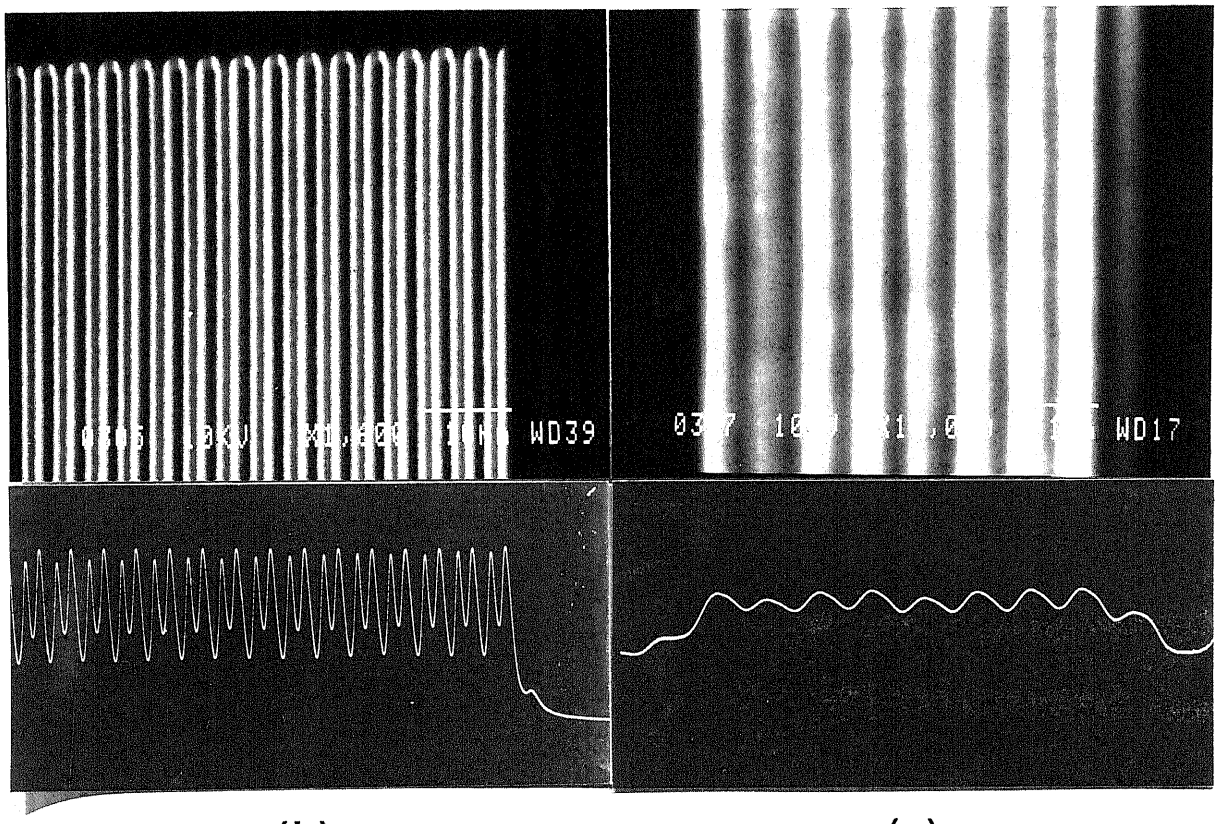

(b) (c)

Fig. 2.9 (a) A SEM micrograph of a nipi-structure reverse-biased at 5 V. The period is 4 μm. (b) An EBIC image and its line profile of the nipi-structure with a period of 4 μm. (c) An EBIC image and a line profile of the nipi-structure with a period of 1 μm.

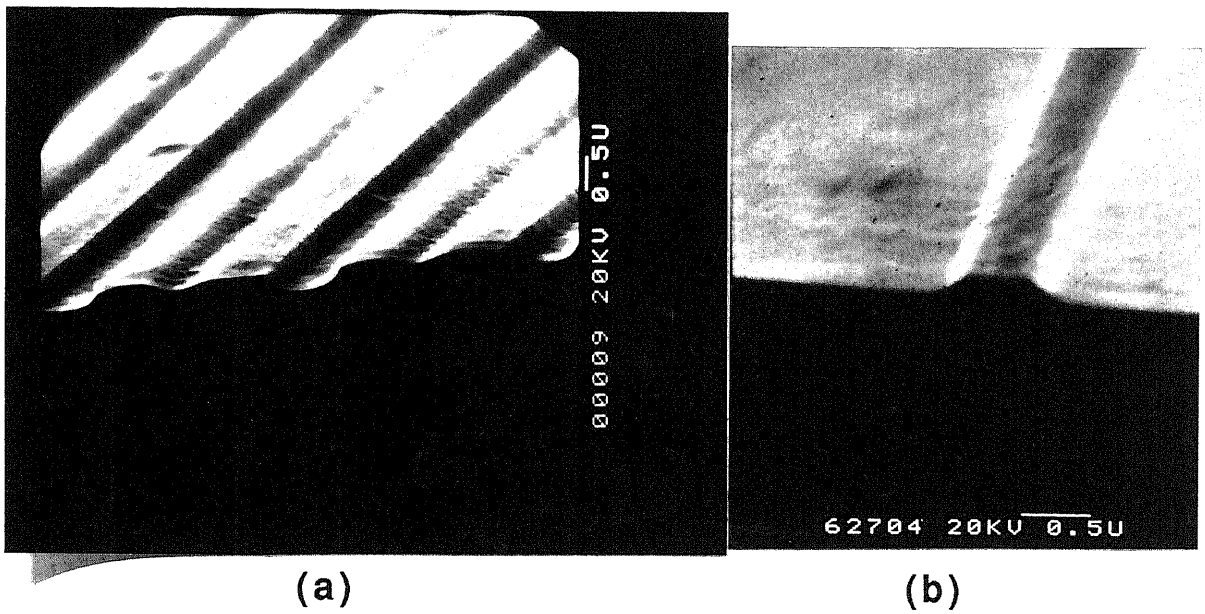

Fig. 2.10 The microstructures fabricated by the FIB implantation and stain-etching. (a) Etched under condition A. Both Si- (smaller grooves) and Be- (larger grooves) implanted regions are selectively etched. (b) Etched under condition B. The Si-implanted region remains unetched.

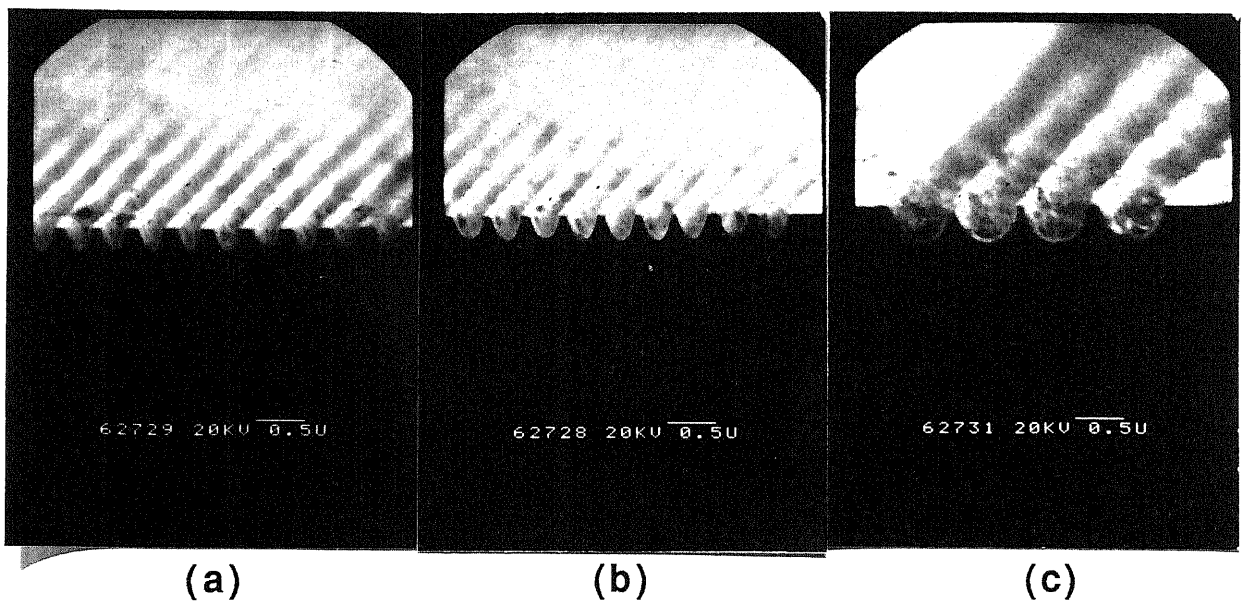

Fig. 2.11 GaAs gratings with submicron periods fabricated by the FIB implantation and the enhanced etching of the damaged regions. The line-doses are (a) 3.0×10^9 cm^{-1}, (b) 3.5×10^9 cm^{-1}, and (c) 4.1×10^{10} cm^{-1}, respectively.

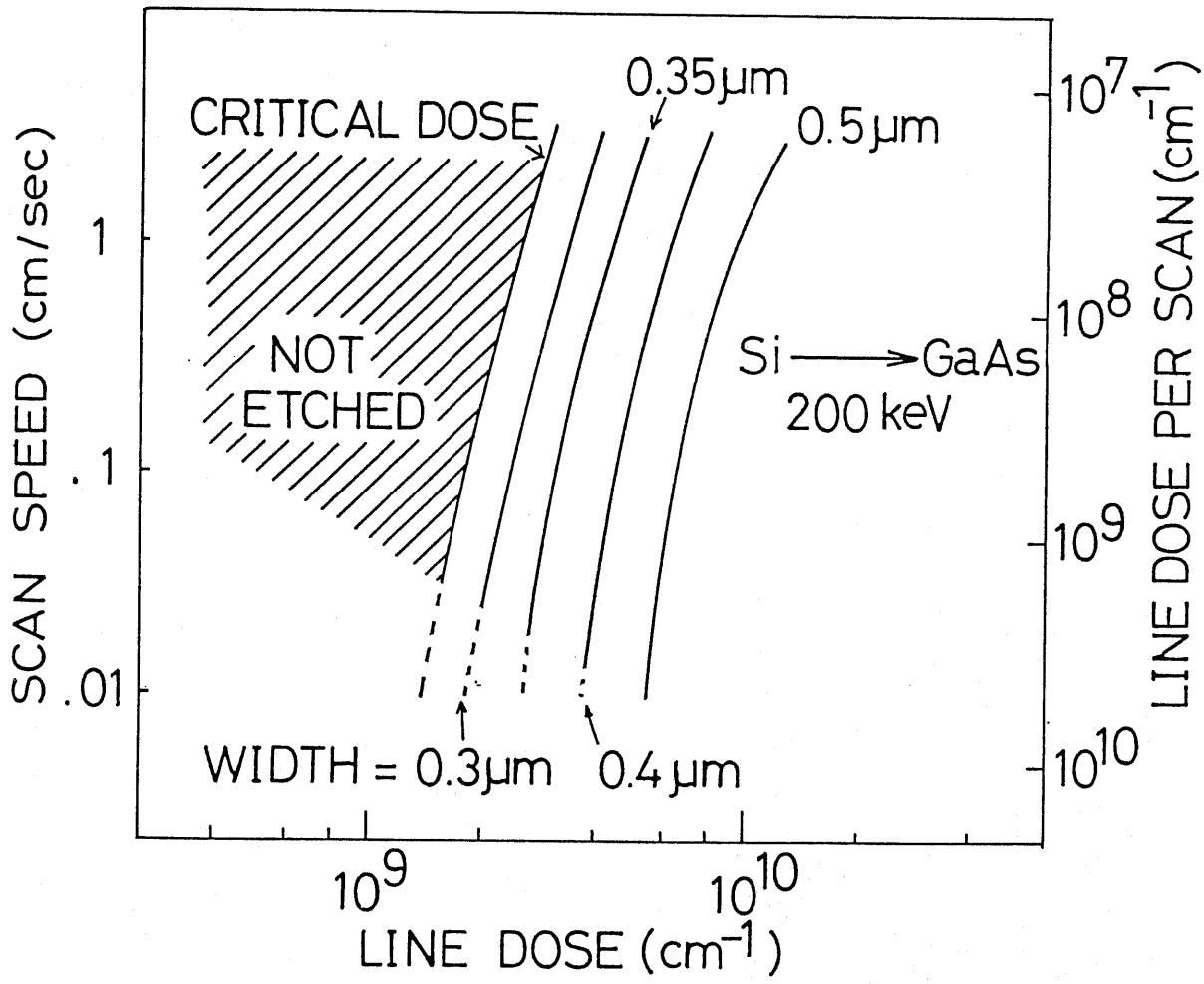

Fig. 2.12 Dependence of the critical dose for the formation of the amorphous region as functions of the line-dose and the scanning rate. The width of the groove is also shown.

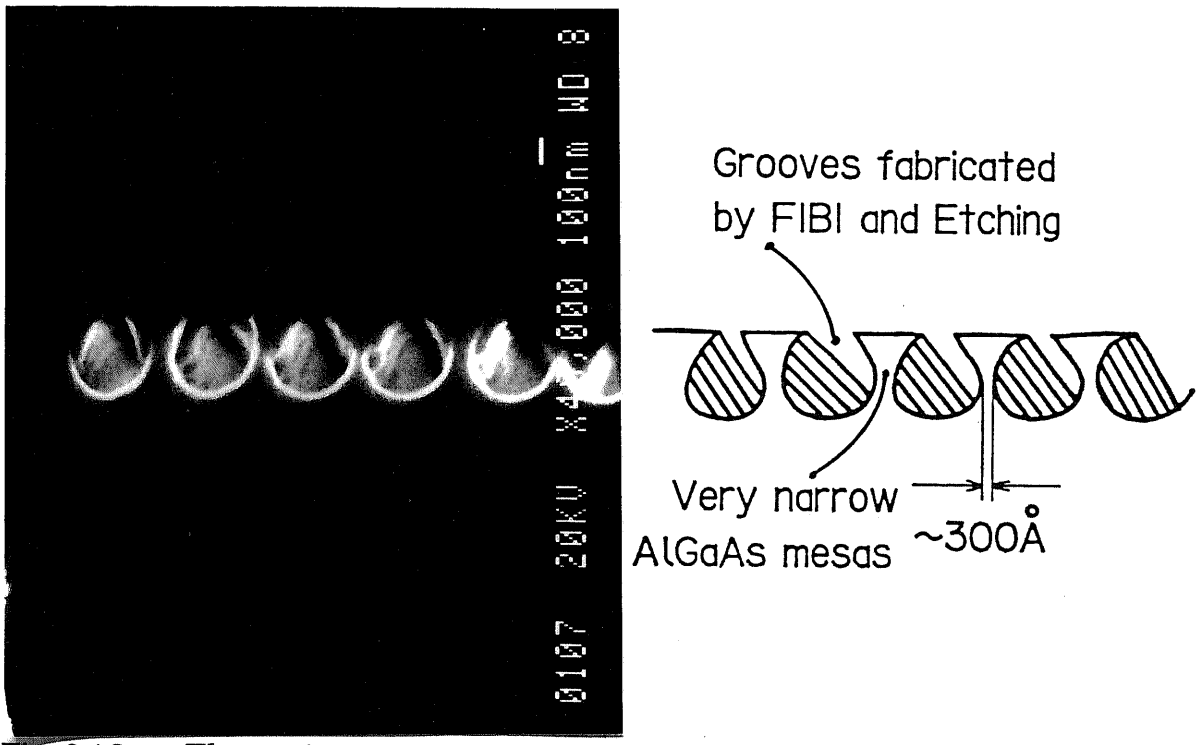

Fig. 2.13 The microstructure of AlGaAs fabricated by the FIB implantation and the wet-etching. The narrowest structure is as small as 30 nm. A schematic illustration of the micrograph is also shown.

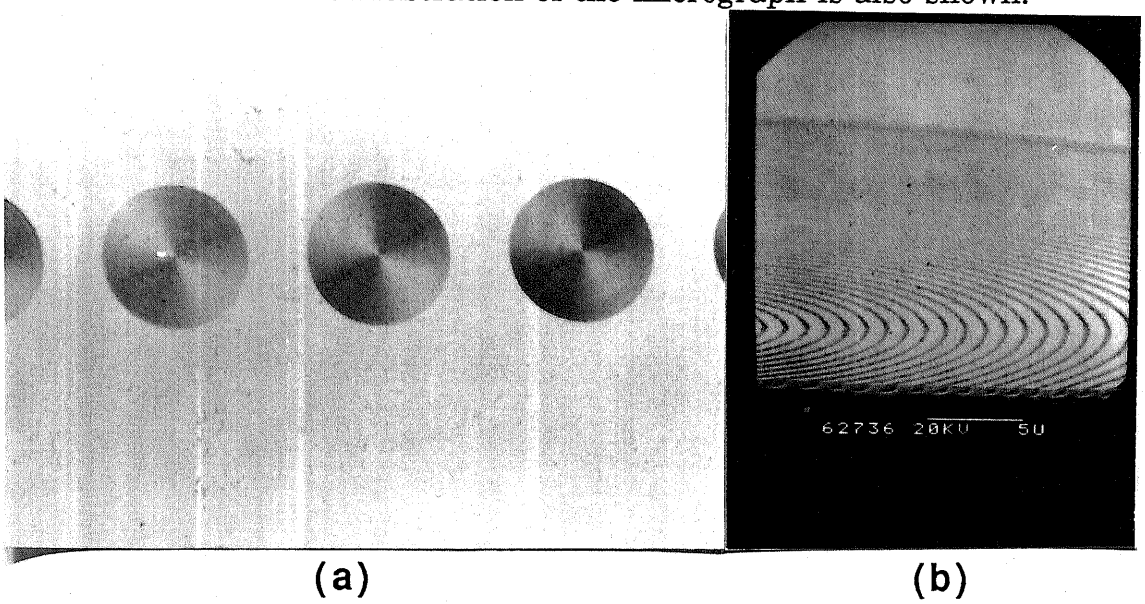

Fig. 2.14 The circular grating of GaAs fabricated by the FIB implantation and the wet-etching. (a) A micrograph of the whole image. The maximum diameter is 1 mm. (b) A SEM micrograph. The separation of each groove is 1 μm.

§ 2.6 Fabrication of GaAs quantum wires

A variety of methods are reported to fabricate very narrow semiconductor structures. In most cases, carriers are confined to two-dimensional (2D) systems in advance by thin film growth techniques such as molecular beam epitaxy (MBE) and metalorganic chemical vapor deposition (MOCVD). For the generation of very small patterns less than 1 μm on the film, the electron beam (EB) lithography[55-66] or the laser holographic lithography[67-71] is generally employed.

The methods for the lateral confinement of carriers are generally classified into two: physical confinement and electrostatically confinement. In the first method, the semiconductors are etched with the submicron lithography patterns as a mask, and the carriers are physically confined into very narrow regions.[55-60,70-73] Reactive ion etching (RIE) is often used for the etching process.[55-59,70,71] In the other method, submicron gates[65-69,74-77] or pn-junctions[78] are formed on the basis of the lithography patterns and the carriers are electrostatically confined into very small regions. The heterointerfaces in regrowth structures[79,80] or intermixed quantum wells[22,64] are also employed for the electrostatic lateral confinement. In any case, the process is very complicated because it consists of the film growth, lithography, etching or evaporation, and so on. It is desirable to develop a new simple process to fabricate narrow semiconductor structures.

The FIB implantation technique is one of the most promising methods to fabricate semiconductor quantum wires. The advantages of the FIB implantation are described in the previous sections. It is very simple, very fine, precisely controlled, and applied to various meanings. However, the FIB implantation has a disadvantage: the implanted ions spread by collisions in semiconductors even if the ion beam is focused.[24] The ions spread further by diffusion during annealing for activation.[24] This disadvantage has to be overcome by some method.

In this section, novel and simple processes are developed to fabricate quasi-one-dimensional GaAs quantum wires by utilizing the FIB implantation. In the first method, a gap space between two high-resistivity regions formed by FIB implantation works as a current path.[20,21] The other method utilizes the expansion of depletion layers in a pn-junction to make a very narrow wire.[21] The minimum width of the fabricated wires is as small as 20 nm.

2.6.1 High-resistivity method

The microstructure fabricated by the FIB implantation[21] is shown in Fig. 2.13. This micrograph is very suggestive for the application of the FIB implantation to the formation of very narrow wire structures. It is shown in the figure that the ions spread in semiconductor to about 0.3 μm even if the ion-beam has 0.1 μm diameter. Here, it should be noted that the dimension of the microstructures formed between the grooves is as small as 30 nm. It is suggested that, although the implanted ions spread in semiconductors, very small structures with

dimensions less than 0.1 μm can be fabricated between the two implanted regions.

Moreover, it is desirable not to anneal the sample in order to suppress the diffusion of implanted ions. When FIB is implanted to a conducting GaAs layer, the implanted region becomes high-resistive as long as no annealing is performed, because a lot of defects are introduced by the FIB implantation. Therefore, the formation of the high-resistive region by the FIB implantation does not involve any annealing process, and no diffusion of ions takes place.

For the fabrication of very narrow GaAs wires, these two techniques are combined: i. e. the gap space between the two high-resistivity (HR) regions formed by the FIB implantation is utilized (HR method).

Figure 2.15 shows schematic views of the sample structure. The starting material was an undoped semi-insulating (SI) LEC GaAs wafer. First, focused Si-ions were implanted into the GaAs wafer at 40 keV with a dose of 4×10^{13} cm^{-2} (the first-stage implantation). The implanted area was 100 μm × 20 μm and the projected range of the ions was 34 nm. Next, rapid thermal annealing (RTA) was carried out to recover the implantation damages and to activate the ions.[37] As a result, a very thin conductive layer with a width of 20 μm was formed on SI GaAs.

Then, a focused Si-ion-beam with a 0.1 μm diameter was implanted into two regions on the sample at 200 keV with a dose of 1.1×10^{12} cm^{-2} (the second-stage implantation). No anneal was performed

after the second implantation. The implanted regions became high-resistive. As shown in the figure, these two high-resistivity regions confine the conducting layer into a very narrow wire. The designed gap spacing d between the second-stage implanted patterns was varied from 0.2 μm to 1.0 μm as a parameter. The designed length of the channel was 2.0 μm. This is one of the simplest methods ever reported to fabricate one-dimensional structures.

Figure 2.16 shows the measured conductance G of the fabricated GaAs wires as a function of d. G decreases linearly with decreasing d and becomes zero when $d = d_0 = 0.48$ μm at 4.2 K. $d_0/2$ is considered to represent the sum of the lateral spread of the implanted ions and the depletion region width. Therefore, the effective width d_{eff} of the wires is given by $d_{eff} = d - d_0$ and the effective length L_{eff} of the wires is 2.48 μm (= 2.0 μm + d_0).

The slope in Fig. 2.16 gives a conductivity in the narrow channel, which is found to be almost the same as that of the original conductive layer. This indicates that the narrow channels are separated from implantation damage by the depletion region formed between the high-resistivity region and the conducting wire. It should be noted that the conductance increases linearly with d_{eff}, indicating that the FIB implantation is well controlled. The minimum d_{eff} of the fabricated wires is as small as 20 nm. This width is in good agreement with the minimum dimension of the microstructures in Fig. 2.13.

2.6.2 pn-junction method

When a focused Si-ion-beam is line-implanted into SI GaAs, an n-type conducting wire structure is easily formed. In this case, however, the width is not so narrow because the ions spread in the substrate. When the focused Si-ion beam is line-implanted into p-type GaAs, it is expected that the n-type wire structure becomes narrower because the depletion region across the pn-junction can expand to the n-type region (the conducting wire) by a reverse-bias. A narrow GaAs wire is fabricated by this method (PN method).

Figure 2.17 shows schematic views of the sample structure. The starting material was an undoped SI LEC GaAs wafer. First, focused Be-ions were implanted into SI GaAs in an area of 100 μm × 13 μm. The energy was 100 keV and the dose was 6×10^{12} cm^{-2}. Then, the focused Si-ion-beam with a 0.1 μm diameter was line-implanted across the Be-implanted area as shown in the figure. The energy was 80 keV and the line-dose was 9×10^{8} cm^{-1}. RTA was performed at 1000 °C for 1 s to activate both Be and Si ions and to suppress the diffusion of implanted Si. Consequently, an n-GaAs wire is formed in p-GaAs.

The measured conductance of the wire decreased with increasing the reverse-bias voltage across the pn-junction, indicating that the wire became narrower by expanding the depletion region between p-GaAs and the n-GaAs wire. The width of the wire will be estimated in § 3.2.

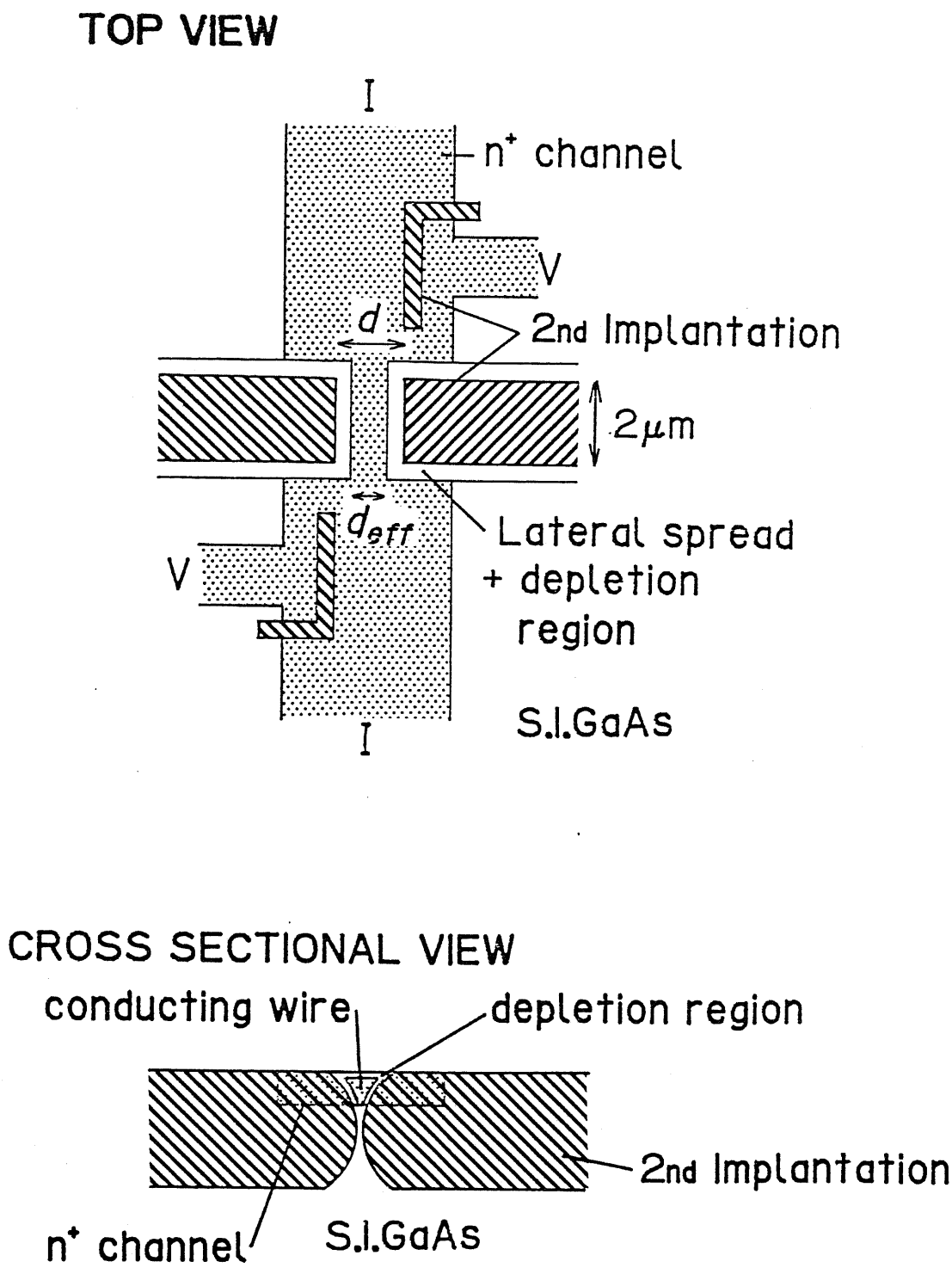

Fig. 2.15 Schematic views of the GaAs wire by the HR method: (a) top view and (b) cross-sectional view.

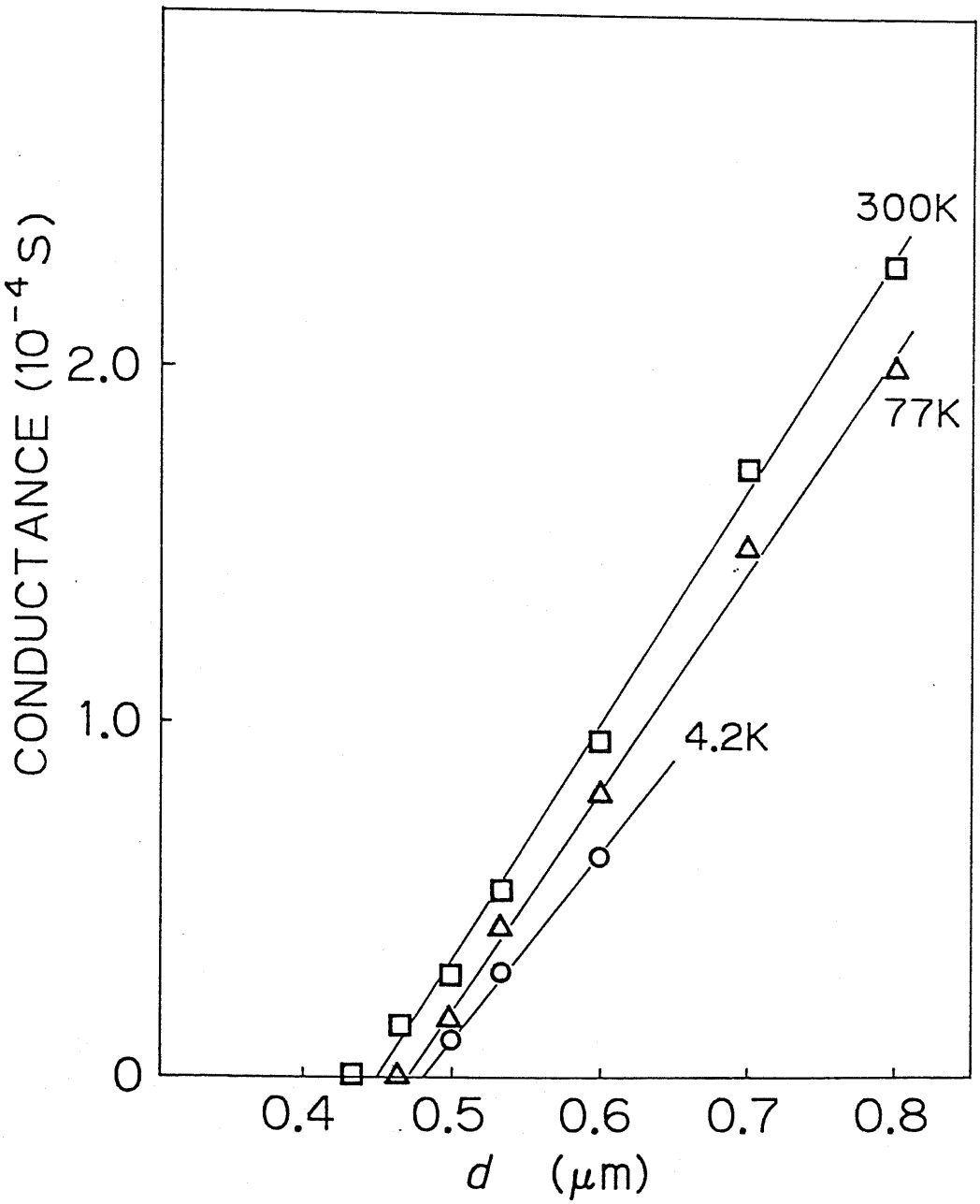

Fig. 2.16 Measured conductance G of the fabricated GaAs wires by the HR method as a function of the designed gap spacing d between the 2nd-stage implanted patterns. Measurements were done at three temperatures: T = 300 K, 77 K, and 4.2 K.

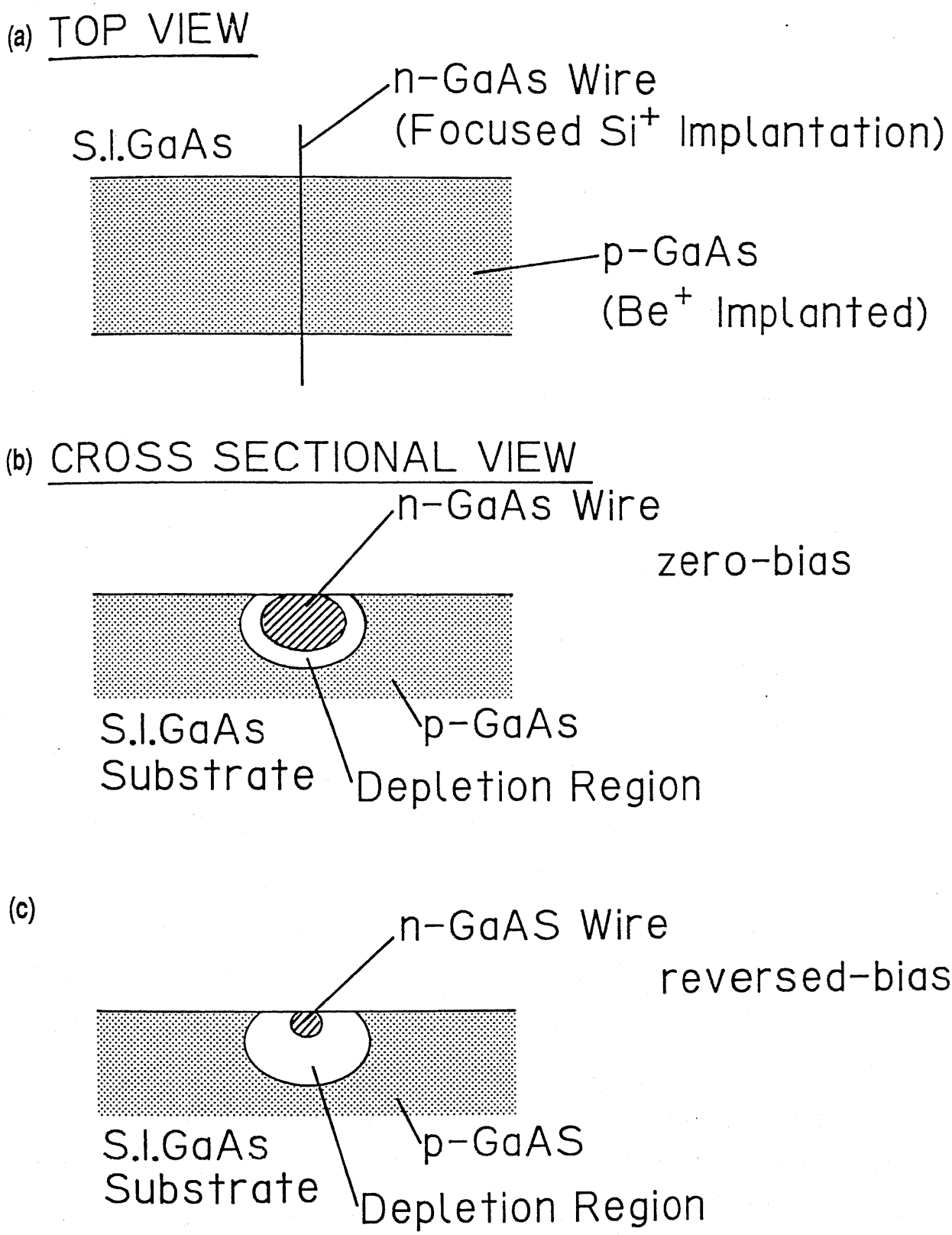

Fig. 2.17 Schematic views of the GaAs wire by the PN method: (a) top view, (b) cross-sectional view at zero-bias, and (c) cross-sectional view at reverse-bias.

§2.7 Conclusion

The microfabrication process of III-V semiconductors by the FIB implantation is demonstrated.

It is shown that electrical properties of focused Si-implanted GaAs are comparable to those of unfocused Si-implanted GaAs when annealed at temperatures higher than 1000 °C by RTA. The activation efficiency of focused Be-ions implanted into GaAs increases with raising the RTA temperature and reaches more than 90 % at 1000 °C annealing. Consequently, the optimal RTA condition of FIB-implanted GaAs is at 1000 ~ 1100 °C for 1 s.

The profiles of FIB implanted ions in GaAs are studied experimentally and theoretically. It is shown that the Be ions spread to about 1 μm in GaAs even if the diameter of the ion-beam is 0.1 μm. The profiles are well predicted by the simple calculation as long as RTA is performed for the post-annealing. It is found that anomalous diffusion of Be takes place when the annealing is longer than 10 min. These results show the RTA process is essential for the FIB implantation.

Fabrication of microstructures of GaAs and AlGaAs is demonstrated. Surface nipi-structures are fabricated by the FIB implantation as an example of the modulated semiconductor structures. The minimum period is 1 μm. An enhance etching of damaged GaAs which is induced by the FIB implantation is applied to the formation of the fine GaAs gratings and very small structures. The GaAs gratings with 0.37 μm period are successfully fabricated. It is found that scanning

speed of the FIB implantation affects the degree of damage in GaAs and, thus, the width of the grooves, due to a high current-density effect of the FIB implantation. The minimum dimension of the fabricated microstructures is as small as 30 nm.

Quasi-one-dimensional GaAs conducting wires are fabricated by two methods using the FIB implantation. In the first method, the high-resistive regions are selectively formed in conducting GaAs layers by the FIB implantation. A narrow conducting wire structure is left between the two high-resistive regions. In the other method, focused Si-ion-beam is line-implanted into p-GaAs to form an n-type conducting wire in p-GaAs. Then negative-bias is applied across the pn-junction to make the n-GaAs wire narrower. The minimum width of the fabricated GaAs wires is as small as 20 nm.

These results show excellent feasibility of the FIB implantation for fabricating various fine structures of III-V semiconductors.

Chapter 3

Phase Coherence Length and Phase Breaking Mechanisms of Electron Waves in GaAs Quantum Wires

Abstract

The phase coherence length L_ϕ and the phase breaking mechanisms of electron waves in GaAs quantum wires are systematically studied. The quantum wires are fabricated both in n-GaAs and in selectively doped AlGaAs/GaAs heterostructures. The positive magneto-conductance, which is due to the weak localization effect, is observed in these wires at low temperature at low magnetic field. L_ϕ in the n-GaAs is estimated by fitting the one-dimensional weak localization theory to the data. It is shown that the theory in "dirty limit" is not applicable to the high-mobility AlGaAs/GaAs wires. L_ϕ in the AlGaAs/GaAs wires at 1.3 K, derived by the modified theory, is ~1.2 μm, 9 times longer than that in the n-GaAs wires. This difference in L_ϕ is well explained by the mobility dependence of L_ϕ, demonstrating that the selectively doped structure is advantageous to obtain long L_ϕ. L_ϕ increases with increasing conductance G as $L_\phi \sim G^{0.85}$ at 4.2 K. This dependence suggests that the main phase breaking mechanism at 4.2 K might be the inelastic electron-electron scattering. L_ϕ is found to increase with decreasing temperature but saturate below around 3 K, indicating the existence of some temperature-independent phase breaking mechanisms at low temperatures.

§ 3.1 Introduction

When the size of the semiconductor structures is so small that the electron wavefunction retains its phase information within the structure, the electron wave which passes through different paths would interfere each other and the interference would play an important role in electron transport. This quantum interference effect of electron waves has been of great interest in solid state physics.[6,11-14] Recently, the applications of the quantum interference to electron devices were proposed[15-17] and their advantages, such as high speed, low power dissipation, and multifunction, were discussed. Since then, the quantum interference has attracted much attention from the technological point of view as well.

One of the most important parameters in the quantum interference effect is the phase coherence length, L_ϕ, of electron waves. This is the distance over which the phase of an electron wavefunction is maintained. When the sample size L is larger than L_ϕ, the quantum interference effect such as the Aharonov-Bohm (AB) effect is smeared out. Therefore, the quantum interference devices must be smaller than L_ϕ.

The phase coherence length L_ϕ is usually estimated from the weak localization effect. Especially in two dimensional (2D) systems, the theory of the weak localization was developed by Hikami *et al.*[81] and Altshuler *et al.*,[82] and L_ϕ (or the phase breaking time τ_ϕ) has been extensively investigated in metal films[83-87] and semiconductors.[18,88-90] In one-dimensional (1D) systems, the weak localization

theory was developed by Altshuler and Aronov.[91] However, there has been very few experimental reports on L_ϕ in narrow quantum wires and L_ϕ in the 1D systems is still controversial. In addition, most of the proposed quantum interference devices are composed of narrow wire structures. Therefore, it is very important to investigate L_ϕ in 1D quantum wires and also to clarify the phase breaking mechanisms which determine L_ϕ in the 1D systems.

In this Chapter, a special attention is focused on the phase coherence length L_ϕ and the phase breaking mechanisms of electron waves in GaAs quantum wires. The dependences of L_ϕ on the electron mobility, on the conductance of the wire, and on the temperature are systematically studied, and the phase breaking mechanisms are discussed.

§ 3.2 describes the phase coherence length L_ϕ in n-type GaAs quantum wires, in which the electron mobility is about 1000 cm^2/Vs. It is shown that L_ϕ can be derived by fitting the theory of the one-dimensional weak localization to the experimental magneto-conductance data. The derived value of L_ϕ at 1.3 K is about 0.13 μm.

In § 3.3, L_ϕ in selectively doped AlGaAs/GaAs quantum wires is investigated. It is shown that the weak localization theory in "dirty limit" is not applicable to the present samples with high mobility. L_ϕ is estimated by fitting the modified theory which takes into account the boundary scattering and the high-mobility effect. Derived L_ϕ is about 1.2 μm at 0.3 K, 9 times longer than that in the n-GaAs wires. The increased L_ϕ is well explained by the mobility dependence of L_ϕ, and

demonstrates the advantage of the use of the selectively doped structures to obtain long L_{ϕ}.

§ 3.4 is devoted to the study on the phase breaking mechanisms in GaAs quantum wires. The conductance dependence and the temperature dependence of L_{ϕ} reveal that the main phase-breaking mechanism at 4.2 K might be the inelastic electron-electron scattering and that some unknown temperature-independent phase-breaking mechanisms are present at lower temperatures.

§ 3.2 Phase coherence length in n-GaAs quantum wires

Novel, simple techniques are developed to fabricate very narrow GaAs quantum wires by the focused ion beam (FIB) implantation, as described in § 2.6. In this section, the magnetoconductance and the phase coherence length L_ϕ of the n-type GaAs wires are described.[20,21]

3.2.1 Preparation of n-type GaAs quantum wires

The narrow n-type GaAs quantum wires are fabricated by two methods using the FIB implantation.[20,21] In the first method, FIB is implanted into n-type GaAs conducting layers to form high-resistivity (HR) regions. The narrow GaAs wire structure is left between the two HR regions (HR method). Three wires are fabricated. From the conductance of the wire, the effective widths d_{eff} of the wires are derived to be 120, 53, 20 nm, respectively. The length L of the wires is 2.5 μm. The fabrication process is described in detail in § 2.6.1.

In the second method, the focused Si-ion-beam is line-implanted into p-GaAs to form an n-type GaAs wire in p-GaAs. The bias-voltage is applied across the pn-junction to control the width of the wire. The length L of the wire is 13 μm. The detailed process is described in § 2.6.2.

3.2.2 Magnetoconductance of n-GaAs quantum wires

In order to investigate the quantum interference effect in the n-type GaAs quantum wires, the magnetoconductances of the wires were measured at low temperatures. The samples were set to the cryostat and cooled down to 1.3 K. The conductances were precisely measured by the lock-in technique with the four-terminal method (for the wires by the HR method) or the two-terminal method (for the wires by the PN method). The current for measuring was set to 3×10^{-9} A to avoid the electron heating effect.[92]

Figure 3.1 shows magnetoconductance spectra of the three n-GaAs wires fabricated by the HR method measured at 1.3 K at low magnetic fields. The conductance is normalized to $G_{univ} = e^2/h$, where e is the electron charge and h the Planck constant. As shown in the figure, the conductance increases with increasing the magnetic field. The increase in the conductance is larger in wider wire.

Figure 3.2 shows magnetoconductance spectra of the n-GaAs wire fabricated by the PN method measured at 1.3 K at several bias-voltages. The positive magnetoconductance (i. e., the negative magnetoresistance) is also observed as shown in the figure. When the bias voltage across the pn-junction is changed from 0 to -6.5 V, the increase in the conductance becomes small. These behaviors are explained by the theory of the weak localization.

3.2.3 Theory of weak localization

It was predicted by Anderson in 1958 that in disordered materials the electron wavefunction would be spatially localized.[7] At finite temperatures, the electron can transfer from a localized level to another by the thermal energy (variable range hopping). However, when the temperature is low enough and the sample size is larger than the localized length ξ, the conductivity will vanish.

Suppose the k-space in a metallic sample where an electron of momentum $\boldsymbol{k}$ travels diffusively with elastic scatterings and the momentum is changed from $\boldsymbol{k}$ to $-\boldsymbol{k}$ as follows (see Fig. 3.3).[93]

$$\boldsymbol{k} \longrightarrow \boldsymbol{k}'_1 \longrightarrow \boldsymbol{k}'_2 \longrightarrow \cdots\cdots \longrightarrow \boldsymbol{k}'_{n-1} \longrightarrow \boldsymbol{k}'_n = -\boldsymbol{k}$$

Here, the momentum transfers are $\boldsymbol{g}_1, \boldsymbol{g}_2, \cdots\cdots, \boldsymbol{g}_n$. When the scatterings are time-reversal, there is an equal possibility for the electron $\boldsymbol{k}$ to be scattered from the state $\boldsymbol{k}$ into $-\boldsymbol{k}$ via the sequence

$$\boldsymbol{k} \longrightarrow \boldsymbol{k}''_1 \longrightarrow \boldsymbol{k}''_2 \longrightarrow \cdots\cdots \longrightarrow \boldsymbol{k}''_{n-1} \longrightarrow \boldsymbol{k}''_n = -\boldsymbol{k}$$

where the momentum transfers are $\boldsymbol{g}_n, \cdots\cdots, \boldsymbol{g}_2, \boldsymbol{g}_1$. This complementary scattering series have the same changes of momentum in opposite sequence. The amplitude of the wavefunction at the final state $-\boldsymbol{k}$ is identical for the both sequences because of the time-reversibility.

When the final amplitudes A' and A'' are phase coherent and equal, $A' = A'' = A$, the final intensity is

$$\begin{aligned} |A' + A''|^2 &= |A'|^2 + |A''|^2 + A'^*A'' + A'A''^* \\ &= 4|A|^2. \end{aligned} \tag{3.1}$$

This amplitude is composed of two different groups. $|A'|^2 + |A''|^2 (= 2|A|^2)$ corresponds exactly to the classical scattering events. $A'^*A'' + A'A''^* (= 2|A|^2)$ corresponds to the interference term, which is neglected in the classical theories. The interference between the two sequences is always constructive because the phase shift is identical for both processes. Therefore, the intensity or the probability of the backscattered electrons is twice as large as in the classical diffusion problem.

It is noted that if the two processes are not coherent, the total scattering intensity is only $2|A|^2$. This also means that the probability of the backscattering in the coherent process is twice as large as in the case of the incoherent scattering. This additional scattering intensity in the coherent process exists only in the backscattering direction. For the other states at the Fermi surface, there is only an incoherent superposition of every two processes.

In a coherent sample, therefore, the probability of backscattering is enhanced. This means that, in the real space, the possibility that an electron returns to the original point is enhanced. This leads to the interference between a propagating electron wave e^{ikr} and the backscattered wave e^{-ikr}, causing a standing wave and thus, a

reduction of the conductivity. Since this effect is thought of as a precursor of the localization, it is called "weak localization".

When the magnetic field is applied, the weak localization effect is suppressed, because the time reversibility is no longer satisfied. Therefore, the conductance of the sample in weak localization regime increases with increasing the magnetic field. This positive magneto-conductance (i. e. negative magnetoresistance) is one of the characteristic features in the weak localization.

The weak localization effect depends on the coherency of the electrons in the sample. If there are some inelastic scatterings the electron wave does not interfere, as mentioned above. The weak localization effect also depends on the dimensionality of the sample: it is enhanced when the dimensionality is reduced, because the probability of the electron backscattering is increased in the lower dimensionality.

The dimensionality in the weak localization is determined by the phase coherence length L_ϕ.[91] The quantum correction to the Drude conductivity due to the weak localization in a disordered one-dimensional system ($W < L_\phi$) was given by Altshuler and Aronov (AA),[91] where W is the width of the one-dimensional system. The reduction of the conductance due to the weak localization is,

$$\begin{aligned}\Delta G(B) &= -\frac{e^2}{h}\frac{2\sqrt{D}}{L}\left[\left(\frac{1}{\tau_\phi}+\frac{1}{\tau_B}\right)^{-1/2}\right] \\ &= -\frac{e^2}{h}\frac{2}{L}\left(\frac{1}{L_\phi^2}+\frac{1}{L_H^2}\right)^{-1/2},\end{aligned} \qquad (3.2)$$

where B is the magnetic field, D ($= \frac{1}{2} v_F^2 \tau_e$) the diffusion coefficient, τ_ϕ the phase breaking time, τ_B the phase relaxation time by the magnetic field, τ_e the elastic scattering time, L_H ($= \sqrt{D\tau_B} = \sqrt{3}\hbar/(eBW)$) the magnetic length in a one-dimensional system of rectangular cross section, L_ϕ ($= \sqrt{D\tau_\phi}$) the phase coherence length, v_F the Fermi velocity, L the length of the wire, and $\hbar = h/2\pi$. Eq. (3.2) is valid for $W < L_\phi$ and

$$B < B_m = \frac{h}{2eW^2} . \tag{3.3}$$

When W = 120 nm, for example, B_m = 0.14 T. The deviation of conductance from the value at B = 0 is given as,

$$\begin{aligned} dG(B) &= \Delta G(B) - \Delta G(0) \\ &= \frac{e^2}{h}\frac{2}{L}\left(L_\phi - \left(\frac{1}{L_\phi^2} + \frac{1}{L_H^2} \right)^{-1/2} \right). \end{aligned} \tag{3.4}$$

Eq. (3.2) or (3.4) contains L_ϕ and W. It should be noted that they are the only unknown parameters. Therefore, L_ϕ and W can be derived by fitting the Eq. (3.4) to the experimental magnetoconductance data.

3.2.4 Estimation of phase coherence length

In order to estimate L_ϕ, Eq. (3.4) was fitted to the experimental data in Figs. 3.1 and 3.2. First, the fitting was performed to the data in Fig. 3.1, with L_ϕ as a fitting parameter. The values of the effective wire widths d_{eff} obtained from Fig. 2.16 were used for W. As shown in Fig.

3.1, the theoretical calculations with L_ϕ = 0.12 μm ~ 0.13 μm, which are shown by solid lines in the figure, are best fitted to the experimental data. It is noted that derived L_ϕ is larger than W, indicating that the fabricated GaAs wires are in the one-dimensional weak localization regime and thus are in the range where Eq. (3.4) is valid. It is also noted that the values of L_ϕ are almost the same for the three wires with different d_{eff}'s.

Then, Eq. (3.4) was fitted to the data in Fig. 3.2. In this case, the fitting parameters are L_ϕ and W. When L_ϕ is set to 0.12 μm, the theory is best fitted to all the data. Although the condition of the one-dimensional localization ($W < L_\phi$) is not satisfied at the bias voltages from 0 to -5 V, the width W is considered to be estimated by this fitting when $W < \pi L_\phi$.[77,94] As shown in the figure, the decrease in magnetoconductance with increasing the negative bias-voltage indicates that the wire becomes narrower with the bias voltage. W is changed from 0.23 μm to 0.09 μm as the bias voltage is varied from 0 to -6.5 V. For reverse-bias voltage higher than 6 V, W becomes smaller than L_ϕ and the wire behaves as a "one-dimensional conductor" in the weak localization regime. The minimum width of the wire fabricated by the PN method was about 90 nm at -6.5 V bias.

These results show that the phase coherence length L_ϕ in n-GaAs wires is 0.12 ~ 0.13 μm. This value is too small in terms of device applications of the quantum interference effect. It is, therefore, desirable to obtain longer L_ϕ in order to realize quantum interference devices.

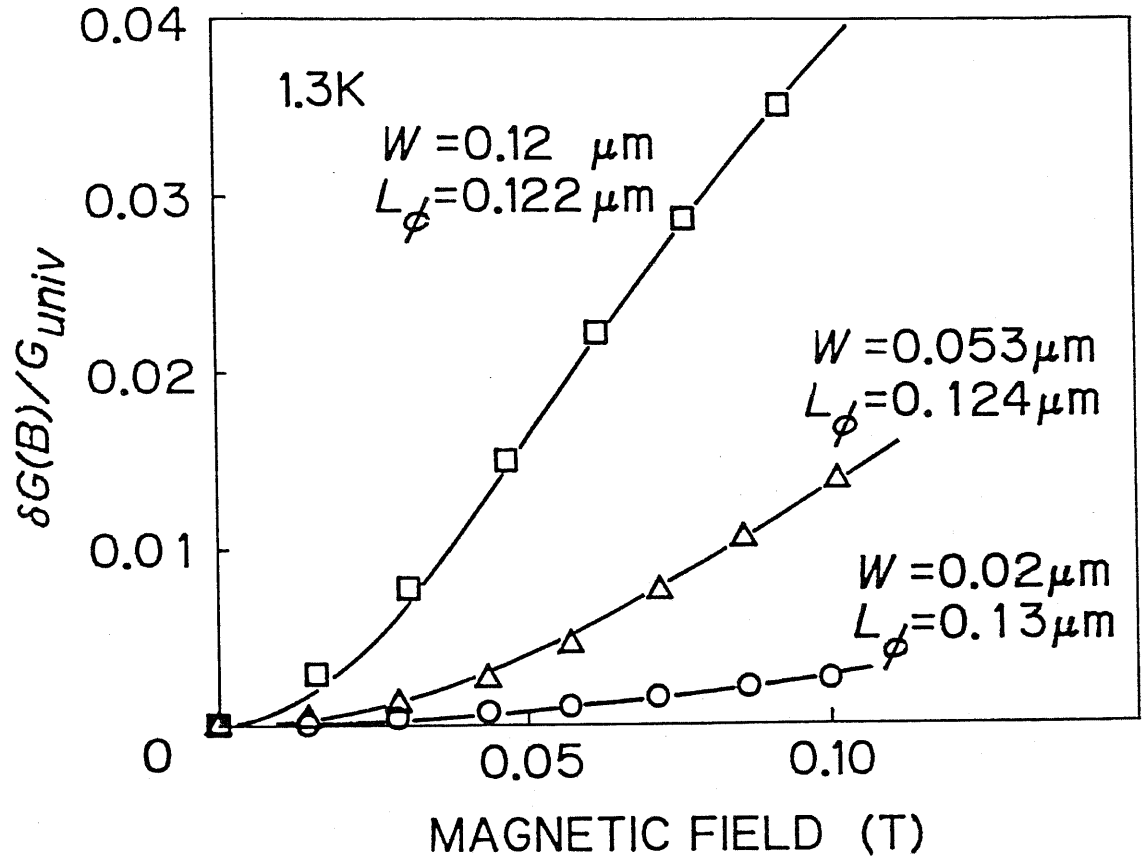

Fig. 3.1 Magnetoconductance spectra of the three n-GaAs wires fabricated by the HR method measured at 1.3 K at low magnetic field. The effective widths d_{eff} of the wires are 120, 53, and 20 nm. The conductance is normalized to $G_{univ} = e^2/h$. The solid curves are the theoretical fittings by Eq. (3.4). The fitting parameter is L_ϕ, and W is set to be d_{eff}.

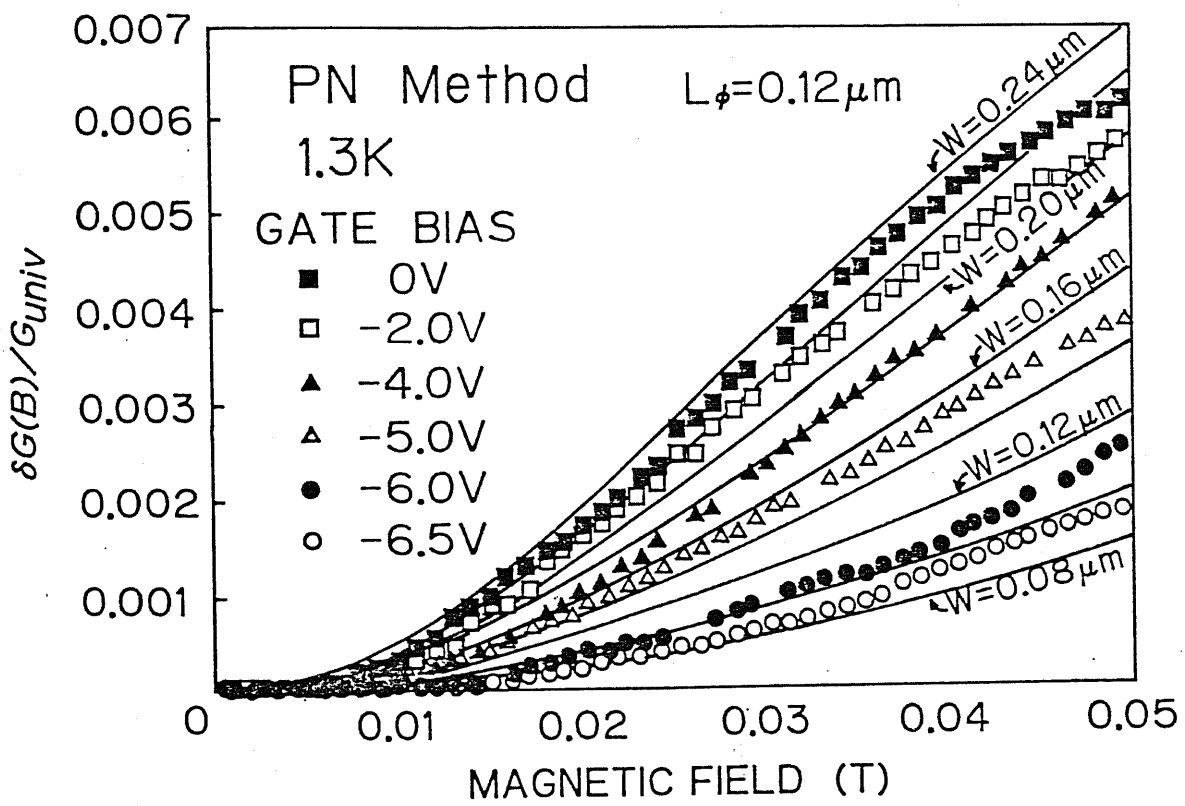

Fig. 3.2 Magnetoconductance spectra of the n-GaAs wire fabricated by the PN method measured at 1.3 K at low magnetic field. The spectra at several bias-voltages are shown. The curves are the theoretical fittings by Eq. (3.4). The fitting parameters are L_ϕ and W.

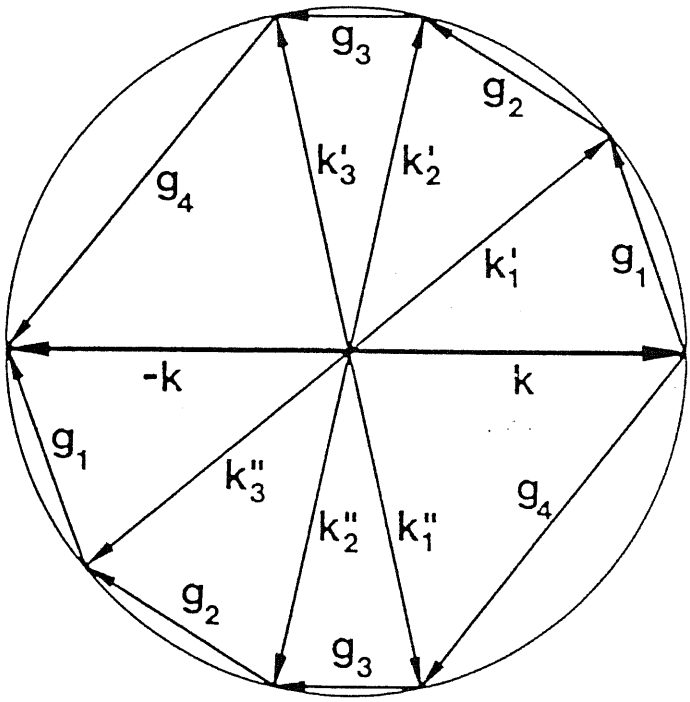

Fig. 3.3 The two sequences in which the electron in the eigenstate of momentum k is scattered from the state k into $-k$. The change of momentum is $g_1, g_2, \cdots, g_n$ for the first series and $g_n, \cdots, g_2, g_1$ for the second. The amplitudes in the final state $-k$ are identical and interfere constructively, yielding an echo in backscattering direction.

§3.3 Phase coherence length in AlGaAs/GaAs quantum wires

The phase coherence length L_ϕ in the n-type GaAs quantum wires is ~0.13 μm, as described in the previous section. The electron mobility in the n-GaAs wires is very small (about 1000 cm^2/Vs) because the original GaAs conducting layers are formed by the Si-implantation and successive rapid thermal annealing. Since the elastic scatterings do not break the phase memory of the electron waves, the low-mobility has nothing to do with the phase breaking. However, it is expected that L_ϕ will become longer when the electron mobility is increased, because the diffusion coefficient D will increase.

This section describes the experimental results on the phase coherence length L_ϕ in GaAs quantum wires which are fabricated in selectively doped AlGaAs/GaAs heterostructures.[95,96] L_ϕ is estimated to be about 1.2 μm at 0.3 K; 9 times longer than in the n-GaAs wires because of the high mobility. This demonstrates that selectively doped heterostructures are advantageous to obtain long L_ϕ.

3.3.1 Fabrication of AlGaAs/GaAs quantum wires

The starting material was a selectively doped AlGaAs/GaAs single heterojunction grown by molecular beam epitaxy (MBE). The two-dimensional (2D) electron density n_s and the Hall mobility μ at 77 K were 5×10^{11} cm^{-2} and 1.7×10^5 cm^2/Vs, respectively. Figure 3.4 shows a schematic cross-section of the AlGaAs/GaAs quantum wire. A focused Si-ion-beam of a 0.1 μm diameter was implanted into two hatched regions to confine a narrow conducting wire structure by the

two high-resistive regions. The dose was 2×10^{11} cm^{-2} and the implantation energy was 200 keV. A very narrow conducting wire was left between the two implanted regions. The designed gap-spacing d was varied from 0.93 μm to 1.2 μm. The length of the wires is 1.9 μm.

Figure 3.5 shows the conductance of the three AlGaAs/GaAs wires at 4.2 K as a function of d. The conductance decreases linearly with decreasing d, and becomes zero when d_0 = 0.9 μm. The effective channel width d_{eff} is given by $d - d_0$. Therefore, the three samples have 300, 100, and 30 nm effective channel widths, respectively. Table II summarizes the structural parameters and characteristics of the two narrower samples, #44 and #34. For comparison, the parameters of the n-type GaAs wire with d_{eff} of 53 nm (#16) are also listed.

3.3.2 Magnetoconductance of AlGaAs/GaAs wires

Figure 3.6 shows magnetoconductance of the two AlGaAs/GaAs wires, #44 (d_{eff} = 100 nm) and #34 (d_{eff} = 30nm), measured at 0.3 K at low magnetic field. The conductance increases with increasing magnetic field, and the increase in conductance is larger in the wider wire. This behavior is similar to that of the n-GaAs wire as shown in Figs. 3.1 and 3.2.

3.3.3 The limit of the AA theory

As described in § 3.2.3, the theory for the magnetoconductance in the one-dimensional weak localization regime was given by Al'tshuler and Aronov (AA).[91] However, this theory is based on the diffusive transport in dirty metals, where $\tau_\phi >> \tau_e$ and $l << W$. Here, τ_ϕ is the phase breaking time, τ_e the elastic scattering time, l the mean free path, and W the width. In high-mobility quantum wires, however, the above conditions are not always satisfied. For example, when $l > W$, the boundary will directly affect the electron transport. When L_ϕ is comparable to l (i. e., $\tau_\phi \sim \tau_e$), the weak localization effect will be reduced because of less elastic backscatterings.

In order to clarify whether or not the AA theory is valid in the AlGaAs/GaAs quantum wires, the AA theory (Eq. (3.4)) was fitted to the data in Fig. 3.6. When L_ϕ was taken as an adjustable parameter with $W = d_{eff}$, a good fitting was obtained only when $B < 500$ G for the two wires (#44 and #34), as shown in Fig. 3.7 (dotted lines). The AA theory should be valid for #44 up to 2 kG (from Eq. (3.3)) and hence, the fitting is not regarded as satisfactory. When both L_ϕ and W were taken as adjustable parameters,[72] we obtained better fitting up to 1 kG as shown in Fig. 3.7 (broken lines) with: L_ϕ =0.7 μm, W = 50 nm for the wire #44 (d_{eff} = 100 nm); and L_ϕ = 0.5 μm, W = 50 nm for #34 (d_{eff} = 30 nm). τ_ϕ and l were estimated, from L_ϕ, W, conductance G, length L and n_s, as $\tau_\phi/\tau_e \sim 2$ and $l/W \sim 10$. Since the AA theory should apply to $\tau_\phi >> \tau_e$ and $l << W$, these values violate these conditions. Therefore, the AA theory is not applicable to the present case.

3.3.4 Modified weak localization theory

The AA theory should be modified to estimate L_ϕ in the high-mobility AlGaAs/GaAs wires. The matters that should be considered are the boundary scattering and the long mean free path. Beenakker and van Houten (BvH)[97] modified the AA theory by taking these effects into account.

When the electron mobility is very high and the elastic scattering time τ_e becomes comparable to the phase breaking time τ_ϕ, the weak localization effect is reduced. This is because the electron must experience at least one elastic scattering before it is backscattered from the state $\boldsymbol{k}$ into $-\boldsymbol{k}$. The probability of the backscattering is thus reduced when $\tau_e \sim \tau_\phi$. In the BvH theory,[97] the reduction factor of the backscattering probability is taken as $(1-e^{-t/\tau_e})$, where t is the time it takes for the electron to be backscattered. Then, the quantum correction to the conductivity is given by

$$\Delta G(B) = -\frac{e^2}{h}\frac{2\sqrt{D}}{L}\left[\left(\frac{1}{\tau_\phi}+\frac{1}{\tau_B}\right)^{-1/2} - \left(\frac{1}{\tau_\phi}+\frac{1}{\tau_B}+\frac{1}{\tau_e}\right)^{-1/2}\right]. \qquad (3.5)$$

In the AA theory (i. e., in the diffusive regime where $\tau_e << \tau_\phi$), the second term between the square brackets, which results from the reduction of the backscattering, is neglected.

When the electron mobility is high and $l > W$, the boundaries directly affect the motion of the electrons, while in the AA theory the boundaries just act as the restriction of the lateral diffusion. BvH

calculated the phase relaxation time τ_B for the boundary scattering[97] and found that for $l_c > W$

$$\tau_B = \frac{l_c^4}{K_1 W^3 v_F} + \frac{l_c^2 \tau_e}{K_2 W^2}, \tag{3.6}$$

where $l_c = (\sqrt{\hbar/eB})$ is the cyclotron radius. If the boundary scattering is specular $K_1 = 0.11$ and $K_2 = 0.23$, and if the boundary is diffusive $K_1 = \frac{1}{4\pi}$ and $K_2 = \frac{1}{3}$. They also found that the diffusion coefficient D strongly depends on the boundary scattering and that

$$D = \frac{1}{2} v_F l \left(1 - \frac{4l}{\pi W} \int_0^1 ds\, s^2 (1 - \exp[-(1-s^2)^{-1/2} W/l\,])\right), \tag{3.7}$$

for the diffusive boundary scattering, while $D = \frac{1}{2} v_F l$ for the specular boundary scattering.

3.3.5 Estimation of phase coherence length

Then, we fit the BvH theory to the data for the both cases of diffusive and specular boundary scatterings. Adjustable parameters are L_ϕ, W, and τ_e, but the number of the independent parameters is reduced to two if G, L, and n_s are known. Therefore, the two-parameter (L_ϕ and W) fitting can be made.

First, the BvH theory is fitted to the data, assuming that the boundary scattering is diffusive. As shown in Fig. 3.8 (broken lines), the theory can be fitted up to 1 kG for both AlGaAs/GaAs wires. The values of L_ϕ

and W are: L_ϕ = 0.8 μm and W = 60 nm for the wire #44 (d_{eff} = 100 nm); and L_ϕ = 0.62 μm and W = 70 nm for #34 (d_{eff} = 30 nm). However, some of the derived parameters are unrealistic. For example, W is narrower in #44 than in #34. Moreover, the diffusion coefficient D in the sample #44 is very small due to the diffusive boundary scattering, i. e. $D = \frac{1}{2} v_F l \times 0.053$ in Eq. (3.7), while the reduction of D is much smaller in the sample #34, $D = \frac{1}{2} v_F l \times 0.25$. This leads to very long τ_ϕ in #44 (τ_ϕ = 100 ps), while τ_ϕ in #34 is 27 ps. Since the both samples (#44 and #34) are considered to have similar characteristics, as listed in Table II, it is not likely that the two samples have so different values of D and τ_ϕ.

Then, the BvH theory is fitted, assuming that the boundary is specular. The best fit data are shown in Fig. 3.8 (solid lines) with: L_ϕ = 1.2 μm, W = 90 nm for the wire #44 (d_{eff} = 100 nm); and L_ϕ = 0.9 μm, W = 70 nm for #34 (d_{eff} = 30 nm). In this case, all the derived parameters are reasonable. From these values, we obtain $\tau_\phi/\tau_e \sim 10$, $L_\phi/l \sim 2$, and $l/W \sim 5$, indicating that the BvH theory is valid in these samples. It should be noted that the electron transport is still diffusive rather than ballistic, since $\tau_\phi \sim 10\tau_e$,.

We consider that these values derived by using the BvH theory for the specular boundary scattering are more reliable, and conclude that the boundary scattering in the AlGaAs/GaAs wires fabricated by the FIB implantation is specular rather than diffusive. This conclusion agrees with the results by BvH in the AlGaAs/GaAs wires fabricated by the reactive ion etching.[98] In our case, L_ϕ's are 1.2 μm and 0.9 μm in the

wire with W of 90 nm and 70 nm, respectively. This result shows that L_ϕ in the AlGaAs/GaAs wires is longer (~9 times longer) than that in the n-GaAs wire (0.13 μm) which is prepared by the FIB implantation. The obtained parameters both in the AlGaAs/GaAs wires and the n-GaAs wire are summarized in Table III.

3.3.6 Mobility dependence of phase coherence length

The difference in L_ϕ in the AlGaAs/GaAs wires and the n-GaAs wires is well explained by considering the fact that the phase coherence length L_ϕ is given by

$$L_\phi = \sqrt{D\tau_\phi}, \tag{3.8}$$

if the electron transport is diffusive. The diffusion coefficient D is given by

$$D = \frac{1}{2} v_F l = \frac{1}{2} v_F^2 \tau_e. \tag{3.9}$$

These equations mean that, if τ_ϕ is assumed to be constant, longer L_ϕ can be achieved in materials with higher electron density and higher mobility, because v_F^2 is proportional to sheet carrier density n_s (in two-dimensions) and τ_e is proportional to mobility μ. The selectively doped heterostructure is the very material that accumulates electrons with both high density and high mobility at the same time. Therefore, the selectively doped structures have the great advantage to obtain long L_ϕ.

It should be noted that L_ϕ depends on the electron mobility. The elastic scattering does not destroy the phase information of the electron waves. Hence, the phase breaking time τ_ϕ is almost independent of the electron mobility. However, the diffusion coefficient D is strongly affected by the mobility. Therefore, longer L_ϕ is achieved in the wires with higher mobility if n_s and τ_ϕ are the same.

The electron mobility in the AlGaAs/GaAs wire #44 (W = 90 nm) is estimated to be ~44000 cm^2/Vs, whereas the mobility in the n-GaAs wire #16 is only ~900 cm^2/Vs. The Fermi velocity v_F is ~3×10^7 cm/s in the AlGaAs/GaAs wire #44, and ~5×10^7 cm/s in the n-GaAs wire #16. From these values, it is predicted by Eqs. (3.8) and (3.9) that the AlGaAs/GaAs wire should have 4.2 times longer L_ϕ than the n-GaAs wire. Although there is about a factor 2 difference between this estimation and the experimental value, the difference in L_ϕ in the two types of the wires is qualitatively explained by the difference in mobility. The discrepancy between the theoretical (4.2 times) and experimental (9 times) results is probably caused by the dependence of τ_ϕ on the conductivity and the width. These results show that the selectively doped structure is suitable to obtain long L_ϕ.

The difference in L_ϕ in the two AlGaAs/GaAs wires (1.2 μm in #44 and 0.9 μm in #34) is also qualitatively explained by the difference in mobility, because the estimated values of mobility in these wires are 44000 and 31000 cm^2/Vs, respectively. Please note that τ_ϕ is almost identical for the two wires (17 ps in #44 and 15 ps in #34) in spite of the difference in the mobility. This is a clear demonstration that the

electron mobility (and thus, the elastic scattering) hardly affects τ_{ϕ}, but L_{ϕ}.

The width W determined by the fitting is not exactly equal to d_{eff} determined from the channel conductance. d_{eff} was estimated on the assumption that the conductivity and the distribution of the damage were the same for all the wires. This assumption is, to the first-order approximation, correct as seen in Fig. 3.5. However, there would be some scatter in the conductivity of the wires due to the inhomogeneity of the fabrication process and of the original epitaxial film. The fluctuation of the focused ion beam would also cause the inhomogeneity of the damage distribution. On the other hand, W was determined for each sample by the two-parameter fitting of the BvH theory; the theory itself has some uncertainty.[97] The two-parameter fitting also leaves a 10 ~ 20 % uncertainty in the parameter W. These effects would result in a discrepancy between W and d_{eff}.

The dependence of L_{ϕ} on the electron density and the electron mobility will be confirmed again in § 3.4.3, where the conductance dependence of L_{ϕ} is investigated.

Table II. The structural parameters and characteristics of the two AlGaAs/GaAs wires and the n-GaAs wire. Here, d_{eff} is the effective width, L the length, G the conductance, n_s the sheet carrier density, E_F the Fermi energy, v_F the Fermi velocity. Listed are the values at 1.3 K. n_s of the sample #44 is obtained by the Shubnikov de Haas oscillation. n_s of #34 is assumed to be the same as that of #44. E_F of the n-GaAs wire is estimated by the state density of the three-dimensional electrons.

sample	d_{eff} (nm)	L (μm)	G (μS)	n_s (cm^{-2})	E_F (meV)	v_F (10^5 m/s)
#44 (AlGaAs/GaAs)	100	1.9	170	5×10^{11}	18	3.1
#34 (AlGaAs/GaAs)	30	1.9	90	5×10^{11}	18	3.1
#16 (n-GaAs)	53	2.5	32	1×10^{13}	54	5.3

Table III. The electrical parameters in the two AlGaAs/GaAs quantum wires and the n-GaAs quantum wire. The values for the AlGaAs/GaAs wires are derived by fitting the BvH theory to the data, assuming that the boundary scattering is specular.

sample	d_{eff} (nm)	W (nm)	L_ϕ (μm)	τ_ϕ (ps)	μ (m^2/Vs)	τ_e (ps)	l (μm)	D (m^2/s)
#44 (AlGaAs/GaAs)	100	90	1.2	17	4.4	1.7	0.52	0.079
#34 (AlGaAs/GaAs)	30	70	0.9	15	3.1	1.2	0.36	0.055
#16 (n-GaAs)	53	53	0.13	3.4	0.09	0.034	0.018	0.0048

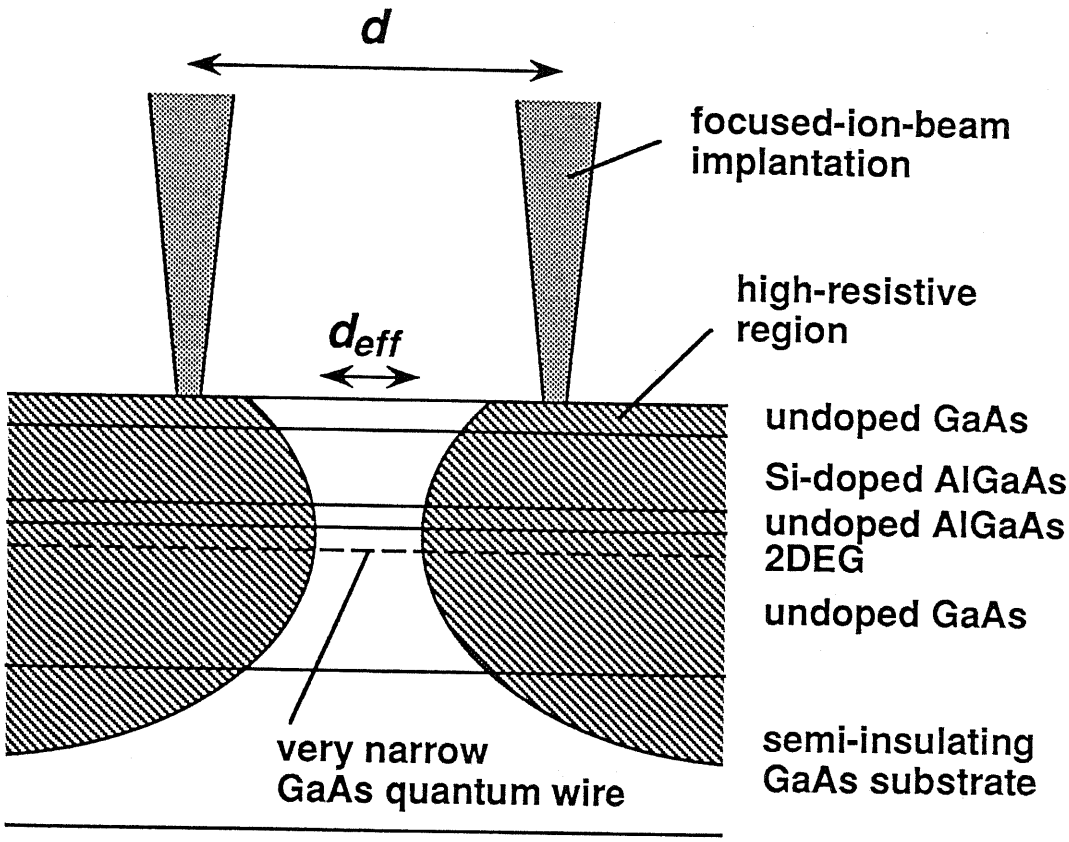

Fig. 3.4 A schematic cross-sectional view of a GaAs quantum wire fabricated in a selectively doped AlGaAs/GaAs heterostructure (AlGaAs/GaAs wire).

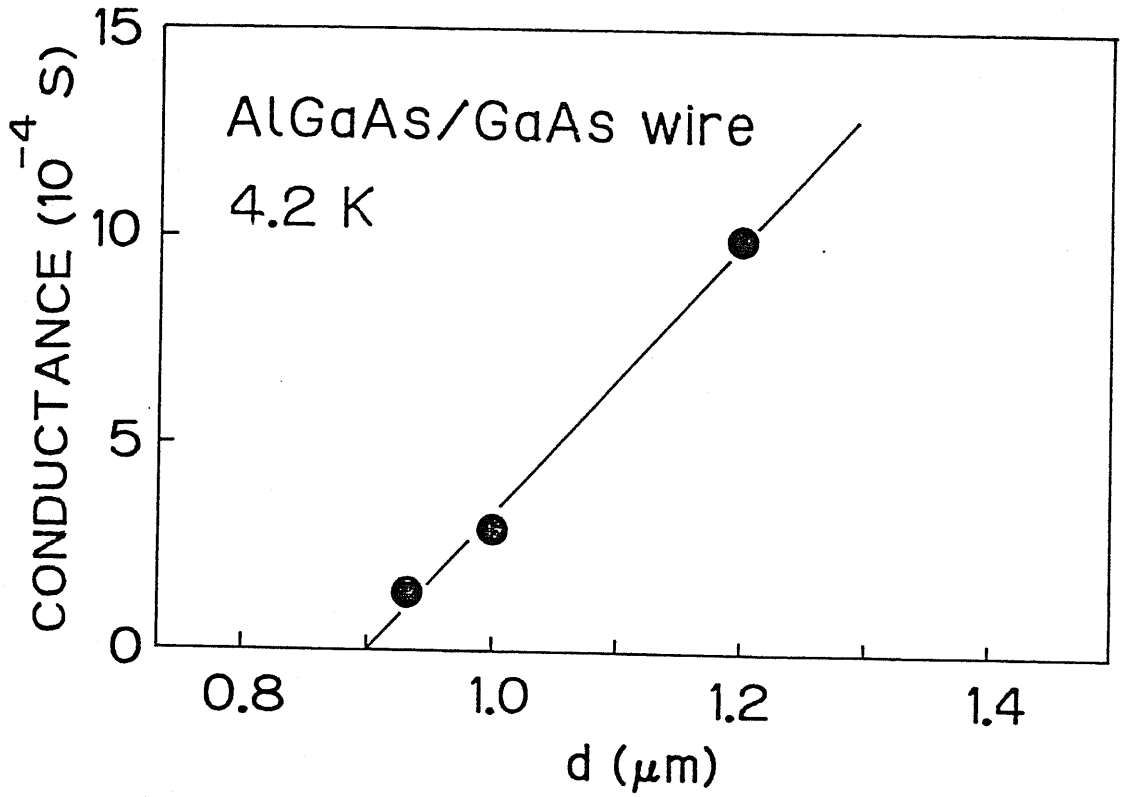

Fig. 3.5 Conductance of the three AlGaAs/GaAs wires at 4.2 K as a function of the designed gap spacing d. Conductnace becomes zero when d = d_0 = 0.9 μm. The effective width d_{eff} is given by d - d_0.

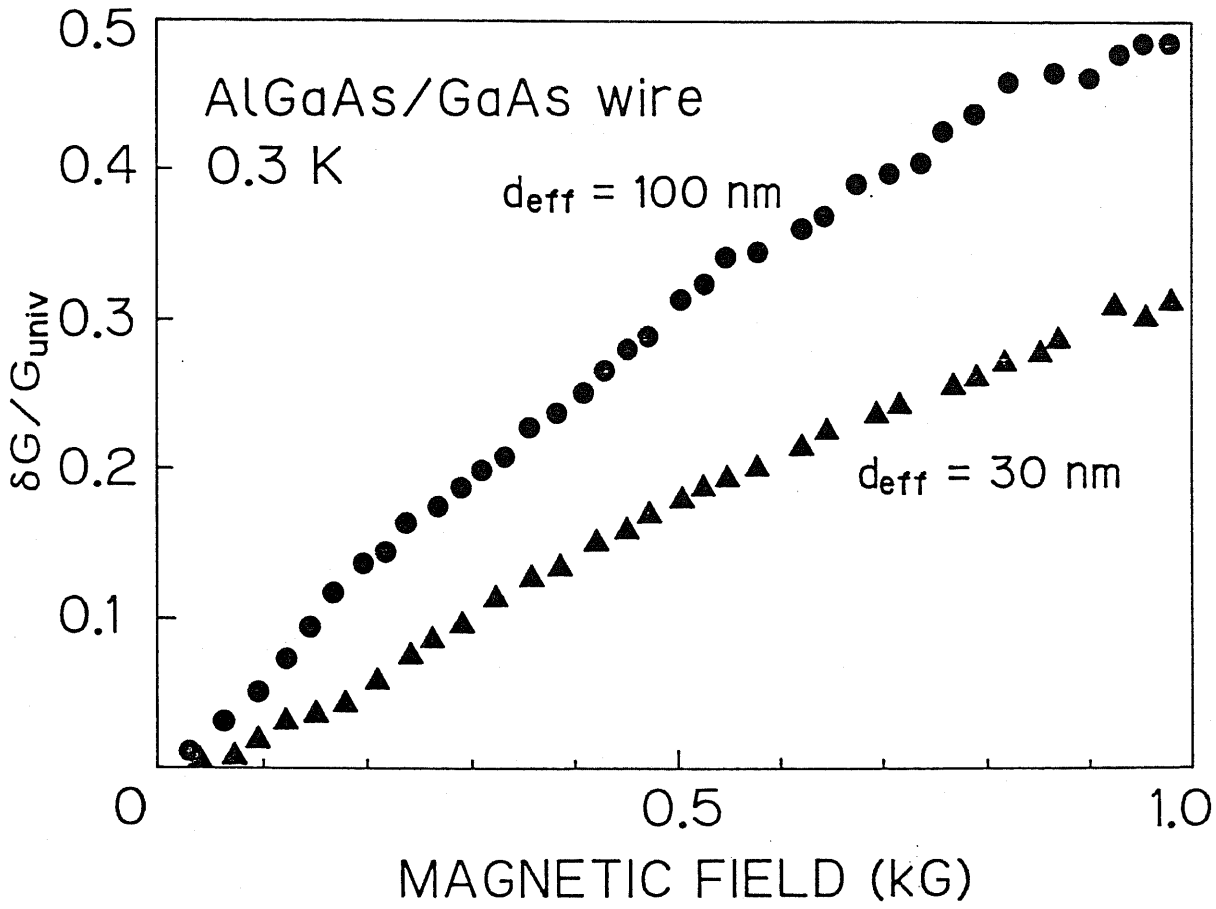

Fig. 3.6 Magnetoconductance spectra of the two AlGaAs/GaAs wires at 0.3 K. The effective widths d_{eff} are 100 nm for the wire #44 and 30 nm for #34. The conductance is normalized to $G_{univ} = e^2/h$.

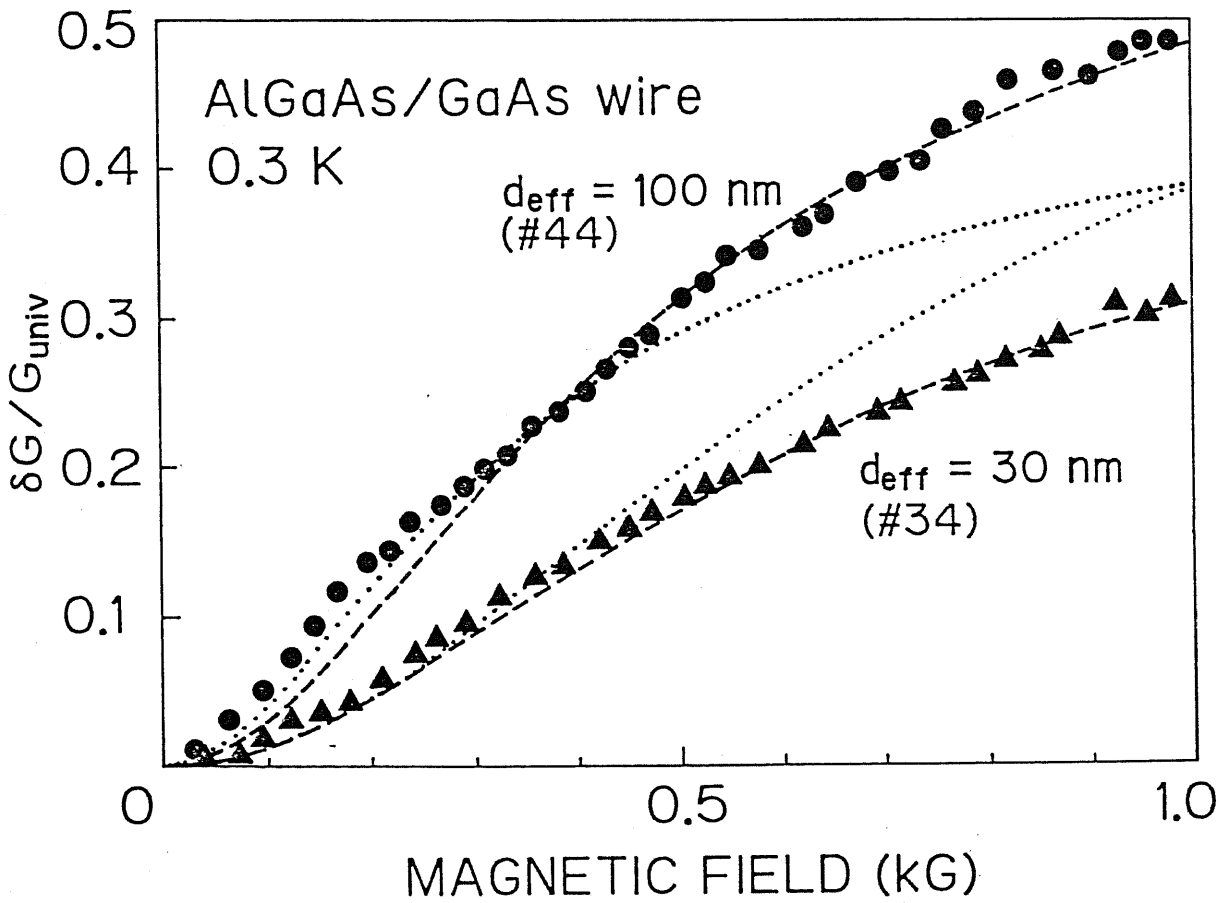

Fig. 3.7 The theoretical fittings of the AA theory (Eq. (3.4)) to the data in Fig. 3.6. The lines show the best theoretical fittings. Dotted lines: the fitting parameter is L_ϕ with $W = d_{eff}$. L_ϕ = 0.48 μm for the wire #44 (d_{eff} = 100 nm); and L_ϕ = 0.7 μm for #34 (d_{eff} = 30 nm). Broken lines: the fitting parameters are L_ϕ and W. L_ϕ =0.7 μm, W = 50 nm for the wire #44 (d_{eff} = 100 nm); and L_ϕ = 0.5 μm, W = 50 nm for #34 (d_{eff} = 30 nm).

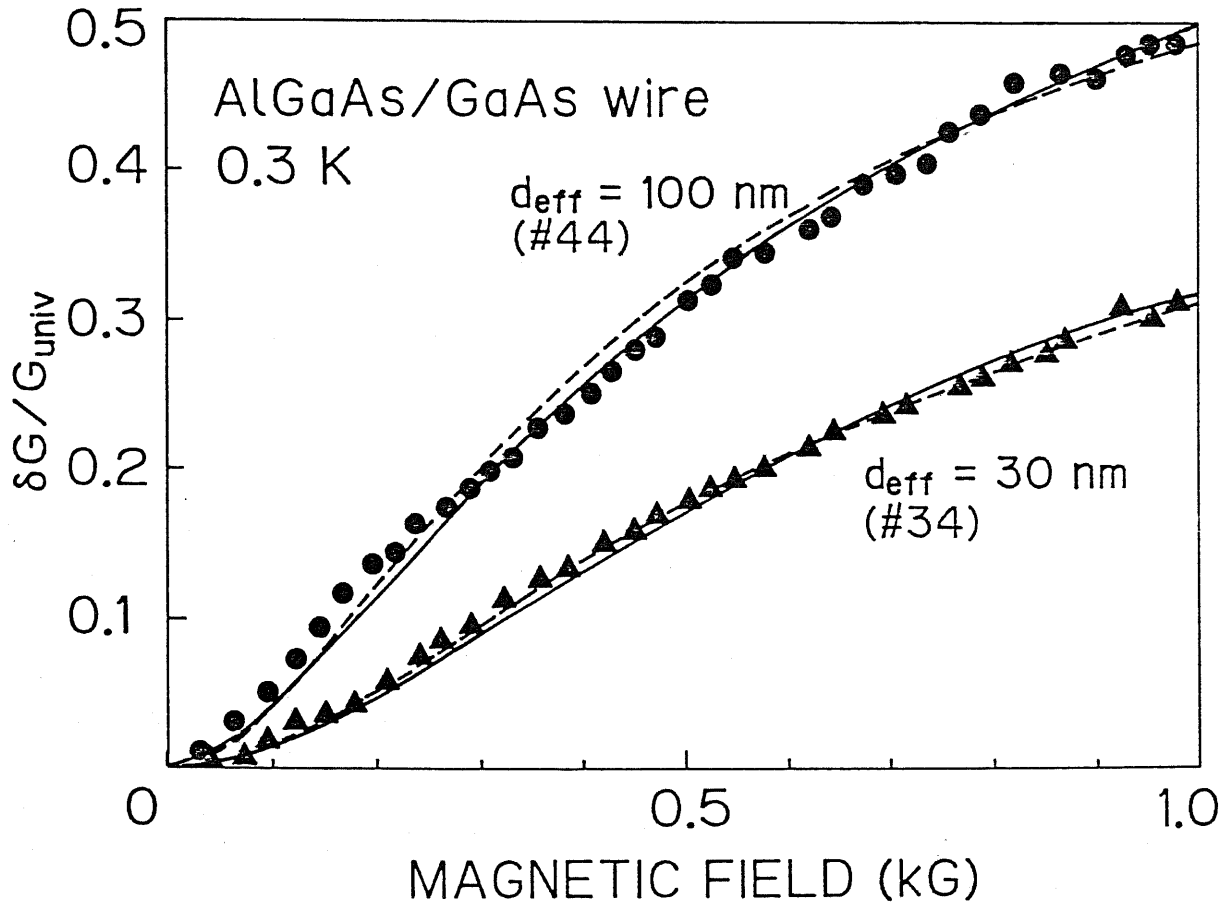

Fig. 3.8 The theoretical fittings of the BvH theory (Eq. (3.5)) to the data in Fig. 3.6. The lines show the best theoretical fittings. Broken lines for the diffusive boundary scattering; L_ϕ = 0.8 μm, W = 60 nm for the wire #44 (d_{eff} = 100 nm); and L_ϕ = 0.62 μm, W = 70 nm for #34 (d_{eff} = 30 nm). Solid lines for the BvH theory for the specular boundary scattering; L_ϕ = 1.2 μm, W = 90 nm for the wire #44 (d_{eff} = 100 nm); and L_ϕ = 0.9 μm, W = 70 nm for #34 (d_{eff} = 30 nm).

§3.4 Phase breaking mechanisms in GaAs quantum wires

The phase coherence length L_ϕ of electron waves is given by

$$L_\phi = \sqrt{D\tau_\phi}. \tag{3.8}$$

It is shown, in the previous section, that the diffusion coefficient D is strongly depends on the electron mobility and the electron density, and that longer L_ϕ can be achieved in materials with higher mobility and higher density, if τ_ϕ is assumed to be constant.

This section is focused on the phase breaking time τ_ϕ, the other parameter that determines L_ϕ. The temperature dependence[96,99] and the conductance dependence[100,101] of L_ϕ (and thus, τ_ϕ) are systematically investigated, and the phase breaking mechanisms of electron waves are discussed.

3.4.1 Theory of electron-electron scattering

The phase memory of the electron wavefunction is not broken by the elastic scattering. This fact has been confirmed by the observation of the Aharonov-Bohm oscillation in metal rings and also in the previous section. It is the inelastic scattering that breaks the phase information. If the electron is scattered inelastically, the energy of the electron is changed and thus its wavelength is varied. Therefore, the phase memory is no longer preserved.

The main inelastic scattering in condensed matters is the electron-phonon scattering at room temperature. At sufficiently low temperatures where the quantum interference effect can be observed, the electron-electron scattering is the dominant inelastic scattering.

In a clean material with no disorder, the electron-electron scattering time τ_{ee} is[102]

$$\tau_{ee}^{-1} = \frac{1}{\hbar}\frac{(kT)^2}{E_F}, \tag{3.10}$$

where k is the Boltzmann constant and E_F the Fermi energy. However, when there is disorder in the material, the inelastic electron-electron scattering is affected by the disordered potential (ex. the potential of the ionized impurity), and Eq. (3.10) is completely modified. In this case, τ_{ee} depends on the dimensionality of the system. The criterion for the dimensionality of the electron-electron scattering is the thermal diffusion length L_T, which is given by[103]

$$L_T = \left(\frac{\hbar D}{kT}\right)^{-1/2}. \tag{3.11}$$

When the width of the system is narrower than L_T, $W < L_T$, the electron-electron scattering is one-dimensional and τ_{ee} is given by[104]

$$\tau_{\phi}^{-1} = \tau_{ee}^{-1} = \frac{e^2 D}{\hbar \sigma W}\left(\frac{kT}{\hbar D}\right)^{1/2}, \tag{3.12}$$

where σ is the sheet conductivity of the system. Accordingly, L_ϕ is given by

$$L_\phi = L_{ee} \equiv \sqrt{D\tau_{ee}} = \left(\frac{\hbar\sigma W}{e^2}\right)^{1/2}\left(\frac{\hbar D}{kT}\right)^{1/4} \sim \sigma^{3/4}W^{1/2}T^{-1/4}. \qquad (kT\tau_\phi < \hbar) \quad (3.13)$$

On the other hand, Altshuler *et al.* argued the electron-electron scattering with small energy transfer, i. e., quasi-elastic scattering.[104] When the electron experiences the quasi-elastic scatterings many times, it looses its phase memory. They found that the phase relaxation time of the quasi-elastic scattering corresponds to the electron scattering time by the electromagnetic fluctuations and is equal to the Nyquist time τ_N. When τ_ϕ is longer than $\hbar/kT$, τ_N dominates over the inelastic electron-electron scattering time τ_{ee}. Then, τ_ϕ is given by[104]

$$\tau_\phi^{-1} = \tau_N^{-1} = \left(\frac{\sqrt{2D}e^2kT}{\sigma W\hbar^2}\right)^{2/3}. \qquad (kT\tau_\phi > \hbar) \quad (3.14)$$

L_ϕ is

$$L_\phi = L_N \equiv \sqrt{D\tau_N} = \left(\frac{D\sigma W\hbar^2}{\sqrt{2}e^2kT}\right)^{1/3} \sim \sigma^{2/3}W^{1/3}T^{-1/3}. \qquad (kT\tau_\phi > \hbar) \quad (3.15)$$

τ_{ee} and τ_N (i. e., L_{ee} and L_N) have different temperature dependences. The electron-electron scattering in narrow wire structures has been investigated by measuring the temperature dependence of τ_ϕ or

L_ϕ.[84-86,105-108] In fact, the existence of the electron scattering with small energy transfer has been confirmed in narrow metal wires, by the observation of the $T^{-2/3}$ dependence of τ_ϕ.[107,108] However, the electron-electron scattering in semiconductor quantum wires is still unclear. Thornton *et al.*[65] (AlGaAs/GaAs wires) and Pooke *et al.*[109] (Si MOS) observed $T^{-1/3}$ dependence of L_ϕ, while Takagaki *et al.*[110] (AlGaAs/GaAs wires) and Wheeler *et al.*[74] (Si MOS) observed $T^{-1/4}$ dependence of L_ϕ. These two dependences suggest, respectively, that τ_N and τ_{ee} are the dominant phase breaking time.

3.4.2 Temperature dependence of phase coherence length

The temperature dependence of L_ϕ is measured in the GaAs quantum wires in the wide temperature range from 0.3 K to 30 K, in order to clarify the above problems. Figure 3.9 (a) shows the temperature dependence of L_ϕ in the two AlGaAs/GaAs wires, #44 and #34, and the n-GaAs wire #16. L_ϕ increases with decreasing temperature from 30 K down to 3K. The strong temperature dependence of L_ϕ around 20 ~ 30 K is considered to be due to the electron-phonon scattering. The weak temperature dependence around 3 ~ 10 K is probably due to the electron-electron scattering. However, the temperature dependence (i. e., the slope in Fig. 3.9 (a)) is different for the three samples, and the phase breaking mechanism is not determined.

At temperatures lower than 3 K, L_ϕ becomes constant. Since the electron mobility and the electron density are constant in this temperature range, our data indicate the saturation of τ_ϕ at low temperatures. This saturation of τ_ϕ (and, therefore, of L_ϕ) is not

caused by electron heating because no change of L_ϕ was observed when the current for measuring conductance was changed from 1 to 100 nA as shown in Fig. 3.9 (b). From Eqs. (3.13) and (3.15), L_ϕ should depend on temperature as $L_\phi \sim T^{-1/3\sim-1/4}$ when τ_ϕ is governed by one-dimensional electron-electron scattering and D is constant. The temperature dependence of our data below 3 K clearly suggests that some temperature-independent phase-breaking mechanisms other than the electron-electron scattering are present at low temperatures.

Taylor *et al.* investigated the temperature dependence of τ_ϕ in n^+-GaAs wires by analyzing conductance fluctuation spectra and found that τ_ϕ contains a temperature-independent contribution, which they ascribed to a surface scattering process.[111] However, surface scatterings such as boundary scattering at AlGaAs/GaAs interface are usually elastic scattering. Although they cause a reduction in the electron mobility,[112] they are not likely to contribute to the saturation of τ_ϕ. Another possible mechanism is the spin-spin scattering. In metal wires, the saturation of τ_ϕ was attributed to this scattering by residual magnetic impurities.[85,86] In the present samples, very few magnetic impurities are present. However, such scattering might be present due to defects introduced by implantation. The mechanism of the saturation of τ_ϕ is not clear at present.

3.4.3 Conductance dependence of phase coherence length

The phase coherence length L_ϕ depends on conductivity and width, other than on temperature, as shown in Eqs. (3.13) and (3.15), if the

phase breaking time τ_ϕ is governed by τ_{ee} or τ_N. Moreover, L_{ee} and L_N have different conductivity dependences and width dependences. It is hard to investigate the width dependence of L_ϕ because of the limited number of the samples. Here, we investigate the conductance dependence of L_ϕ in gated AlGaAs/GaAs wires in order to obtain further information on the phase breaking mechanisms. The temperature is 4.2 K, where the unknown temperature-independent mechanism as described in § 3.4.2 are not dominant.

Figure 3.10 shows a schematic cross-sectional view of a gated AlGaAs/GaAs wire. The starting material was a selectively doped AlGaAs/GaAs/AlGaAs double heterostructure grown by molecular beam epitaxy (MBE). Al was evaporated onto the channel to form gate electrodes. The thickness of the Al film was 1600 Å. Then, a focused Si-ion-beam with a 0.1 μm diameter was implanted at 200 keV through the Al film into two regions as shown in Fig. 3.10. Since the projected range of Si in Al is 2430 Å, most of the implanted ions penetrate the Al film. The implanted GaAs quantum well is thus depleted by a lot of damage. A very narrow wire structure is formed between the two implanted regions as shown in the figure. The electron density in the wire can be precisely controlled by the gate voltage.

Figure 3.11 shows magnetoconductance spectra of the 220-nm wide gated AlGaAs/GaAs wire at 4.2 K with conductance as a parameter. The observed positive magnetoconductance is due to the weak localization effect. The increase in the conductance with magnetic field is larger at larger conductance. To evaluate L_ϕ and W, the

modified one-dimensional weak localization theory Eq. (3.5) was fitted to the data with L_ϕ and W as fitting parameters. It is assumed that the boundary scattering is specular. As shown by solid lines in the figure, theoretical curves with W = 220 nm are well fitted to all the magnetoconductance data, indicating that the width of the wire is almost constant in this range even when the gate voltage is applied to change the conductance.

Figure 3.12 shows L_ϕ in the gated AlGaAs/GaAs wire as a function of the conductance G of the wire. L_ϕ increases with increasing G, as expected from Eqs. (3.13) and (3.15). This result clearly shows that longer L_ϕ can be obtained in materials with higher electron density and higher electron mobility, as discussed in § 3.3. This result is very important in realizing a quantum interference devices, where long L_ϕ is necessary.

In the present case, the thermal diffusion length L_T at 4.2 K is 0.48 μm and larger than W, which confirms that the wire is one-dimensional in terms of the electron-electron scattering. In our sample, $kT\tau_\phi/\hbar$ = 2 ~ 4, which means that both L_{ee} and L_N would contribute to the phase breaking. If we assume $L_\phi \sim G^p$, we obtain p = 0.85 from Fig. 3.12. This value more favorably agrees with that of inelastic electron-electron scattering L_{ee} in Eq. (3.13) rather than that of electron scattering by small energy transfer L_N in Eq. (3.15). Since these theories are based on the theories for the dirty metals, they are insufficient to discuss the phase breaking mechanisms in the AlGaAs/GaAs quantum wires in more detail. We call for further

refinement of the theory for the electron-electron scattering in high-mobility systems.

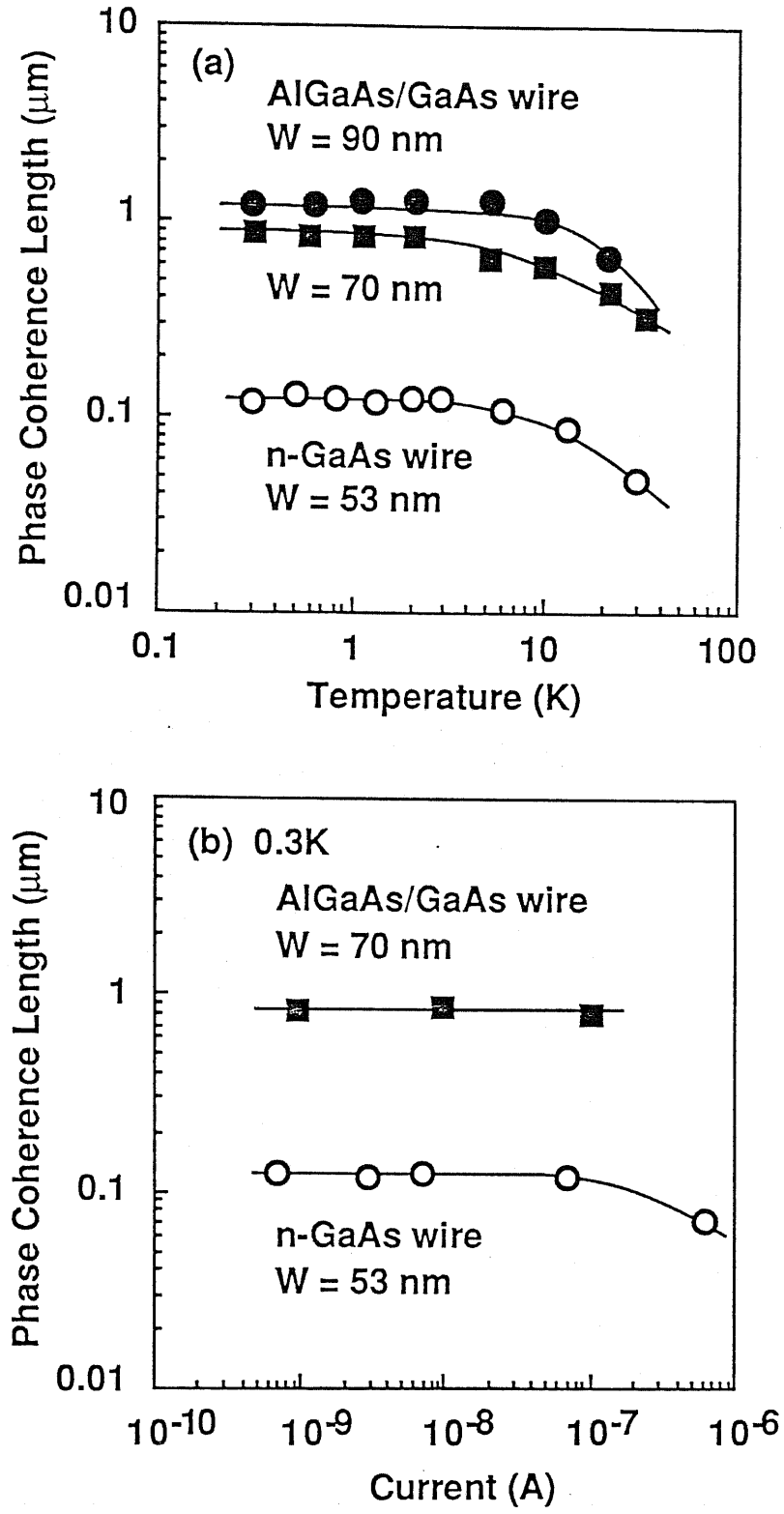

Fig. 3.9 (a) Temperature and (b) current dependence of phase coherence length L_ϕ of the two AlGaAs/GaAs wires and the n-GaAs wire.

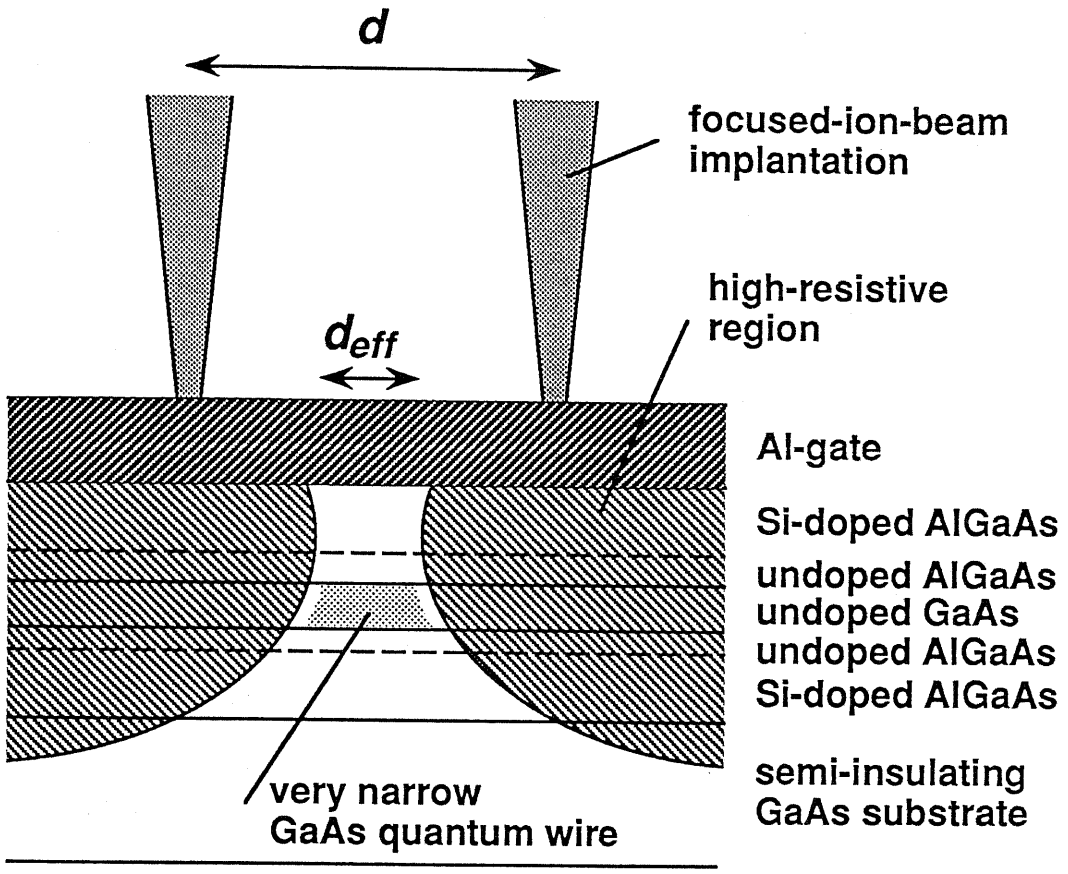

Fig. 3.10 A schematic cross-sectional view of the gated quantum wire fabricated in a selectively doped AlGaAs/GaAs/AlGaAs double heterostructure. Focused Si ions are implanted through the Al gate electrode.

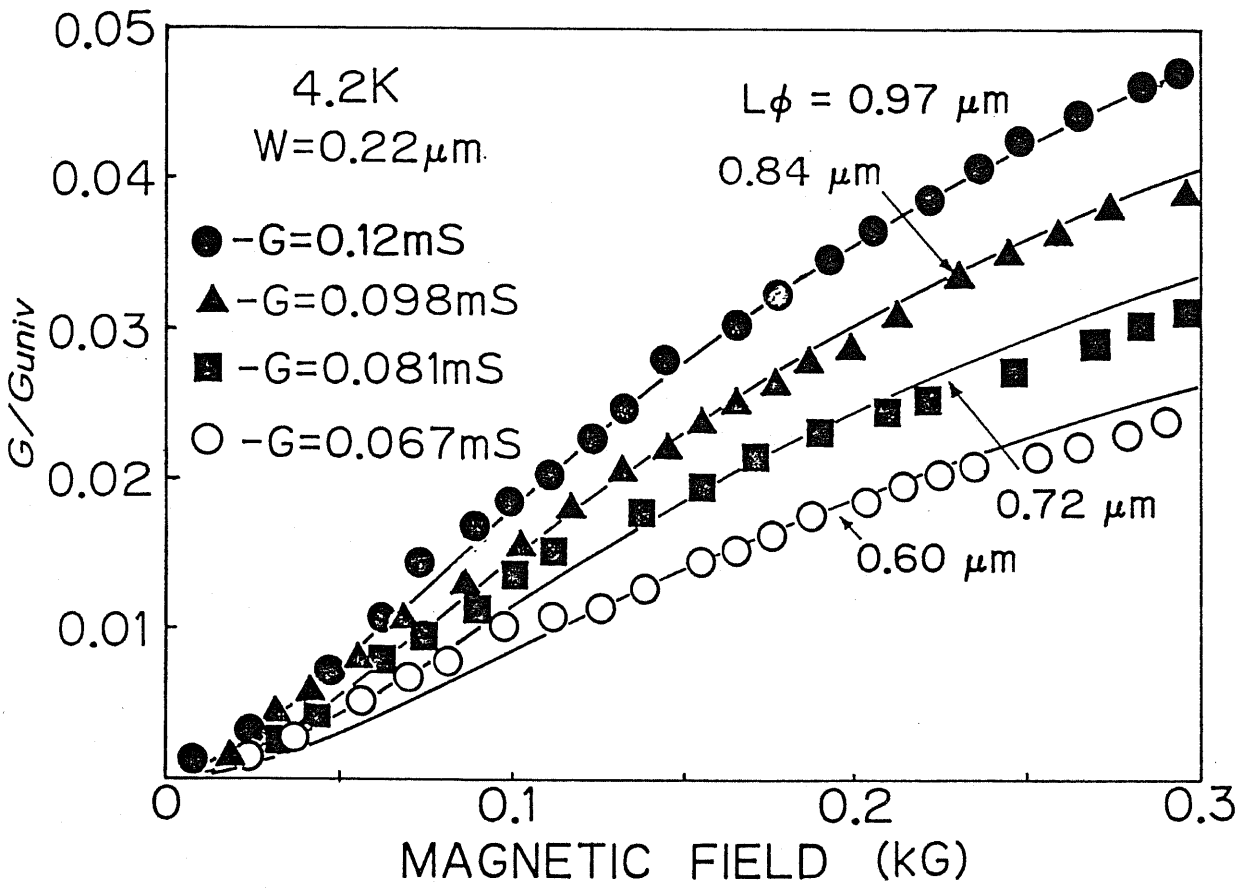

Fig. 3.11 Magnetoconductance spectra of the gated AlGaAs/GaAs wire at several conductances at 4.2 K. The width, length, electron density, and electron mobility at V_g = 0 V (G = 0.12 mS) are 220 nm, 10 μm, 5.8 $\times 10^{11}$ cm^{-2}, and 66000 cm^2/Vs, respectively. The solid lines show the theoretical fittings of the BvH theory (Eq. (3.5)), assuming that the boundary scattering is specular.

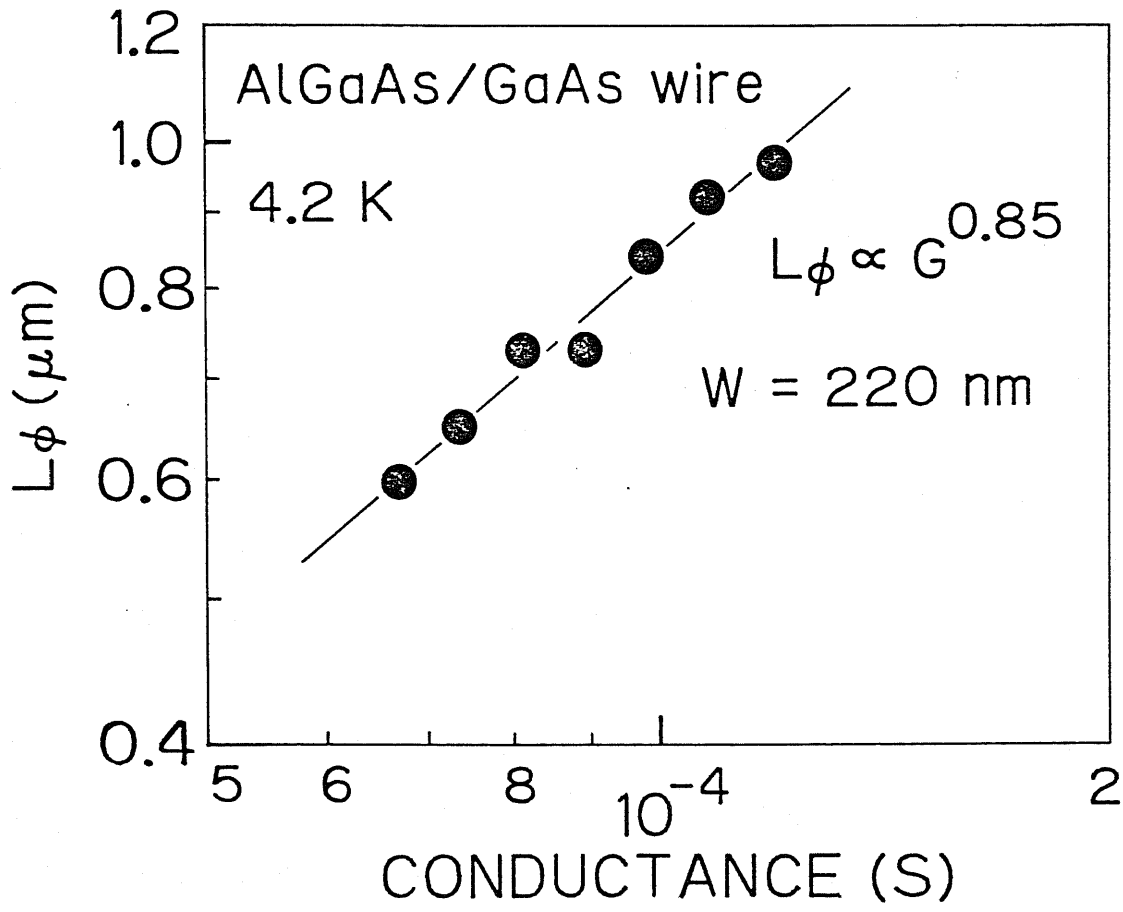

Fig. 3.12 Conductance dependence of phase coherence length in the gated AlGaAs/GaAs wire.

§3.5 Conclusions

The phase coherence length L_ϕ and the phase breaking mechanisms of electron waves are systematically studied in GaAs quantum wires, which are fabricated both in n-type GaAs and in selectively doped AlGaAs/GaAs heterostructures. The weak localization due to the quantum interference effect manifests itself in the positive magneto-conductance at low temperatures at low magnetic field.

L_ϕ in the n-GaAs wires can be estimated by fitting the one-dimensional weak localization theory to the magnetoconductance data. It is shown, however, that the theory in the dirty limit is not applicable to the AlGaAs/GaAs wires with high-mobility. The modified weak localization theory, which takes the boundary scattering and the less elastic scattering into consideration, is applied to the estimation of L_ϕ in the AlGaAs/GaAs wires.

It is found that longer L_ϕ can be achieved in materials with both higher electron mobility and higher electron density at the same time. This is demonstrated by the difference in L_ϕ in the n-GaAs wires and the selectively doped AlGaAs/GaAs wires. The AlGaAs/GaAs wire has L_ϕ of 1.2 μm; 9 times longer than the n-GaAs wire has. Moreover, L_ϕ is increased with increasing the conductance in the gated AlGaAs/GaAs wire. These results show the advantage of the selectively doped structure to obtain long L_ϕ.

L_ϕ increases with decreasing temperature but saturates below around 3 K, indicating the existence of some temperature-independent

phase-breaking mechanisms. The conductance dependence of L_ϕ, $L_\phi \sim G^{0.85}$, indicates that the main phase-breaking mechanism at 4.2 K might be the inelastic electron-electron scattering.

The value of L_ϕ, 1.2 μm, at 0.3 K is considered to be long enough to realize the quantum interference devices by the state-of-the-art technology. The selectively doped structures are the most suitable for these devices. The temperature dependence of L_ϕ shows that L_ϕ is long enough at 4.2 K and even at 10 K, suggesting that it is not necessary for the quantum interference devices to be cooled down below 4.2 K in order to maintain long L_ϕ, as long as the selectively doped AlGaAs/GaAs heterostructures are chosen as the material.

Chapter 4

Conductance Fluctuations and Correlation Energy in GaAs Quantum Wires

Abstract

Conductance fluctuations in narrow GaAs wires are studied. The conductance of the GaAs wires fluctuates randomly with the magnetic field at low temperatures. It is found that the amplitude of the conductance fluctuations in n-GaAs wires depends on the width of the wire even when the widths are narrower than the phase coherence length L_{ϕ}. This result is in disagreement with the present theory of the universal conductance fluctuations. It is shown that the conductance also fluctuates with the Fermi energy in gated AlGaAs/GaAs wires. The correlation energy E_c in GaAs wires is, for the first time, estimated experimentally to be ~1 meV, which is in agreement with the theory. It is shown that E_c corresponds to the energy scale of broadening of coherent electrons. This value of E_c is much larger than that in metals, and corresponds to a temperature of ~10 K. This result suggests that the reduction of the quantum interference effect by the energy averaging is not important in semiconductors and that the operation of the quantum interference devices at ~10 K would be possible.

§4.1 Introduction

The random conductance fluctuations as a function of magnetic field were first discovered by Umbach *et al.* in Au rings at very low temperatures below 1 K.[6] They also observed the fluctuations even in a single Au wire. The fluctuations are not noise (i. e., time-dependent changes in conductance), but are time-independent stochastic magnetoconductance patterns. The patterns vary between samples even though the samples have the identical geometry, but are reproducible at a given temperature within a given sample. This is why the patterns are often called "magnetofingerprints".

The conductance fluctuations are observed in degenerated semiconductor wires, such as narrow Si MOSFETs[113-116] and GaAs wires.[58,59,61,117-119] In Si MOSFETs, the conductance fluctuates as a function of the Fermi energy (gate voltage)[113-115] as well as of the magnetic field.

The theoretical work on the fluctuations was also developed. Stone performed a numerical simulation of the magnetoconductance of very small wires and showed sample-specific, aperiodic structures due to the non-self-averaging nature in small wires.[120] This simulation agreed with the experiments very well, and it was found that the random fluctuations were the results of the quantum interference of electron waves (the Aharonov-Bohm (AB) effect) caused by the magnetic flux piercing the wire.

The fluctuation patterns disappear smoothly as temperature is increased in a given sample. This is because the two temperature-dependent length scales become shorter than the sample size L with increasing temperature. The one length scale is the phase coherence length L_ϕ, which is discussed in Chapter 3. If $L < L_\phi$, the amplitude of the conductance fluctuations is reduced by the self-averaging effect. The other length scale is the thermal diffusion length L_T, which is given by

$$L_T = \left(\frac{\hbar D}{kT}\right)^{1/2}. \tag{4.1}$$

This length is considered to correspond roughly to the coherence length in terms of the energy broadening due to the finite temperature. L_T is related to the energy averaging effect.

At finite temperatures, the electron energy distribution has an energy broadening of the order of kT. Within some energy bandwidth, it would be expected that the electron states have spatial correlation.[121] The bandwidth is called the correlation energy E_c, and this is a very important parameter in the energy averaging effect. If $kT > E_c$, which corresponds to $L' > \pi L_T$, where L' is the smaller of L and L_ϕ, the fluctuation patterns between the uncorrelated bands are averaged (energy averaging) and the fluctuation amplitudes are reduced. Therefore, E_c gives a maximum limit to the temperature at which the quantum interference can be observed.

Since E_c in metals is very small (ex. E_c/k = 0.035 K in Au rings[121]), the AB oscillation and the conductance fluctuations in metals are observable only at low temperatures. In semiconductors, E_c is expected to be much larger than in metals. However, there are very few experimental reports on E_c in semiconductor wires. It is very important to investigate E_c in semiconductor wires in order to clarify at how high temperature the quantum interference devices can operate.

In this Chapter, conductance fluctuations and correlation energy in GaAs quantum wires are studied. The experimental results on the amplitudes of the fluctuations, the correlation field, and the correlation energy are compared with the theory of the universal conductance fluctuations.

§ 4.2 describes the conductance fluctuations in n-type GaAs quantum wires. it is shown that the amplitude of the conductance fluctuations depends on the width W of the wire even when $W < L_\phi$. This result disagrees with the existing theory.

In §4.3, conductance fluctuations in gated AlGaAs/GaAs wires as a function of not only the magnetic field but also the Fermi energy are investigated. The correlation energy E_c in the GaAs quantum wire is obtained for the first time directly from the experiment. The physical meaning of E_c is discussed. The maximum temperature at which the quantum interference devices can operate is also discussed.

§4.2 Conductance fluctuations in n-GaAs wires

This section describes the experimental results on the magneto-conductance at high magnetic field of the n-type GaAs wires.[20,21] Two types of n-GaAs wires, fabricated by the HR method and the PN method, are investigated. The fabrication processes are described in § 2.6. The amplitudes of the conductance fluctuations are compared with the theory.

4.2.1 Magnetoconductance at higher magnetic field

Figure 4.1 shows the magnetoconductance of the three wires fabricated by the HR method measured at higher magnetic field at 1.3 K. The length of the wires is 2.5 μm and the widths are 120, 53, and 20 nm. At low magnetic field less than ~0.3 T, a rapid increase in conductance is observed in all the wires. This positive magneto-conductance is due to the weak localization effect described in the previous chapter. At higher magnetic field, the conductance randomly fluctuates. These fluctuation patterns are reproducible, but change after an external stimulus such as light or heat is applied.

Figure 4.2 shows the magnetoconductance spectra of the n-GaAs wires fabricated by the PN method measured at 1.3 K. The length of the wire is 13 μm. Four spectra at different bias-voltages are shown. The width of the wire at each bias-voltage is shown in Fig. 3.2. The conductance also fluctuates randomly at all the bias-voltages. This phenomenon observed in Figs. 4.1 and 4.2 is the "universal conductance fluctuations" due to the quantum interference effect.

4.2.2 Theory of the universal conductance fluctuations

The conductance fluctuation patterns in the magnetoconductance spectra are the superposition of all the interferences in a sample. The interference is caused by an electron which passes through different paths in the fluctuated potentials due to ionized impurities. Therefore, the fluctuation patterns strongly depends on the distribution of the ionized impurities. It is considered that the external stimulus such as light or heat would change the charge distribution due to the ionized impurities, causing the changes in the fluctuation patterns. When there is no external stimulus, the patterns are reproducible and sample-specific because the configuration of the ionized impurities is invariant.

It should be noted that the sample-specific conductance fluctuations are the manifestations of the statistical fluctuations from the ensemble average of the conductance of many samples, which differ only in their microscopic impurity configuration. This understanding leads to the introduction of an ergodic hypothesis which connects the theoretical analysis and the experimental results,[19] as discussed below.

In order to estimate the amplitude of the conductance fluctuations, Lee and Stone[14], and Altshuler[13] calculated the following correlation function,

$$F(\Delta E, \Delta B) = \langle g(E, B)g(E+\Delta E, B+\Delta B)\rangle - \langle g(E, B)\rangle^2, \qquad (4.2)$$

where the angular brackets denote the ensemble averaging over the impurity configuration, g is conductance in unit of $G_{univ} = e^2/h$. Please note that

$$\begin{aligned} F(0, 0) &= \langle g(E, B)^2 \rangle - \langle g(E, B) \rangle^2 \\ &= (g(E, B) - \langle g(E, B) \rangle)^2 \\ &= (\Delta g)^2. \end{aligned} \tag{4.3}$$

This deviation is the statistical deviation. In experiment, however, it is impossible to analyze the statistical fluctuations from the ensemble average because the number of the samples is limited. It is impossible to compare the theory and the experiment. Therefore, the ergodic hypothesis is assumed:[14,19] an ensemble average at fixed E, ΔE, B, and ΔB is equivalent to an average over many values of E and B at fixed ΔE and ΔB. Thus, the calculated deviations can be directly compared with the experiment in a single sample, such as the deviation of conductance as a function of magnetic field.

A surprising conclusion was derived from this calculation: as long as the phase coherence of the electron waves remains, $F(0, 0)$ is independent of the sample size and the degree of the disorder, and is of order unity. This means that in a completely coherent sample, the amplitude of the conductance fluctuations, both with magnetic field and with the Fermi energy, is universal, namely

$$\Delta G = \frac{e^2}{h} \sqrt{F(0, 0)} \sim \frac{e^2}{h}. \tag{4.4}$$

This is called the "universal conductance fluctuations".[13,14]

When there are some inelastic scatterings and the sample size becomes shorter than the phase coherence length L_ϕ, the amplitude of the conductance fluctuations is reduced. Suppose a subunit with size of $L_\phi \times L_\phi$ and divide the sample into these subunits.[116] The phase coherence is maintained within each subunit and the fluctuation amplitude is $\sim e^2/h$ in each subunit, but the electron states in different subunits are uncorrelated. The number of the subunits is $MN = (W/L_\phi)\,(L/L_\phi)$, where W and L are the width and length of the wire, respectively. Then, the amplitude of the fluctuation is reduced by the self-averaging among the uncorrelated subunits and is given by,[116]

$$\Delta G = \frac{M}{N}\frac{1}{\sqrt{MN}}\frac{e^2}{h} = \left(\frac{W}{L_\phi}\right)^{1/2}\left(\frac{L_\phi}{L}\right)^{3/2}\frac{e^2}{h}. \qquad (W > L_\phi) \qquad (4.5)$$

When $W < L_\phi$, M equals to unity and

$$\Delta G = \left(\frac{L_\phi}{L}\right)^{3/2}\frac{e^2}{h}. \qquad (W < L_\phi) \qquad (4.6)$$

From Eq. (4.5), when $W > L_\phi$, ΔG increases with increasing W as $\Delta G \sim W^{1/2}$, but the relative conductance fluctuation $\Delta G/G_0$ is reduced as $\Delta G/G_0 \sim W^{-1/2}$. On the other hand, when $W < L_\phi$, Eq. (4.6) shows that ΔG depends only on L_ϕ and L, and is not dependent on W.

4.2.3 Amplitude of the conductance fluctuations

The three wires in Fig. 4.1 are in the regime of $W < L_\phi$. In this case, the values of L_ϕ are estimated from the weak localization theory. The amplitudes of the fluctuations predicted by Eq. (4.6) are indicated by bars in the figure. The order of magnitudes of the fluctuations is in agreement with the experimental results. However, please note that in the 120 nm-wide wire the amplitude of the fluctuations is larger than the predicted ΔG. Furthermore, the observed fluctuations become smaller as the GaAs wire becomes narrower.

It was reported by Skocpol *et al.*[116] that the measured magnitude of conductance fluctuations in Si inversion-layer nanostructures is in excellent agreement with the theoretical predictions of Eqs. (4.5) and (4.6). However, Ishibashi *et al.*[118] observed in a narrow GaAs wire with mesa width of 0.3 μm the fluctuations larger than the prediction from Eq. (4.5) in which L_ϕ deduced from the weak localization effect was adopted. Thornton *et al.*[122] also observed very large fluctuations and derived a long L_ϕ (2 μm at 0.35 K) from Eq. (4.6) in a narrow GaAs/AlGaAs channel with width of ~0.2 μm, while they obtained[65] much shorter L_ϕ (~0.22 μm at 0.41 K) from the one-dimensional localization experiments on a similar sample.

On the other hand, our data show that the amplitude of the fluctuations is dependent on the width of the wires even when the width W is narrower than L_ϕ: in wide wires ($W \sim L_\phi$) the amplitude is larger than the predicted value $(L_\phi/L)^{3/2}$ (e^2/h), while in very narrow wires ($W << L_\phi$) the amplitude becomes smaller than the prediction.

This result clearly disagrees with Eq. (4.6) which shows no width dependence of the fluctuation amplitude.

It has been recently understood that the universality of the amplitude of the conductance fluctuations does not hold when the distance between the voltage probes is less than L_ϕ.[123-125] This results from the nonlocality of the electron wavefunction:[124-126] the electron waves can propagate into voltage probes up to a distance of L_ϕ. In our samples, however, the length L (2.5 μm) is much smaller than L_ϕ, and the samples are in the regime where the theory of the universal conductance fluctuations should apply. This unsolved problem calls for further study.

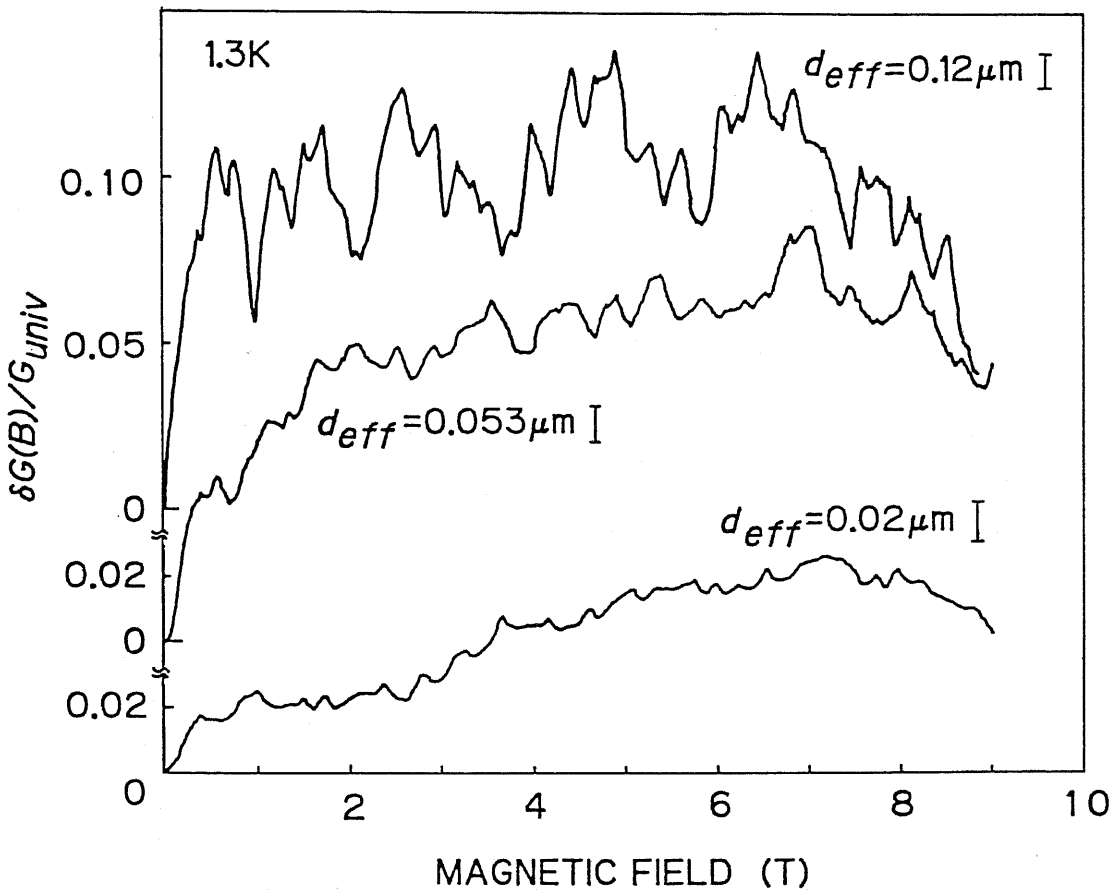

Fig. 4.1 Magnetoconductance spectra of the three n-GaAs wires fabricated by the HR method measured at high magnetic field at 1.3K. The conductance randomly fluctuates. The bars indicate the amplitudes of the conductance fluctuations predicted by Eq. (4.6).

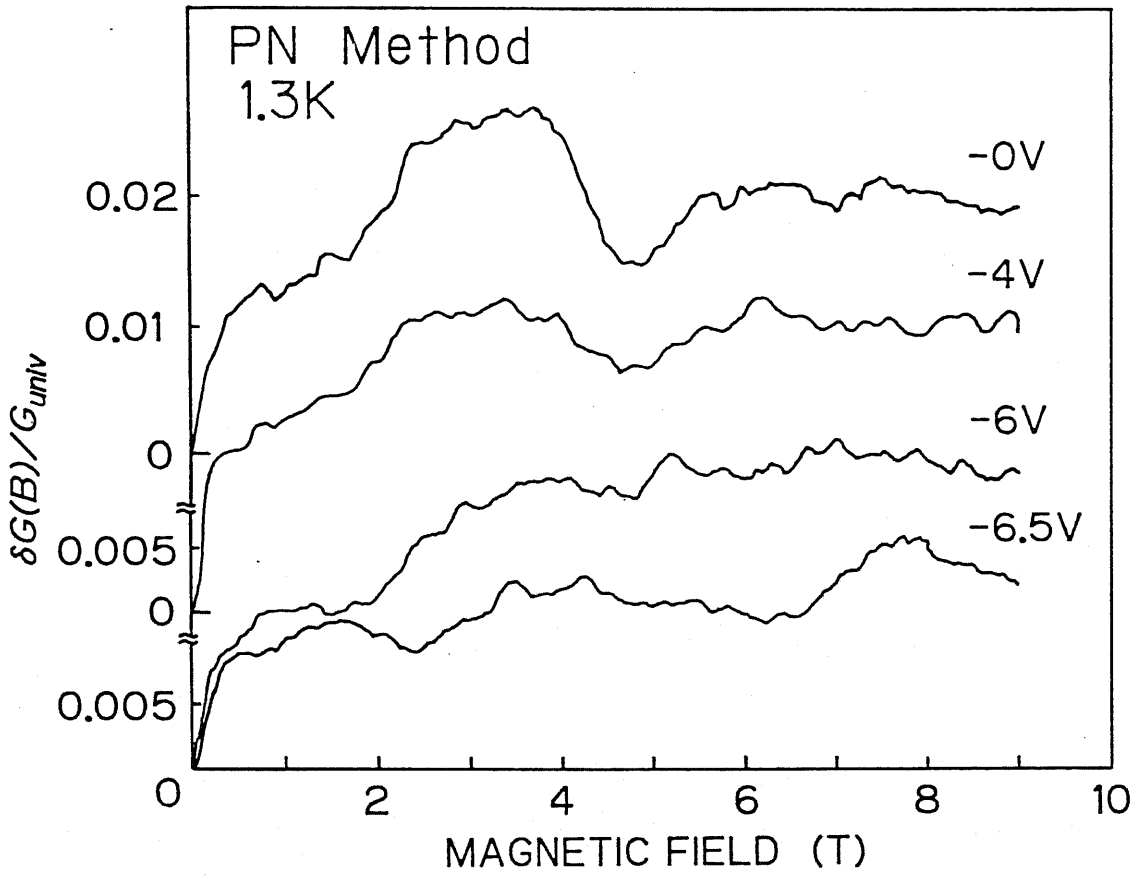

Fig. 4.2 Magnetoconductance spectra of the n-GaAs wires fabricated by the PN method measured at high magnetic field at 1.3K. The spectra at various bias-voltages are shown.

§4.3 Conductance fluctuations in gated AlGaAs/GaAs wires

The Fermi energy E_F should be changed precisely to obtain the correlation energy E_c experimentally. For this purpose, AlGaAs/GaAs quantum wires with gate electrodes are fabricated by the focused-ion-beam implantation and their conductances are measured at low temperatures as functions of both magnetic field and gate voltage.[100] The fabrication process of the wires is described in § 3.4.3. The experimental values of the correlation field B_c and the correlation energy E_c are compared with the theory of the universal conductance fluctuations.

4.3.1 Conductance fluctuations in AlGaAs/GaAs wires

Figures 4.3 and 4.4 show magnetoconductance spectra of two gated AlGaAs/GaAs wires (#12 and #22) with different widths measured at 0.3 K. The length of the wires is 10 μm. The width W and L_ϕ at 4.2 K at zero-bias are estimated, by fitting the modified theory of the one-dimensional weak localization to the magnetoconductance data ($B <$ 100 G), to be W = 400 nm, L_ϕ = 680 nm for the wire #12; and W = 350 nm, L_ϕ = 350 nm for the wire #22. The magnetoconductance spectra at various gate voltages are shown. Random oscillation patterns due to the conductance fluctuations are observed in all the spectra. The average period of the random oscillations is apparently shorter in the wire #12 (W = 400 nm) than in #22 (W = 350 nm). This is caused by the difference in the correlation field B_c in two wires.

4.3.2 Correlation field in AlGaAs/GaAs quantum wires

The correlation field B_c is defined as a half-width of the correlation function Eq. (4.2) with respect to B, and corresponds to the typical spacing of the observed fluctuations in B.

B_c is roughly estimated as follows.[116,127] The fluctuation is caused by the interference of an electron which travels in different paths and recombines, making a loop. The size of the loop (i. e., the coherent subunit) is limited by the sample size. If the sample is larger than L_ϕ, the loop size is limited by L_ϕ, because an electron loses the phase memory and cannot interfere in loops larger than L_ϕ. Therefore, the area S of the loop is given by

$$S = \min(L, L_\phi) \times \min(W, L_\phi), \tag{4.7}$$

where min (A, B) represents the smaller of A and B. When the magnetic flux through the loop is h/e, the phase shift of the electron with different paths becomes 2π. Therefore, the expected period of fluctuations B_c is given by

$$B_c = \frac{h/e}{S} = \frac{h/e}{\min(L, L_\phi) \times \min(W, L_\phi)}. \tag{4.8}$$

The estimated values of B_c from Eq. (4.8) are 150 G for the wire #12 (W = 400 nm) and 340 G for #22 (W = 350 nm), which are indicated by bars in Figs. 4.3 and 4.4, respectively. They are in good agreement with the experiment as shown in the figures.

4.3.3 Conductance fluctuations with the Fermi energy

The conductance fluctuation patterns at several gate voltages (and thereby at several Fermi energies) are shown in Figs. 4.3 and 4.4. It is very interesting to see how the fluctuation patterns change with the gate voltage. In the wire #12 (in Fig.4.3), the pattern completely changes when the gate voltage V_g is changed from 0 to -20 mV. However, please note that the pattern hardly changes even when V_g changes from -20 to -22 mV. When V_g is changed to -24,-26, -28, and so on, the pattern does not change suddenly but gradually, and finally at V_g = -36 mV the pattern is quite different from that at V_g= -20 mV.

This behavior is clear in Fig. 4.5 which shows the conductance of the wire #12 (W = 400 nm) as a function of the gate voltage at 0.3 K. The derivative of the conductance is also shown. The conductance also fluctuates randomly with the gate voltage, that is, with the Fermi energy E_F. The average period of the oscillations is about 20 mV, which corresponds to the change in the Fermi energy ΔE_F of about 1 meV.

4.3.4 Correlation energy in gated AlGaAs/GaAs wires

In the theory of the universal conductance fluctuations, the correlation energy E_c is also defined as the half-width of $F(\Delta E, 0)$. Within a bandwidth E_c, the electron states are spatially correlated and all the electrons contribute to the same random pattern of the fluctuations. If the change of the Fermi energy ΔE_F is less than E_c, the fluctuation pattern does not change. However, if ΔE_F exceeds E_c,

the pattern changes, but its amplitude is the same. This means that E_c corresponds to the typical scale of the spacing between the conductance fluctuations in E_F. Therefore, the average period in Fig. 4.5 gives the experimental value of E_c; E_c = 1 meV. This is the first experimental determination of E_c in GaAs quantum wires.

E_c, the half-width of $F(\Delta E, 0)$, is given by[14,19]

$$E_c = \frac{\pi^2 \hbar D}{L'^2}, \tag{4.9a}$$

where L' is the sample size, but when the size is larger than L_ϕ, L' corresponds to L_ϕ. Thus, E_c is

$$E_c = \frac{\pi^2 \hbar D}{(\min(L, L_\phi))^2}. \tag{4.9b}$$

The theoretical value of E_c derived from Eq. (4.9b) is 0.6 meV. This value is in good agreement with the experiment.

It should be noted that Eq. (4.9a) can be re-written as

$$E_c = \frac{\pi^2 \hbar}{t_p} \sim \frac{h}{t_p}, \tag{4.10}$$

where t_p ($= L'^2/D$) is the time it takes for an electron to travel across the length L' by diffusion, where L' is the smaller of the sample size L and L_ϕ. This means that

$$t_p = \min(\tau_\phi, L^2/D) \tag{4.11}$$

and t_p is the life time of the coherent electron in the sample. Therefore, E_c is considered to correspond to the energy broadening of the coherent electrons (i. e. correlated electrons) from the uncertainty principle. If ΔE_F is smaller than E_c, this change is within the energy broadening and no change in conductance will take place. When ΔE_F is larger than E_c, the correlated electron states feel the change of the energy and the conductance changes.

Licini *et al.* reported the experiment similar to the experiment discussed in § 4.3.3 by tuning the gate voltage of a narrow Si MOSFET,[113] in which the fluctuation pattern with respect to the magnetic field was invariant under small changes in E_F, but changed rather sharply once $\Delta E_F > E_c$, and, then, it remained fairly constant again until $\Delta E_F > 2E_c$ and another change was observed.[121] Washburn and Webb insisted that this was a clear demonstration of existence of neighboring bands of internally correlated levels.[121] In our data, however, the pattern changes gradually with the Fermi energy, suggesting that E_c is not the well defined energy band but rather the energy scale of broadening in the quantum interference phenomena, as discussed above.

4.3.5 Energy averaging in semiconductor quantum wires

Here, we compare two energy scales of broadenings: the energy broadening E_c of the uncorrelated electron states and the energy broadening kT by the finite temperature. When $kT < E_c$, all the

electrons are correlated and the fundamental fluctuation pattern only contributes to the conductance. When $kT > E_c$, however, the all the electrons are not correlated and several fluctuation patterns contribute to the conductance. Thus, the amplitude of the observed fluctuation is reduced by the energy averaging. The number of the uncorrelated patterns[121] is simply given by $N = kT/E_c$ and the fluctuation amplitude is proportional to $N^{-1/2} \sim T^{-1/2}$, which was actually observed in a Au ring.[128]

Therefore, E_c puts the upper limit to the temperature at which the conductance fluctuations and the AB oscillation can be clearly observed. The value of E_c in our samples derived from the conductance fluctuations with E_F at 0.3 K is about 1 meV, which corresponds to a temperature of ~10 K. Although the value of E_c depends on temperature because D and L_ϕ in Eq. (4.9) have the temperature dependences, the changes in D and L_ϕ below 10 K are very small and thus the temperature dependence of E_c would be small. This means that the energy averaging in the GaAs quantum wires is not remarkable below 10 K.

To clarify in more detail whether or not the energy averaging effect causes the reduction of the fluctuation amplitude, we compare the temperature dependences of L_ϕ and πL_T in other samples. In the wires #44 and #34, for example, πL_T at 10 K is 0.77 μm and 0.64 μm, respectively. These values mean that at $T < 10$ K, πL_T is always larger than L_ϕ (see Fig. 3.9), because L_T has $T^{-1/2}$ dependence. From this relation and from Eqs. (4.1) and (4.9) (note that $L_\phi < L$ in our samples), we derive $kT < E_c$ at $T < 10$ K. This also shows that the

energy averaging effect is not remarkable below 10 K in the wires #44 and #34. At $T > 10$ K, $L_\phi \sim L_T$, and both the energy averaging and the self-averaging will take place at the same time.

In metals, E_c is very small. For example, the value of E_c in the Au ring is only 0.003 meV, which corresponds to 0.035 K.[121] This is because D in metals is much smaller than in semiconductors though L_ϕ in metals is comparable to that in semiconductors. Therefore, semiconductors are suitable materials for the observation of the quantum interference effect at finite temperatures owing to the large diffusion coefficient.

These results shows that in semiconductors at finite temperatures, the the reduction of the quantum interference is mainly caused by the self-averaging. The energy averaging is less important at low temperatures than the self averaging. It can be said again that the maximum size of the quantum interference is determined by L_ϕ. Even at temperatures higher than 4.2 K, the device will operate as long as the size is less than L_ϕ.

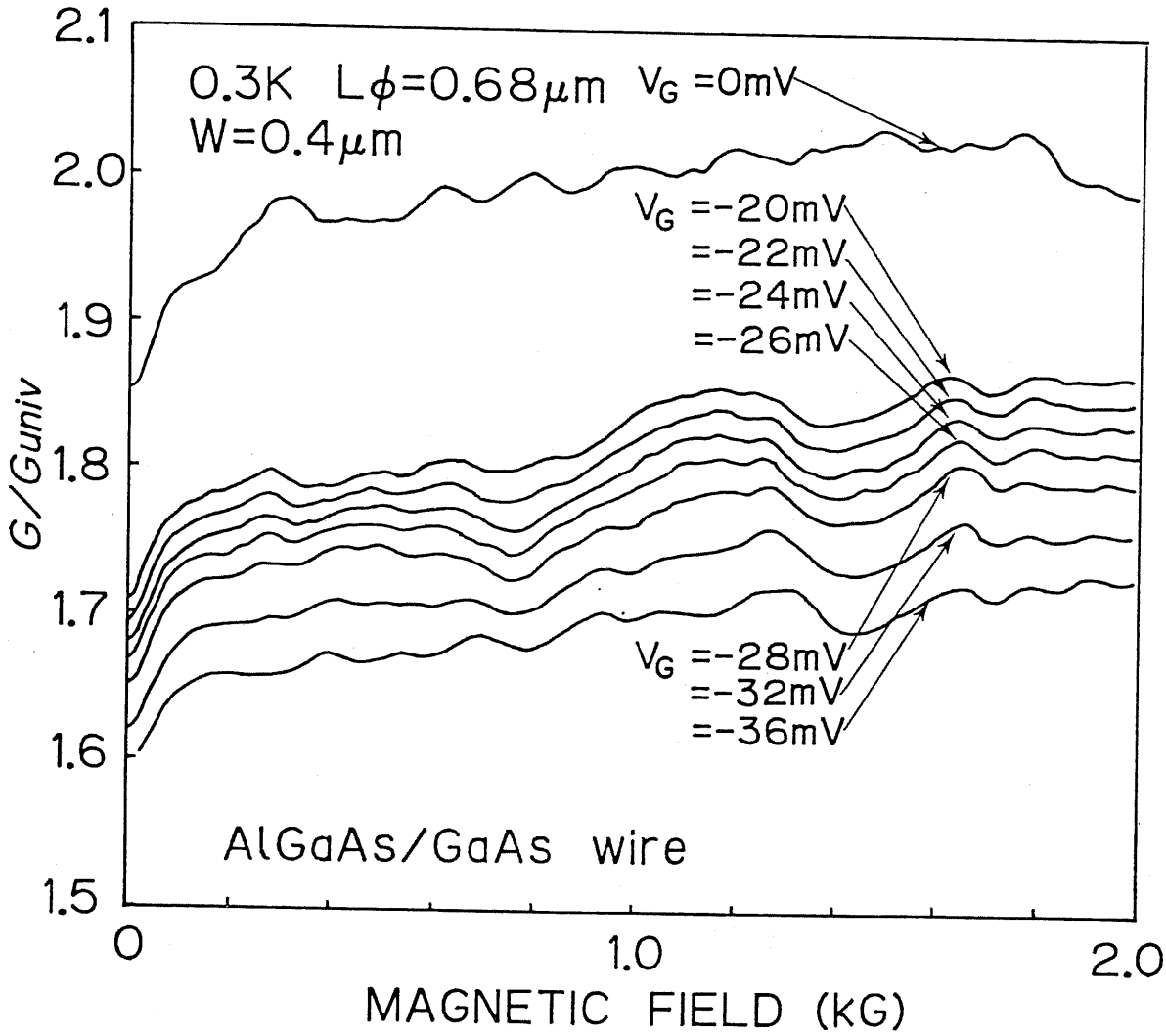

Fig. 4.3 Magnetoconductance spectra of the gated AlGaAs/GaAs wires #12 at 0.3 K. L_ϕ = 680 nm and W = 400 nm at V_g = 0 V. The gate voltage dependence of the magnetoconductance spectra is also shown. The bar indicated the correlation field B_c estimated from Eq. (4.8).

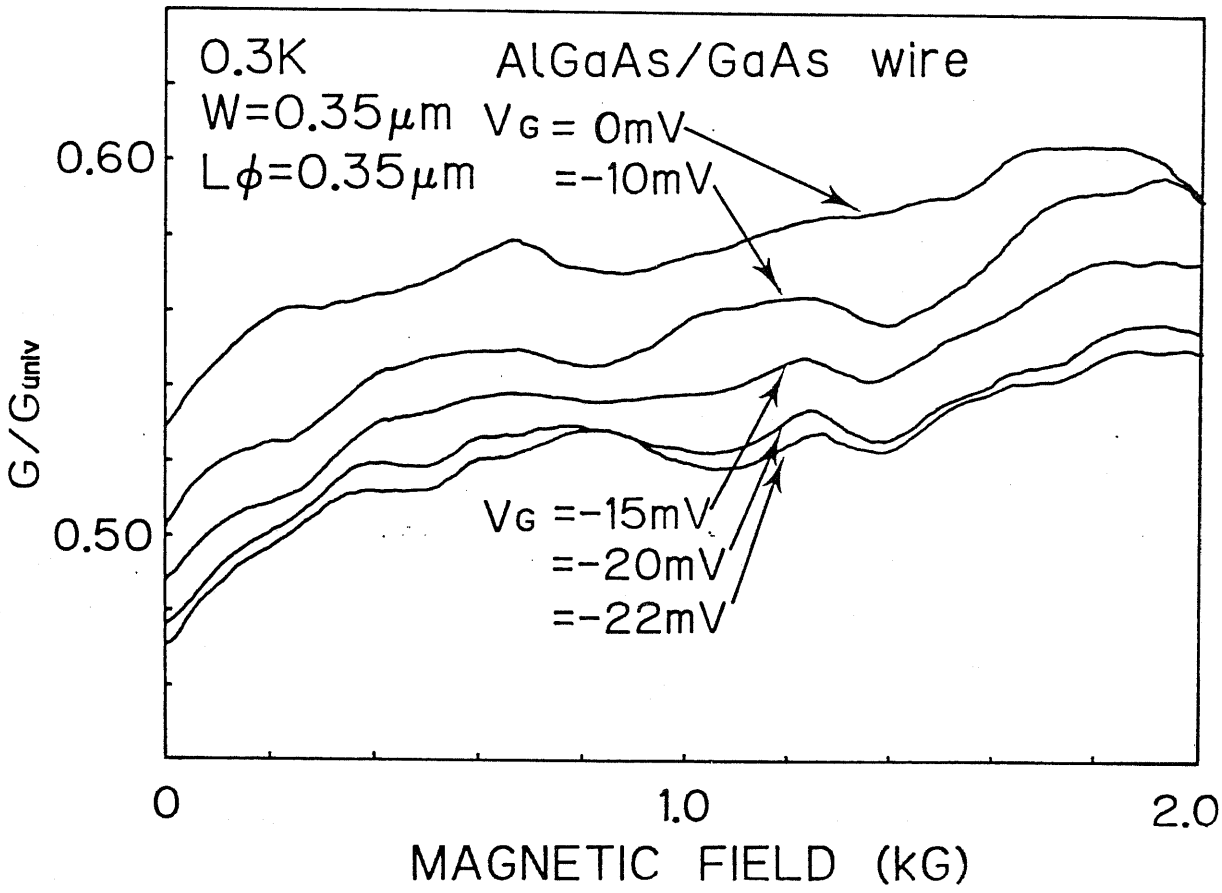

Fig. 4.4 Magnetoconductance spectra of the gated AlGaAs/GaAs wires #22 at 0.3 K. L_ϕ = 350 nm and W = 350 nm at V_g = 0 V. The spectra at various bias-voltages are shown. The bar indicated the correlation field B_c estimated from Eq. (4.8).

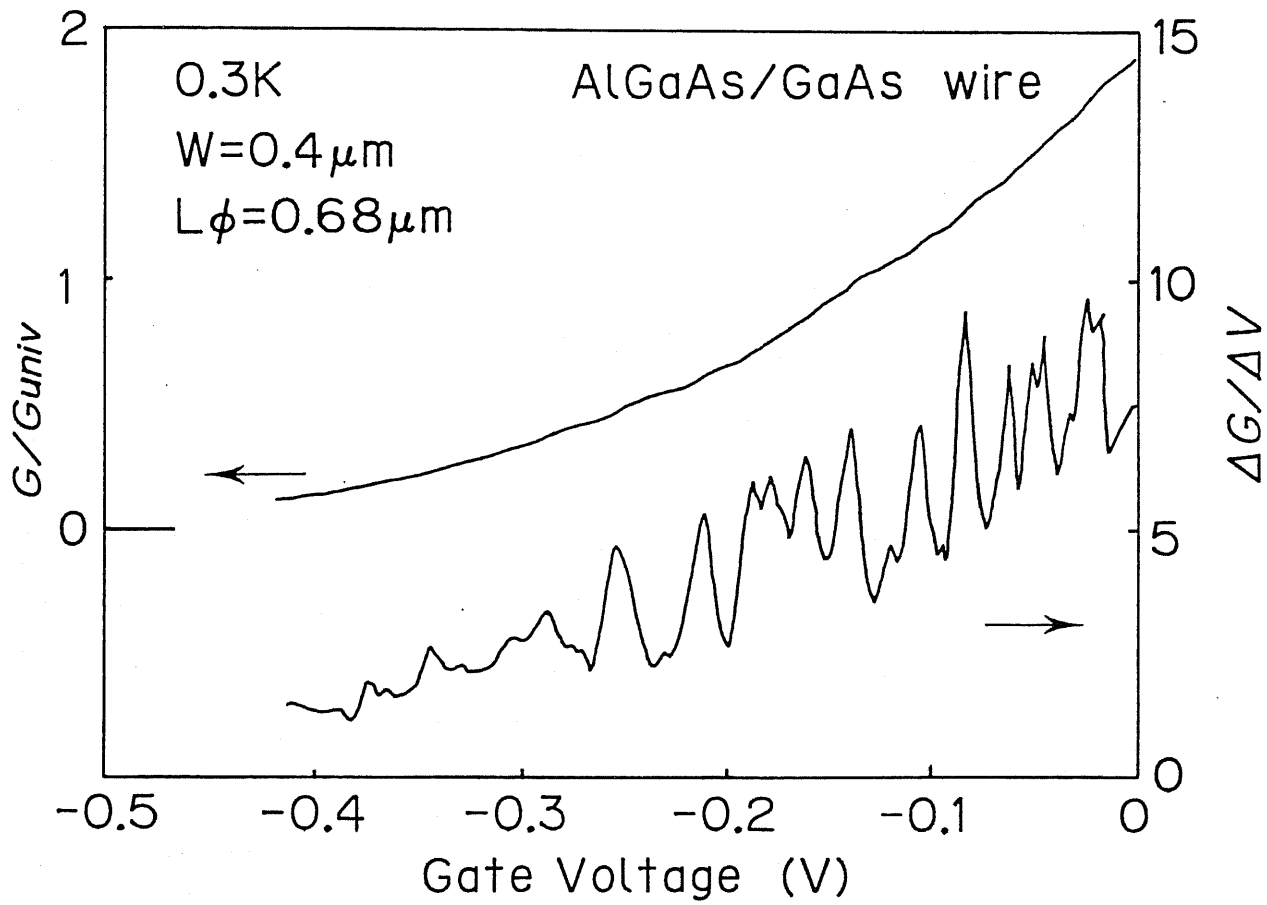

Fig. 4.5 Conductance of the wire #12 at 0.3 K as a function of the gate voltage. The derivative of conductance with respect to the gate voltage is also shown. L_ϕ = 680 nm and W = 400 nm at V_g = 0 V.

§4.4 Conclusions

Conductance fluctuations in narrow GaAs quantum wires are studied. The amplitude of the conductance fluctuations, the correlation magnetic field, and the correlation energy are investigated in n-GaAs wires and gated AlGaAs/GaAs wires.

The conductance of the n-GaAs wires fluctuates randomly with the magnetic field at low temperatures. It is found that the amplitude of the conductance fluctuations in the n-GaAs wires depends on the width of the wire even when the widths are narrower than the phase coherence length L_ϕ. This result is in disagreement with the present theory of the universal conductance fluctuations.

It is shown that in gated AlGaAs/GaAs wires the conductance fluctuates as a function of the Fermi energy as well as of the magnetic field. The experimental and theoretical values of the correlation field B_c are compared. They are in good agreement.

The correlation energy E_c is, for the first time, determined in GaAs wires from the average period of the conductance fluctuation with the Fermi energy. The value of E_c is ~1 meV, which is in agreement with the theory. It is shown that E_c corresponds to the energy broadening of coherent electrons. This value of E_c is much larger than that in metals, and corresponds to a temperature of ~10 K. This result suggests that the reduction of the quantum interference effect by the energy averaging is not important in semiconductors, and

demonstrates that the semiconductors have advantage over metals in terms of the device applications at temperatures higher than 4.2 K.

Chapter 5

GaAs Quantum Wire Transistors

Abstract

Very narrow AlGaAs/GaAs quantum wire transistors with gate length of 10 μm are fabricated by the focused-ion-beam-implantation and their characteristics are investigated as a function of gate voltage V_g at various drain voltages V_{ds} and temperatures T. When the width W of the wire transistor is wide, only the universal conductance fluctuation effect with V_g is observed in the channel conductance g_d. In narrower transistors (W < 350 nm), however, two anomalous behaviors are observed in g_d at low temperatures. One is the anomalous increase of transconductance (i. e., the sharp increase in g_d) at V_g just above the threshold voltage V_{th} and the shift of V_{th} with V_{ds}. This anomaly lasts up to 30 K and $V_{ds} \leq 10$ meV. The other is the anomalous oscillation of the ac channel conductance as a function of V_g observed only at T < 1.3 K and V_{ds} < 1 mV. The negative transconductance is observed due to this oscillation. The origins of these anomalous behaviors are discussed in terms of the strong localization of electron states.

§ 5.1 Introduction

The quantum interference in AlGaAs/GaAs quantum wires has been of great interest in the fields of semiconductor physics and technology. Several quantum interference devices have been proposed.[15-17] Most of them utilize the (electric) field effects, such as the electric-field Aharonov-Bohm effect. However, the electric-field AB effect[129] has not been observed in semiconductors, although the AB effect as a function of magnetic field has been observed in various GaAs rings.[130-133] Moreover, the field-effect on the electron transport in very narrow GaAs quantum wires, especially in the strongly localized regime, is not understood.

In this Chapter, the characteristics of narrow AlGaAs/GaAs quantum wire transistors are investigated at low temperatures. It is shown that the potential fluctuations in the channel, which cause the strong localization of electron wavefunctions, affect the device characteristics, resulting in anomalous behaviors in the channel conductance at low temperatures.

In § 5.2, the fabrication process and the structure of the AlGaAs/GaAs quantum wire transistor are described.

In § 5.3, the channel conductance and transconductance of the AlGaAs/GaAs quantum wire transistors are measured as functions of gate voltage, drain voltage, and temperature. The origins of two anomalous behaviors in the channel conductance, which are observed only at low temperatures and at low drain voltages, are discussed.

§ 5.2 Fabrication of AlGaAs/GaAs quantum wire transistors

Figure 5.1 shows the schematic top view of the AlGaAs/GaAs quantum wire transistor. The starting material was a selectively doped AlGaAs/GaAs/AlGaAs double heterostructure grown by molecular beam epitaxy (MBE). The electron density and mobility of the two-dimensional (2D) electron gas at 77 K are 6×10^{11} cm^{-2} and 26000 cm^2/Vs, respectively. A wide channel with a width of 20 μm was defined by a mesa etch. Al was evaporated on the channel to form a gate electrode. Then, focused Si-ion-beam was implanted through Al films to form two high-resistive regions and to confine the wide channel into very narrow one. This structure acts as a GaAs quantum wire transistor. Each transistor has only a single narrow channel.

Four wire transistors (#11, #12, #22, and #36) were fabricated. The widths W of the channel at zero-bias are estimated by the fitting the modified theory of the one-dimensional localization (Eq. (3.5)) to the experimental magnetoconductance data at 1.3 K, assuming that the boundary scattering is specular. The derived widths are 500, 400, 350, and 150 nm, respectively. The length of the narrow channel is 10 μm. The samples #12 and #22 in § 4.3 and in this Chapter are the identical samples.

As shown in Fig. 5.1, this structure has five electrodes; two current terminals, two voltage probes, and a gate electrode. To avoid the confusion and compare to a normal field effect transistor, the voltage drop between the two voltage probes is denoted by drain-source

voltage V_{ds}, the channel current by drain current I_d, and the dc channel conductance by drain conductance g_d (= I_d/V_{ds}). The trans-conductance g_m is defined similarly:

$$g_m = \frac{\partial I_d}{\partial V_g}\Big|_{V_{ds} = \text{const}}, \tag{5.1}$$

where V_g is the gate voltage. The gate length of the transistor is 10 μm.

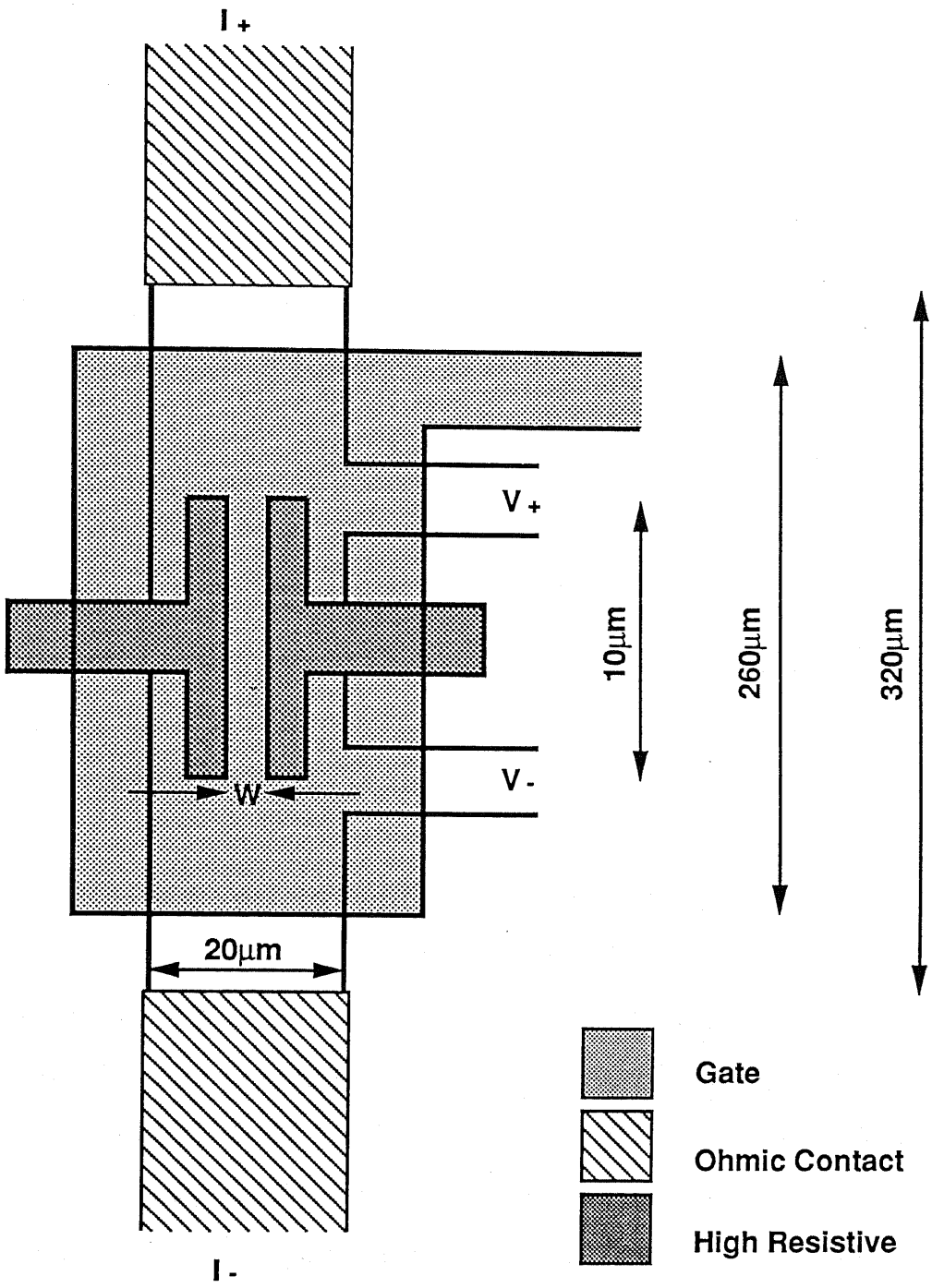

Fig. 5.1 A schematic top view of an AlGaAs/GaAs quantum wire transistor. The length of the narrow channel is 10 μm.

§5.3 Anomalous characteristics in AlGaAs/GaAs wire transistors

In this section, the characteristics of the fabricated GaAs quantum wire transistors are investigated. The channel conductance is precisely determined both by dc measurement at constant V_{ds} (denoted by g_d) and by ac measurement at constant I_d (denoted by G). The transconductance g_m is measured by applying small ac voltage (~10 mV) to the gate electrodes.

5.3.1 I-V characteristics

Figure 5.2 shows the I-V characteristics of the transistor #22 at 4.2 K. The transistor operation in the depletion mode is confirmed.

5.3.2 Anomalous increase in transconductance

Figures 5.3 (a) and (b) show the channel conductance g_d and transconductance g_m of the transistor #22 as a function of the gate voltage V_g at 4.2 K at several drain voltages. g_d decreases with decreasing V_g, but the slope of the g_d-V_g curve suddenly changes at V_g just above the threshold voltage V_{th} (i. e., g_d suddenly drops to zero) for only small V_{ds} (< 7 mV). This causes anomalous increase in g_m just above V_{th} for small V_{ds}, as shown in Fig. 5.3 (b). The resultant high peak in g_m becomes more pronounced as V_{ds} decreases. Moreover, V_{th} shifts from -0.3 to -0.24 V as V_{ds} decreases. This anomalous behavior is not observed in the transistor #12 (W = 400 nm), but only in narrower transistors, #22 and #36 (W = 350 and 150 nm).

Figure 5.4 shows g_m in #36 at various temperatures. Anomalously high g_m just above V_{th} is reduced smoothly with increasing temperature. It can be observed at up to 30 K.

5.3.3 Anomalous oscillation in channel conductance

In Figs. 5.3 (b) and 5.4, small oscillations in g_m are observed for sufficiently larger V_g than V_{th}. These oscillations become anomalously large when temperature is lower than 1.3 K and the channel current is very small. Figure 5.5 shows the gate-voltage dependence of the channel conductance G in the narrow transistor #22 (W = 350 nm) at 0.3 K. The channel current I_d is set to 5 nA. The conductance anomalously oscillates. The transconductance g_m becomes negative by this oscillation.

The gate-voltage dependence of the channel conductance in the wide transistor #12 (W = 400 nm) is discussed in § 4.3 (see Fig. 4.5). The conductance randomly fluctuates with V_g (i. e., with the Fermi energy E_F). This is due to the universal conductance fluctuation effect.

However, the oscillation in Fig. 5.5 is not due to the universal conductance fluctuations for the following reasons.
(1) The oscillation is hardly changed even when magnetic field larger than the correlation field B_c is applied, as shown in Fig. 5.5 (B_c is 340 G in #22).

(2) The amplitude of the oscillation is much larger than the predicted amplitude form Eq. (4.6). The predicted amplitude is only $0.006 \times G_{univ}$.

This kind of oscillation can be observed only at low temperatures less than ~1.3 K, only for small channel current ($I_d \leq 5$ nA), and only in narrow transistors (#22 and #36).

5.3.4 Strong localization

The theory of the universal conductance fluctuation[13,14] is based on the metallic transport in disordered condensed matters. In a metallic sample where the electron states are extended to the whole sample, the amplitude of the conductance fluctuation is $\sim e^2/h$. However, when temperature is decreased, or when the Fermi energy is decreased and becomes comparable to the potential fluctuations in the sample, the localization length ξ becomes shorter than the sample size L (or the phase coherence length L_ϕ). ξ is a length scale in which the envelope of the electron wavefunction decays. Then, the electron states are localized (strong localization). The transition from the extended states to the localized states is called the metal-insulator transition.

The conductivity of the sample vanishes when the electron states change from extended to localized states at zero temperature. Mott[134] discussed the dependence of conductivity on the electron energy in a three-dimensional system. The critical energy at which the transition takes place was called the mobility edge. He argued for a discontinuous transition of conductivity at the mobility edge. The

scaling theory of localization[8] predicted that the conductivity would change continuously.

In the strongly localized regime at finite temperatures, the current is carried by the resonant tunneling[135] and the variable-range hopping.[136] It is theoretically predicted that the fluctuations of the conductance via these two processes are exponentially large, which is actually observed in very narrow Si MOSFET.[75,78,137-139]

In our AlGaAs/GaAs quantum wire transistors, the electron states will be strongly localized when the Fermi energy E_F is decreased by the gate voltage and becomes comparable to the fluctuated potential in the channels. The sudden decrease in the channel conductance just above the threshold voltage in Fig. 5.3 (a) is considered to be the very manifestation of the metal-insulator transition.

5.3.5 The origin of anomalous characteristics

When the gate voltage V_g is sufficiently larger than the threshold voltage V_{th}, the Fermi energy E_F is much larger than the potential fluctuations and the electron states are extended to the whole sample. The conductivity will vanish when V_g is decreased close to V_{th} and E_F becomes comparable to the fluctuated potential. This reduction of conductivity will occur rather rapidly at very low temperatures and for very small drain voltage, because the electrons which contribute to the conductivity have very small energy distribution. On the other hand, at high temperature or for large drain voltage, the reduction will occur slowly due to the large energy broadening of electrons. It

should be noted that, even when the electron states are localized, the electrons exist in the channel, but the mobility of the electron is changed to zero, causing the conductivity to vanish.

The behavior of the channel conductance g_d in Fig. 5.3 (a) is well explained by the above interpretation. For V_{ds} = 240 mV, where the electrons are considered to be heated due to high electric field, g_d increases gradually when V_g exceeds V_{th}. V_{th} is about -0.3 V in this case. For V_{ds} = 75 mV, g_d also gradually increases but V_{th} slightly shifts to -0.28 V. When V_{ds} is 7.0 mV or 0.6 mV, g_d does not appear until V_g = -0.24 V. It is considered that in the range of V_g from -0.3 to -0.24 V, electrons at low V_{ds} are induced but localized, resulting in zero conductance. When V_g exceeds -0.24 V, g_d increases suddenly because of the delocalization. When the energy broadening of conducting electrons is small, the transition to the extended electron states is sharp.

The slope of the g_d-V_g curve in Fig. 5.3 (a) gives the transconductance g_m. The rapid increase in g_d causes high g_m just above V_{th}. Now we focus on the anomalous increase in g_m in Fig. 5.3 (b). The drain current I_d in the linear region (for small V_{ds}) in a normal field effect transistor is given by

$$\begin{aligned} I_d &= (W/L)\, n\, q\, \mu\, V_{ds} \\ &= (W/L)\, \mu\, C\, (V_g - V_{th})\, V_{ds}, \end{aligned} \qquad (5.2)$$

where n is the electron density in the channel, q the electron charge, μ the electron mobility, C the gate capacitance, W the width of the

channel, and L the length of the channel. g_m is given by Eq. (5.1). Therefore, g_m/V_{ds} is

$$g_m/V_{ds} = \frac{\partial I_d}{\partial V_g}\Big|_{V_{ds}=\text{const}} / V_{ds}$$
$$= \frac{qW}{L}\left(\mu\frac{\partial n}{\partial V_g} + n\frac{\partial \mu}{\partial V_g}\right) \qquad (5.3)$$

Usually, g_m in the linear region is simply given by $g_m/V_{ds} = (W/L)\mu C$, ignoring the change in μ (the second term in brackets in Eq. (5.3)). This tempts us to think that the increase in g_m just above V_{th} is due to the increased mobility μ.[68] However, Eq. (5.3) is the correct form of g_m. Using this equation, the high peak in g_m is well explained by the transition of the electron states from the localized to extended states.

When the electron states are strongly localized, n_s is finite but $\mu = 0$, resulting in $g_m = 0$. When V_g exceeds V_{th} and g_d rapidly increases, n_s does not change too much but μ drastically increases because of the delocalization. Thus, $(\partial\mu/\partial V_g)$ becomes very large temporarily, leading to a high peak in g_m. After complete delocalization, μ hardly changes with V_g (i. e., $\partial\mu/\partial V_g \sim 0$) and g_m shows an almost constant value corresponding to $(W/L)\mu C V_{ds}$. Therefore, the anomalous increase in g_m in Fig. 5.3 (b) is not due to the mobility enhancement in a one-dimensional quantum wire predicted by Sakaki,[4] but due to the strong localization.

The localization effect is strongly dependent on the dimensionality of the system. It is considered to depend on the width in one-dimensional system; the electron states are more likely to be localized in narrower

one-dimensional system. This is why the anomalous increase in g_m is observed in narrower wire transistors #22 and #36, and not in wide transistor #12.

The anomalous increase in g_m does not seem to depend on temperature so much below 12 K, as shown in Fig. 5.4. This may be related to the saturation of L_ϕ at low temperatures as discussed in § 3.4.2 (see Fig. 3.9 (a)). This is because at finite temperatures and in samples $L > L_\phi$, the localization takes place when $L_\phi > \xi$. If ξ has no temperature dependence in a given sample, the saturation of L_ϕ at low temperatures will leads no temperature dependence of the anomalous increase in g_m.

The origin of the other anomaly, the large oscillation in the channel conductance G in Fig. 5.5, is not clear at present. One possibility is the variable-range hopping in the strongly localized regime at finite temperatures. The theory[136,138] predicts the width of the peak in conductance due to the hopping is of the order of kT. However, the observed width of the peak at 0.3 K in Fig. 5.5 is about 1 meV, much larger than kT.

Another possible explanation is the observation of the one-dimensional quantization of electrons. Although the width of the channel is rather wide (W = 350 nm) at V_g = 0 V, the width can be locally very narrow for smaller V_g because of the fluctuated potential distribution. When the electrons are quantized into the one-dimensional system, the density of states $D(E)$ of electrons in each quantized level varies with energy as $D(E) \sim E^{-1/2}$. When E_F is changed by the gate voltage and

passes over each quantized energy level, the scattering rate of electrons would be varied and, thus, the conductance would oscillate with E_F. However, the origin of the oscillation is not clear.

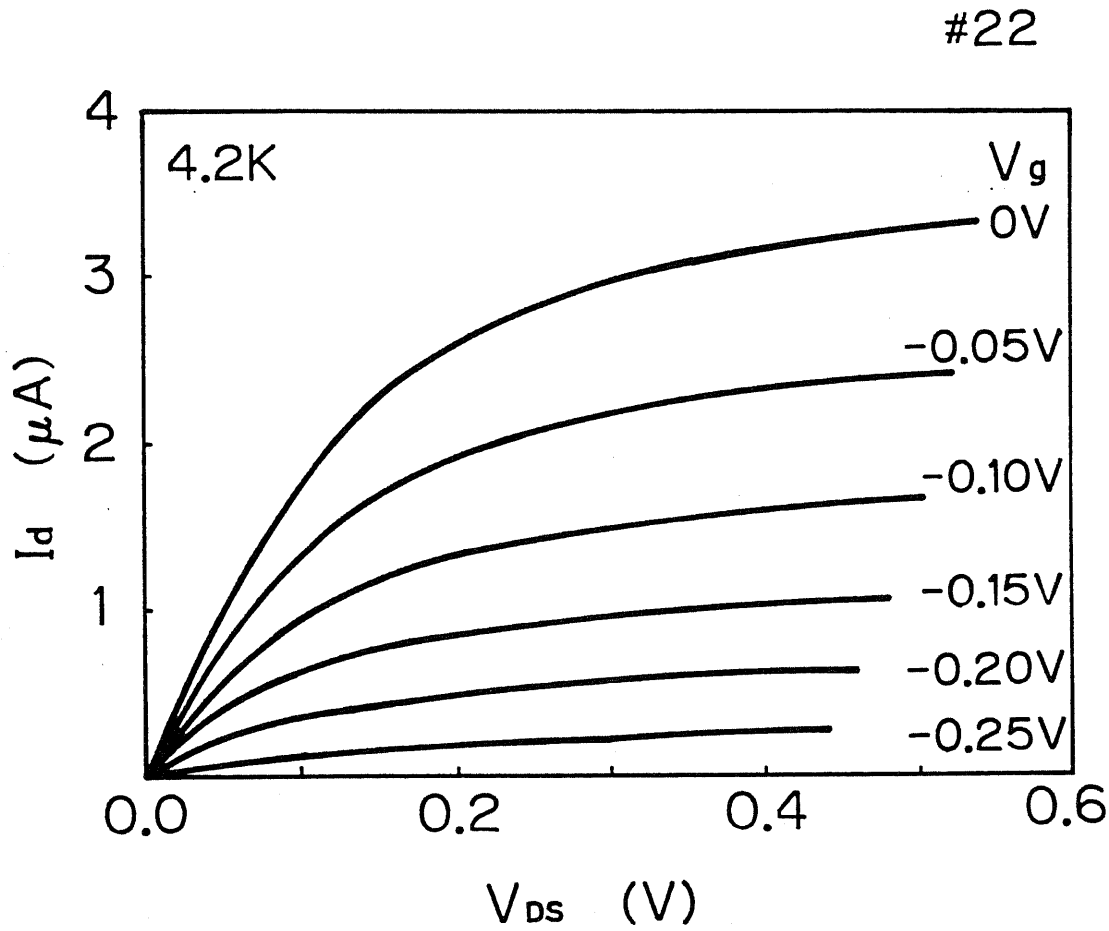

Fig. 5.2 The current-voltage (I_d-V_{ds}) characteristics of the AlGaAs/GaAs quantum wire transistor #22 at 4.2 K. The channel width W at V_g = 0 V is 350 nm.

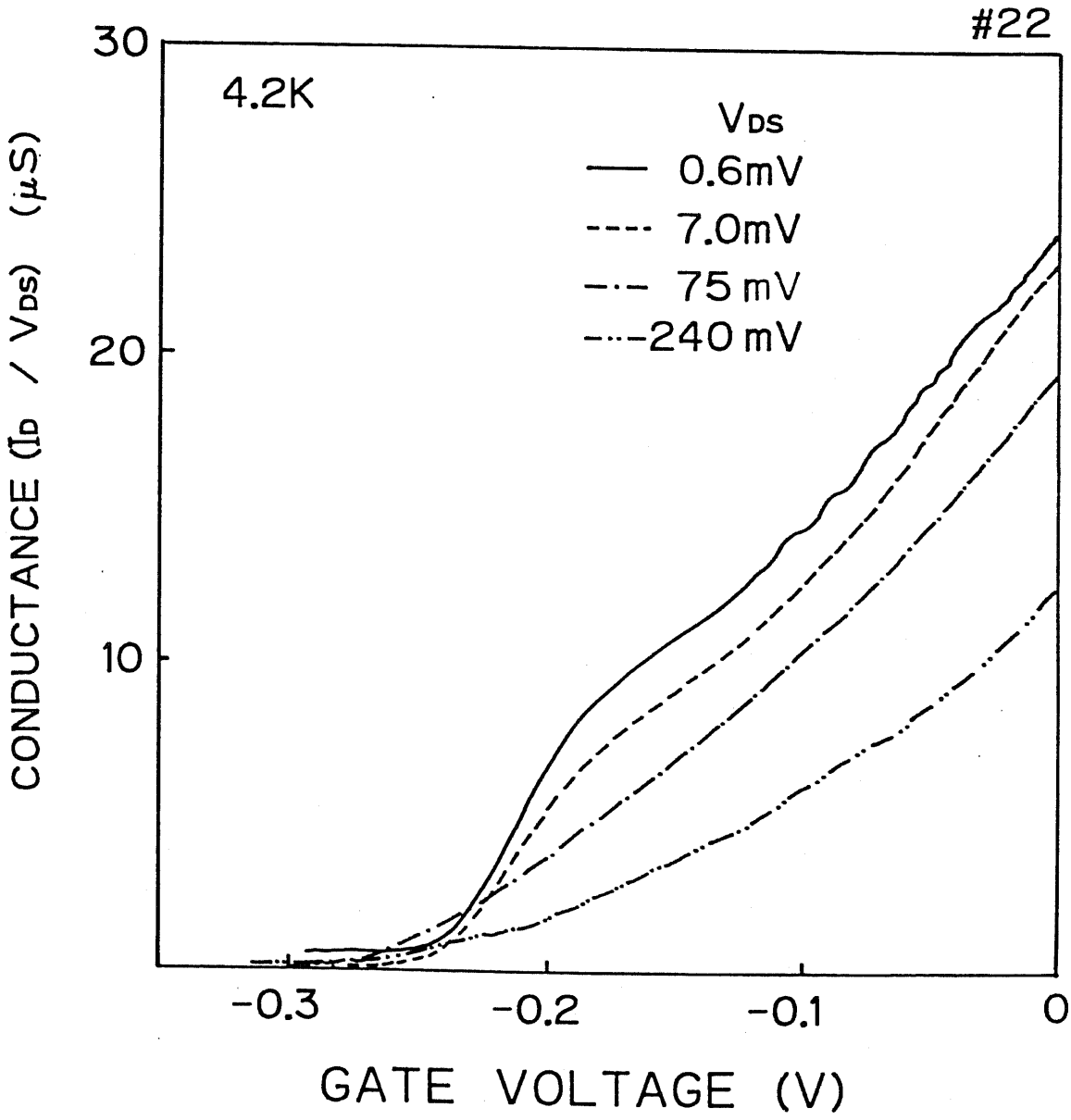

Fig. 5.3 (a) The gate-voltage dependences of the channel conductance g_d (= I_d/V_{ds}) of the AlGaAs/GaAs quantum wire transistor #22 at 4.2 K for different drain voltages.

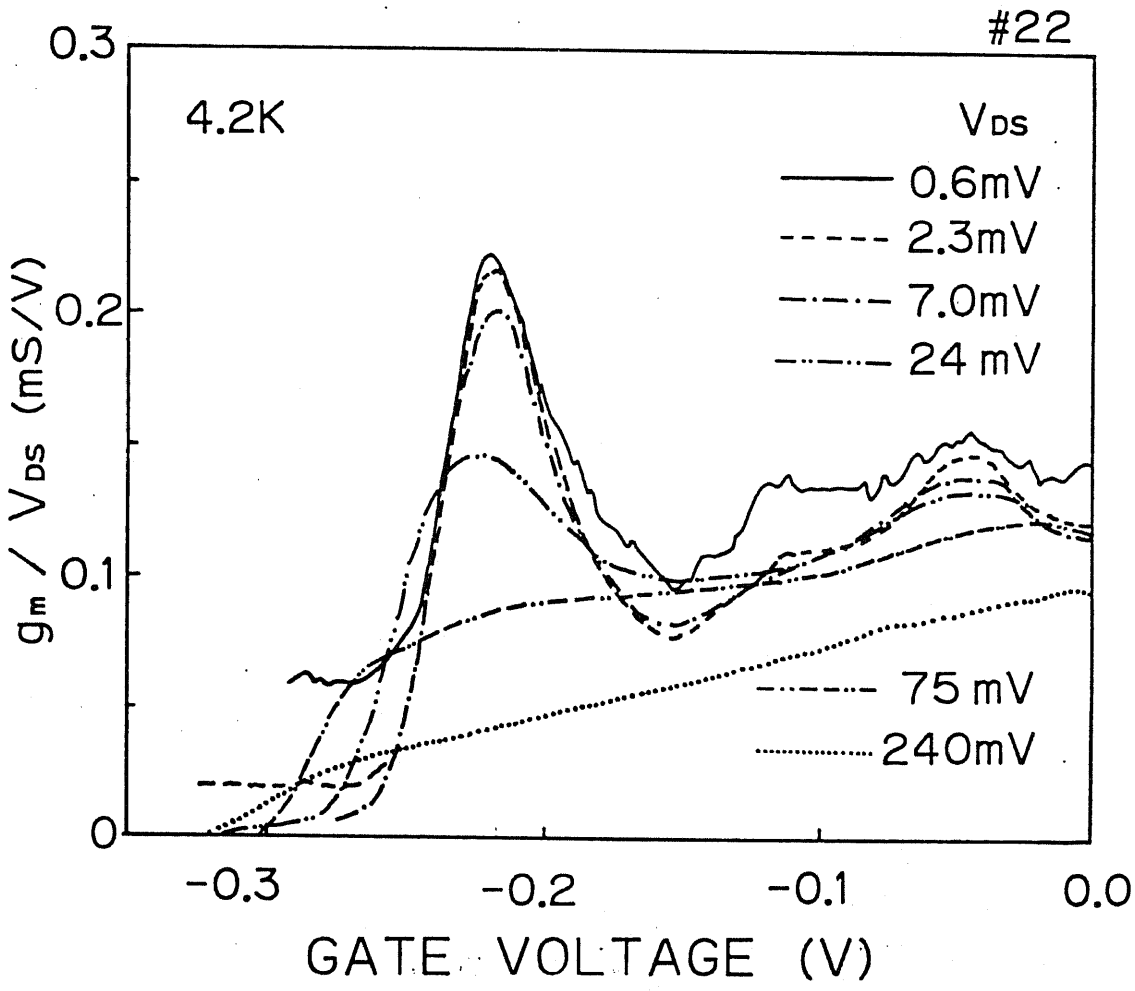

Fig. 5.3 (b) The gate-voltage dependences of the transconductance g_m, normalized to the drain voltage V_{ds}, of the AlGaAs/GaAs quantum wire transistor #22 at 4.2 K for different drain voltages.

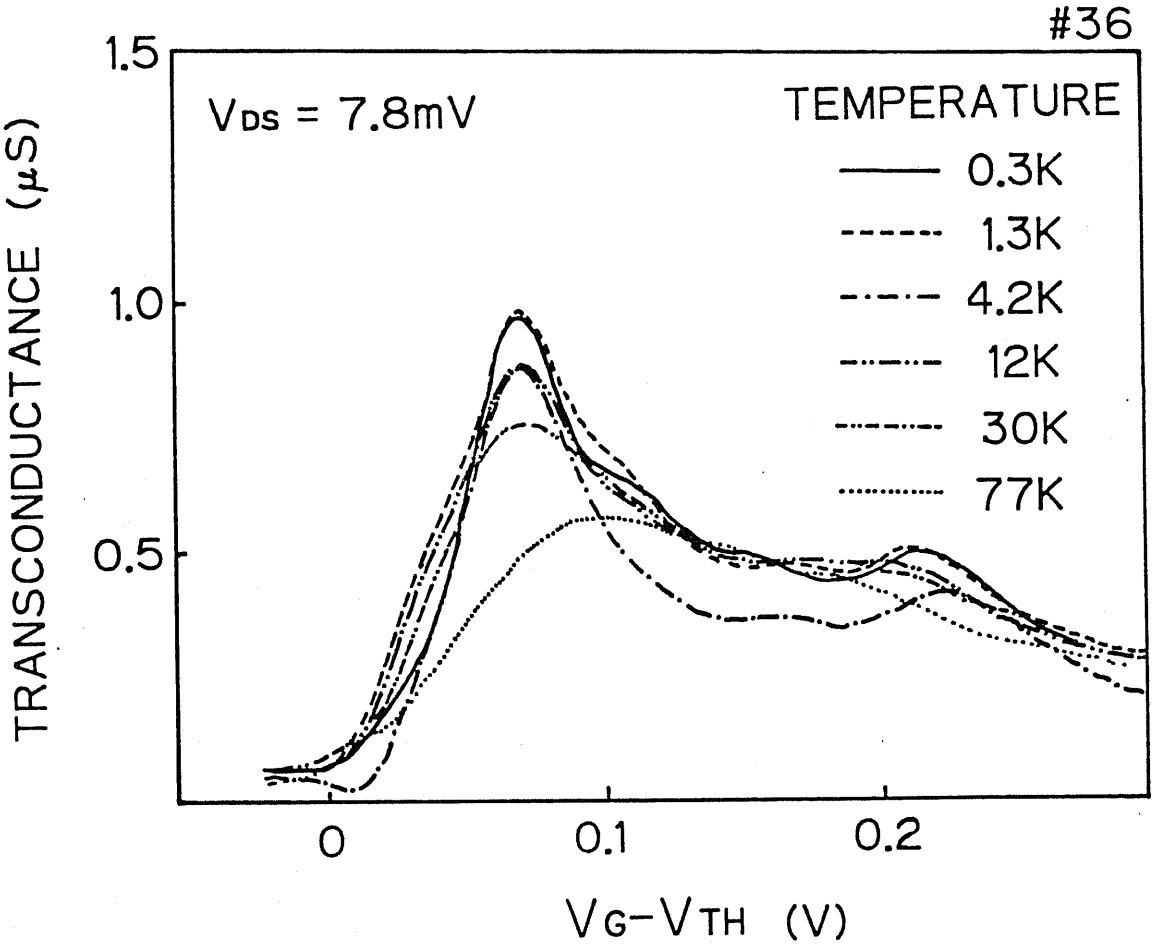

Fig. 5.4 The gate-voltage dependences of the transconductance g_m of the AlGaAs/GaAs quantum wire transistor #36 at several temperatures. The drain voltage V_{ds} is fixed to 7.8 mV.

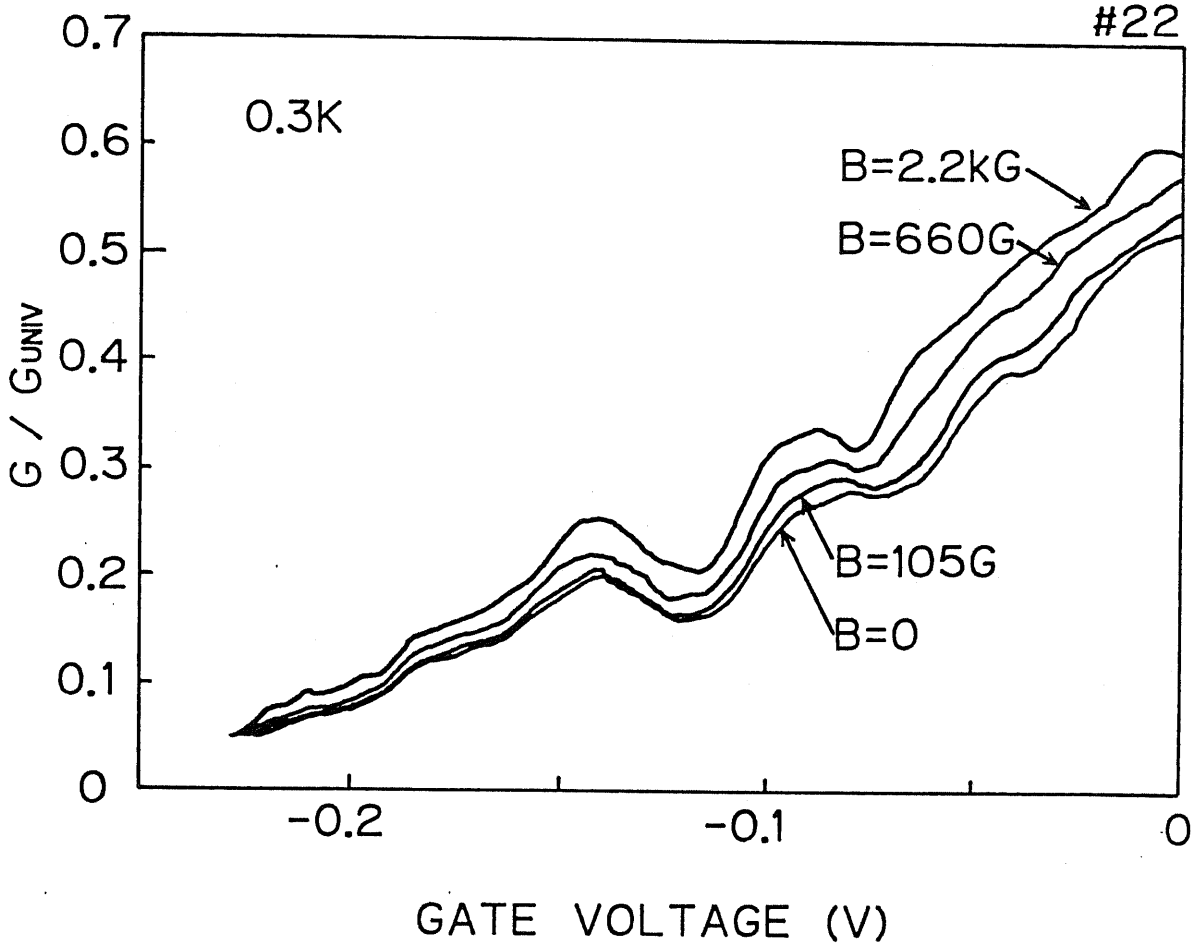

Fig. 5.5 The gate-voltage dependences of the ac conductance G of the AlGaAs/GaAs quantum wire transistor #22 at 0.3 K at several magnetic field. The conductance is normalized to $G_{univ} = e^2/h$. The channel current I_d is set to 5 nA.

§ 5.4 Conclusions

Two anomalous behaviors are observed in the channel conductance of very narrow AlGaAs/GaAs quantum wire transistors at very low temperatures. The threshold voltage shifts to the positive way with decreasing drain voltage and the transconductance is anomalously increased at gate voltage just above the threshold. This behavior is well explained by the transition from extended states to localized states of electrons (metal-insulator transition). The channel conductance anomalously oscillates as a function of gate voltage. The negative transconductance is observed due to this oscillation. It is shown that this is not the universal conductance fluctuations. The origin is discussed in terms of the variable-range hopping and the one-dimensional quantization of electrons.

Chapter 6

Conclusions

We have established qualitative and quantitative understanding of the quantum interference effect of electron waves in semiconductor quantum wires. We have addressed the following four problems which are very important in the quantum interference effect from the technological point of view:

(1) Fabrication process of the semiconductor quantum wires.
(2) Phase coherence length and phase breaking mechanisms of electron waves in GaAs quantum wires.
(3) Correlation energy of electron wavefunctions in GaAs quantum wires.
(4) Effect of localization on characteristics of GaAs quantum wire transistors.

We have clarified these important points in the quantum interference effect and have shown the possibility of the quantum interference devices in semiconductors.

§ 6.1 Fabrication process of semiconductor quantum wires

Novel, simple technique is developed to fabricate very narrow semiconductor quantum wires by the focused-ion-beam (FIB) implantation. The various submicron processing techniques, which are the key technology in realizing the quantum wires, are demonstrated in Chapter 2.

Rapid thermal annealing (RTA) process of FIB-implanted GaAs is developed. Electrical properties of focused Si- and Be-implanted GaAs are comparable to those of unfocused ion-implanted GaAs. It is shown the optimal RTA condition of FIB-implanted GaAs is at 1000 ~ 1100 °C for 1 s.

The profiles of FIB implanted ions in GaAs are studied experimentally and theoretically. The profiles are well predicted by the simple calculation as long as RTA is performed for the post-annealing. The result shows the RTA process is essential for the FIB implantation.

Fabrication of microstructures of GaAs and AlGaAs is demonstrated. Surface nipi-structures with a period of 1μm are fabricated by the FIB implantation. An enhance etching of damaged GaAs, which is induced by the FIB implantation, is applied to the formation of the fine GaAs grating with a period of 0.37 μm and very small structures. The minimum dimension of the fabricated microstructures is as small as 30 nm.

Finally, quasi-one-dimensional GaAs conducting wires are fabricated by the two methods using the FIB implantation. In the first method, the high-resistive regions are selectively formed in conducting GaAs layers by the FIB implantation. A narrow conducting wire structure is left between the two high-resistive regions. In the second method, focused Si-ion-beam is line-implanted into p-GaAs to form an n-type conducting wire in p-GaAs. Then negative-bias is applied across the pn-junction to make the n-GaAs wire narrower. The minimum width of the fabricated GaAs wires is as small as 20 nm.

These results show excellent feasibility of the FIB implantation for fabricating various fine structures and semiconductor quantum wires.

§ 6.2 Phase coherence length and phase breaking mechanisms

The phase coherence length L_ϕ and the phase breaking mechanisms of electron waves are systematically studied in Chapter 3. The semiconductor quantum wires are fabricated both in n-type GaAs and in selectively doped AlGaAs/GaAs heterostructures. The weak localization due to the quantum interference effect manifests itself in the positive magnetoconductance at low temperatures and at low magnetic field.

L_ϕ in the n-GaAs wires can be estimated by fitting the one-dimensional weak localization theory to the magnetoconductance data. It is shown, however, that the theory in the dirty limit is not applicable to the AlGaAs/GaAs wires with high-mobility. The modified weak localization theory, which takes the boundary scattering and the less elastic scattering into consideration, is applied to the estimation of L_ϕ in the AlGaAs/GaAs wires.

It is found that longer L_ϕ can be achieved in materials with both higher electron mobility and higher electron density at the same time. This is demonstrated by the difference in L_ϕ in the n-GaAs wires and the selectively doped AlGaAs/GaAs wires. The AlGaAs/GaAs wire has L_ϕ of 1.2 μm; 9 times longer than the n-GaAs wire has. Moreover, L_ϕ is increased with increasing the conductance in the gated AlGaAs/GaAs wire. These results show the advantage of the selectively doped structure to obtain long L_ϕ.

L_ϕ increases with decreasing temperature but saturates below around 3 K, indicating the existence of some temperature-independent phase-breaking mechanisms. The conductance dependence of L_ϕ, $L_\phi \sim G^{0.85}$, indicates that the main phase-breaking mechanism at 4.2 K might be the inelastic electron-electron scattering.

The value of L_ϕ, 1.2 μm, at 0.3 K is considered to be long enough to realize the quantum interference devices by the state-of-the-art technology. The selectively doped structures are the most suitable for these devices. The temperature dependence of L_ϕ shows that L_ϕ is long enough at 4.2 K and even at 10 K, suggesting that it is not necessary for the quantum interference devices to be cooled down below 4.2 K in order to maintain long L_ϕ, as long as the selectively doped AlGaAs/GaAs heterostructures are chosen as the material.

§ 6.3 Correlation energy of electron wavefunctions

Conductance fluctuations in narrow semiconductor quantum wires are studied in Chapter 4. The amplitude of the conductance fluctuations, the correlation magnetic field, and the correlation energy are investigated in n-GaAs wires and gated AlGaAs/GaAs wires.

The conductance of the n-GaAs wires fluctuates randomly with the magnetic field at low temperatures. It is found that the amplitude of the conductance fluctuations in the n-GaAs wires depends on the width of the wire even when the widths are narrower than the phase coherence length L_ϕ.

It is shown that in gated AlGaAs/GaAs wires the conductance fluctuates as a function of the Fermi energy as well as of the magnetic field. The experimental and theoretical values of the correlation field B_c are in good agreement.

The correlation energy E_c is, for the first time, determined experimentally in GaAs wires from the average period of the conductance fluctuation with the Fermi energy. The value of E_c is ~1 meV, which is in agreement with the theory. It is shown that E_c corresponds to the energy broadening of coherent electrons. This value of E_c is much larger than that in metals, and corresponds to the temperature of ~10 K. It is also shown that the thermal diffusion length L_T is always smaller than L_ϕ when T < 10 K. These results suggest that the reduction of the quantum interference effect by the

energy averaging is less important than that by the self-averaging effect in semiconductors, and demonstrates that the semiconductors have advantage over metals in terms of the device applications at temperatures higher than 4.2 K.

§ 6.4 Effect of localization in the GaAs quantum wire transistors

Very narrow AlGaAs/GaAs quantum wire transistors with gate length of 10 μm are fabricated by the focused-ion-beam-implantation and their characteristics are investigated as a function of gate voltage V_g at various drain voltages V_{ds} and temperatures T in Chapter 5.

Two anomalous behaviors are observed in the channel conductance at very low temperatures. The threshold voltage shifts to the positive way with decreasing drain voltage, and the transconductance is anomalously increased at gate voltage just above the threshold. This behavior is well explained by the transition from extended states to localized states of electrons (metal-insulator transition).

The channel conductance anomalously oscillates as a function of gate voltage. The negative transconductance is observed due to this oscillation. It is shown that this is not due to the universal conductance fluctuations. The origin is discussed in terms of the variable-range hopping in the strongly localized region and the one-dimensional quantization of electrons due to the the fluctuated potential.

§ 6.5 Concluding remarks

We have studied the quantum interference effect of electron waves in semiconductor quantum wires from the technological point of view. The emphasis has been placed on the following four points: (1) the fabrication process, (2) the phase coherence length, (3) the correlation energy, and (4) the quantum wire transistor. Although some of the problems still remain unsolved, most of the properties are clarified qualitatively or quantitatively.

The focused-ion-beam implantation is one of the most excellent techniques for the fabrication of the semiconductor quantum wires.

The selectively doped heterostructure is one of the most suitable materials for the quantum interference devices as well as for the study of the physics of the quantum interference effect. The phase coherence length in this material is more than 1 μm at low temperatures. Moreover, the correlation energy in the material is sufficiently large, and the energy averaging effect is not important. The realization of the quantum interference effect has come very closely to the goal.

The author hopes that the present study will contribute to the comprehensive understanding of the quantum interference effect in the field of the semiconductor technology and that the quantum interference devices will be realized in the near future.

References

[1]L. Esaki and R. Tsu, IBM J. Res. Dev. **14**, 61 (1970).

[2]T. Mimura, S. Hiyamizu, T. Fujii, and K. Nanbu, Jpn. J. Appl. Phys. **19**, L225 (1980).

[3]J. P. van der Ziel, R. Dingle, R. C. Miller, W. Wiegmann, and W. A. Nordland Jr., Appl. Phys. Lett. **26**, 463 (1975).

[4]H. Sakaki, Jpn. J. Appl. Phys. **19**, L735 (1980).

[5]Y. Kawaguchi and S. Kawaji, J. Phys. Soc. Jpn. **48**, 699 (1980).

[6]C. P. Umbach, S. Washburn, R. B. Laibowitz, and R. A. Webb, Phys. Rev. B**30**, 4048 (1984).

[7]P. W. Anderson, Phys. Rev. **109**, 1492 (1958).

[8]E. Abrahams, P. W. Anderson, D. C. Licciardello, and T. V. Ramakrishnan, Phys. Rev. Lett. **42**, 673 (1979).

[9]Y. Aharonov and D. Bohm, Phys. Rev. **115**, 485 (1959).

[10]A. Tonomura, T. Matsuda, R. Suzuki, A. Fukuhara, N. Osakabe, H. Umezaki, J. Endo, K. Shinagawa, Y. Sugita, and H. Fujiwara, Phys. Rev. Lett. **48**, 1443 (1982).

[11]D. Y. Sharvin and Y. V. Sharvin, JETP Lett. **34**, 272 (1981).

[12] R. A. Webb, S. Washburn. C. P. Umbach, and R. B. Laibowitz, Phys. Rev. Lett. **54**, 2696 (1985).

[13]B. L. Al'tshuler, JETP Lett. **41**, 648 (1985).

[14]P. A. Lee and A. D. Stone, Phys. Rev. Lett. **55**, 1622 (1985).

[15]S. Datta, M. R. Melloch, S. Bandyopadhyay, and M. S. Lundstrom, Appl. Phys. Lett. **48**, 487 (1986).

[16]S. Datta, *Extended Abstracts of the 20th International Conference on Solid State Devices and Materials*, Tokyo, Japan, 1988, pp. 491-494.

[17]M. Yamamoto and K. Hohkawa, *Extended Abstracts of the 20th International Conference on Solid State Devices and Materials*, Tokyo, Japan, 1988, pp. 495-498.

[18]D. J. Bishop, R. C. Dynes, and D. C. Tsui, Phys. Rev. B**26**, 773 (1982).

[19]P. A. Lee, A. D. Stone, H. Fukuyama, Phys. Rev. B**35**, 1039 (1987).

[20]T. Hiramoto, K. Hirakawa, Y. Iye, and T. Ikoma, Appl. Phys. Lett. **51**, 1620 (1987).

[21]T. Hiramoto, K. Hirakawa and T. Ikoma, J. Vac. Sci. Technol. **B6**, 1014 (1988).

[22]Y. Hirayama, S. Tarucha, Y. Suzuki, and H. Okamoto, Phys. Rev. B[37], 2774 (1988).

[23]R. L. Seliger, R. L. Kubena, R. D. Olney, J. W. Ward, and V. Wang, J. Vac. Sci. Technol. **16**, 1610 (1979).

[24]T. Hiramoto, T. Odagiri, P. Oldiges, T. Saito, and T. Ikoma, *in Gallium Arsenide and Related Compounds, Las Vegas, 1986*, Inst. Phys. Conf. Ser. No.83, p. 295.

[25]R. L. Kubena, C. L. Anderson, R. L. Seliger, R. A. Jullens, and E. H. Stevens, J. Vac. Sci. Technol. **19**, 916 (1981).

[26]K. Gamo, Y. Ochiai, and S. Namba, Jpn. J. Appl. Phys. **21**, L792 (1982).

[27]K. Gamo, N. Takakura, N. Samoto, R. Shimizu, and S. Namba, Jpn. J. Appl. Phys. **23**, L293 (1984).

[28]K. Saito, H. Onoda, H. Morimoto, T. Katayama, Y. Watakabe, and T. Kato, J. Vac. Sci. Technol. B**6**, 1032 (1988).

29J. R. A. Cleaver, E. C. G. Kirk, R. J. Young, and H. Ahmed, J. Vac. Sci. Technol. B**6**, 1026 (1988).

[30]K. Nakamura, T. Nozaki, T. Shiokawa, K. Toyoda, and S. Namba, Jpn. J. Appl. Phys. **24**, L903 (1985).

[31]Y. Hirayama and H. Okamoto, Jpn. J. Appl. Phys. **24**, L965 (1985).

[32]Y. Hirayama, Y. Suzuki, S. Tarucha, and H. Okamoto, Jpn. J. Appl. Phys. **24**, L516 (1985).

[33]T. Hiramoto, *Master thesis*, University of Tokyo, 1986.

[34]E. Miyauchi, H. Arimoto, H. Hashimoto, T. Utsumi, J. Vac. Sci. Technol. B**1**, 1113, (1983).

[35]Y. Bamba, E. Miyauchi, H. Arimoto, K. Kuramoto, A. Takamori, H. Hashimoto, Jpn. J. Appl. Phys. **22**, L650 (1983).

[36]Y. Bamba, E. Miyauchi, H. Arimoto, A. Takamori, H. Hashimoto, Jpn. J. Appl. Phys. **23**, L515 (1984).

[37]T. Hiramoto, T. Saito, and T. Ikoma, Jpn. J. Appl. Phys. **24**, L193 (1985).

[38]T. Hiramoto, Y. Mochizuki, T. Saito and T. Ikoma, Jpn. J. Appl. Phys. **24**, L921 (1985).

[39]T. Hiramoto, Y. Mochizuki and T. Ikoma, Jpn. J. Appl. Phys. **25**, L830 (1986).

[40]H. Kohzu, M. Kuzuhara, and Y. Takayama, J. Appl. Phys. **54**, 4998 (1983).

[41]R. L. Chapman, J. C. C. Fan, J. P. Donnelly, and B-Y. Tsaur, Appl. Phys. Lett. **40**, 805 (1982).

[42]A. N. M. M. Choudhury, K. Tabatabaie-Alavi, and C. G. Fonstad, Appl. Phys. Lett. **43**, 381 (1983).

[43]T. Hiramoto and T. Ikoma, *Proceedings of the 5th Conference on Semi-Insulating III-V Materials*, Malmö, Sweden, June, 1988, pp. 337.

[44]P. Chambon, M. berth, and B. Prévot, Appl. Phys. Lett. **46**, 162 (1985).

[45]S. J. Pearton, K. D. Cumming, and G. P. Vella-Coleiro, J. Appl. Phys. **58**, 3252 (1985).

[46]K. Maezawa and K. Oe, IEEE Electron Device Lett. EDL**7**, 13 (1986).

[47]M. Uematsu, Jpn. J. Appl. Phys. **26**, L246 (1987).

[48]T. Odagiri, *Master thesis*, University of Tokyo, 1988.

[49]E. A. Poltoratski and V. M. Stuchebnikov, Sov. Phys. Solid State **8** 770 (1966).

[50]R. Dingle, H. L. Stormer, A. C. Gossard, and W. Wiegmann, Appl. Phys. Lett. **33**, 665 (1978).

[51]G. H. Döhler, H. Kunzel, and K. Ploog, Phys. Rev. B**25**, 2616 (1982).

[52]T. Taguchi, T. Nakamura, K. Horiuchi and H. Ishikawa, *17th Symp. on Ion Implantation and Submicron Fabrication*, Wako, Japan, 1986, pp.165.

[53]T. Nakamura and T. Katoda, Jpn. J. Appl. Phys. **23**, L552 (1984).

[54]M. Tamura, S. Shukuri, T. Ishitani, M. Ichikawa, and T. Doi, Jpn. J. Appl. Phys. **23**, L417 (1984).

[55]W. J. Skocpol, L. D. Jackel, E. L. Hu, R. E. Howard, and L. A. Fetter, Phys. Rev. Lett. **49**, 951 (1982).

[56]P. M. Mankiewich, R. E. Howard, L. D. Jackel, W. J. Skocpol, and D. M. Tennant, J. Vac. Sci. Technol. B**4**, 380 (1986).

[57]K. Kash, A. Scherer, J. M. Worlock, H. G. Craighead, and M. C. Tamargo, Appl. Phys. Lett. 49, 1043 (1986).

[58]G. P. Whittington, P. C. Main, L. Eaves, R. P. Taylor, S. Thoms, S. P. Beaumont, C. D. W. Wilkinson, C. R. Stanley, and J. Frost, Superlattices and Microstructures, **2**, 381 (1986).

[59]K. Ishibashi, K. Nagata, K. Gamo, S. Namba, S. Ishida, K. Murase, M. Kawabe, and Y. Aoyagi, Solid State Commun. **61**, 385 (1987).

[60]H. Temkin, G. J. Dolan, M. B. Panish, and S. N. G. Chu, Appl. Phys. Lett. **50**, 413 (1987).

[61]H. van Houten, B. J. van Wees, M. G. J. Heijman, and J. P. André, Appl. Phys. Lett. **49**, 1781 (1986).

[62]A. Scherer, M. L. Roukes, H. G. Craighead, R. M. Ruthen, E. D. Beebe, and J. P. Harbison, Appl. Phys. Lett. **51**, 2133 (1987).

[63]K. Owusu-Sekyere, A. M. Chang, and T. Y. Chang, Appl. Phys. Lett. **52**, 1246 (1988).

[64]J. Cibert, P. M. Petroff, G. J. Dolan, S. J. Pearton, A. C. Gossard, and J. H. English, Appl. Phys. Lett. **49**, 1275 (1986).

[65]T. J. Thornton, M. Pepper, H. Ahmed, D. Andrews, and G. J. Davies, Phys. Rev. Lett. **56**, 1198 (1986).

[66]T. P. Smith, III, H. Arnot, J. M. Hong, C. M. Knoedler, S. E. Laux, and H. Schmid, Phys. Rev. Lett. **59**, 2802 (1987).

[67]W. Hansen, M. Horst, J. P. Kotthaus, U. Merkt, Ch. Sikorski, and K. Ploog, Phys. Rev. Lett. **58**, 2586 (1987).

[68]M. Okada, T. Ohshima, M. Matsuda, N. Yokoyama, and A. Shibatomi, *Extended Abstracts of the 20th International Conference on Solid State Devices and Materials*, Tokyo, Japan, 1988, pp. 503-506.

[69]K. Ismail, W. Chu, D. A. Antoniadis, and H. I. Smith, to appear in Appl. Phys. Lett.

[70]M. Kohl, D. Heitmann, P. Grambow, and K. Ploog, Phys. Rev. B**37**, 10927 (1988).

[71]T. Demel, D. Heitmann, P. Grambow, and K. Ploog, Appl. Phys. Lett. **53**, 2176 (1988).

[72]K. K. Choi, D. C. Tsui, and K. Alavi, Appl. Phys. Lett. **50**, 110 (1987).

[73]A. D. C. Grassie, K. M. Hutchings, M. Lakrimi, C. T. Foxon, and J. J. Harris, Phys. Rev. B**36**, 4551 (1987).

[74]R. G. Wheeler, K. K. Choi, A. Goel, R. Wisnieff, and D. E. Prober, Phys. Rev. Lett. **49**,1674 (1982).

[75]R. F. Kwasnick, M. A. Kastner, J. Melngailis, and P. A. Lee, Phys. Rev. Lett. **52**, 224 (1984).

[76]A. C. Warren, D. A. Antoniadis, and H. Smith, Phys. Rev. Lett. **56**, 1858 (1986).

[77]H. Z. Zheng, H. P. Wei, D. C. Tsui, and G. Weimann, Phys. Rev. B**34**, 5635 (1986).

[78]A. B. Fowler, A. Hartstein, and R. A. Webb, Phys. Rev. Lett, **48**, 196 (1982).

[79]P. M. Petroff, A. C. Gossard, R. A. Logan, and W. Wiegmann, Appl. Phys. Lett. **41**, 635 (1982).

[80]H. Asai, S. Yamada, and T. Fukui, Appl. Phys. Lett. **51**, 1518 (1987).

[81]S. Hikami, A. I. Larkin, and Y. Nagaoka, Prog. Theor. Phys. **63**, 707 (1980).

[82]B. L. Altshuler, D. Khmelnitskii, A. Larkin, and P. A. Lee, Phys. Rev. B**22**, 5142 (1980).

[83]D. Abraham and R. Rosenbaum, Phys. Rev. B**27**, 1413 (1983).

[84]P. Santhanam, S. Wind, and D. E. Prober, Phys. Rev. B**35**, 3188 (1987).

[85]J. J. Lin and N. Giordano, Phys. Rev. B**35**, 1071 (1987).

[86]J. J. Lin and N. Giordano, Phys. Rev. B**35**, 545 (1987).

[87]D. Belitz and S. D. Sarma, Phys. Rev. B**36**, 7701 (1987).

[88]M. J. Uren, R. A. Davies, M. Kaveh, and M. Pepper, J. Phys. C**14**, L395 (1981).

[89]R. G. Wheeler, Phys. Rev. B**24**, 4645 (1981).

[90]T. Nambu, S. Kawaji, K. Kuboki, Y. Kawaguchi, J. Yoshino, and H. Sakaki, J. Phys. Soc. Jpn. **53**, 682 (1984).

[91]B. L. Al'tshuler and A. G. Aronov, JETP Lett. **33**, 499 (1981).

[92]K. Hirakawa and H. Sakaki, Appl. Phys. Lett. **49**, 889 (1986).

[93]G. Bergmann, Phys. Rep. **107**, 1 (1984).

[94]K. K. Choi, D. C. Tsui, and K. Alavi, Phys. Rev. B**36**, 7751 (1987).

[95]T. Hiramoto, K. Hirakawa, Y. Iye, and T. Ikoma, to be published in Material Research Society Symposia Proceedings.

[96]T. Hiramoto, K. Hirakawa, Y. Iye, and T. Ikoma, submitted to Appl. Phys. Lett.

[97]C. W. Beenakker and H. van Houten, Phys. Rev. B**38**, 3232 (1988).

[98]H. van Houten, C. W. Beenakker, B. J. van Wees, and J. E. Mooij, Surf. Sci. **196**, 144 (1988).

[99]T. Hiramoto, K. Hirakawa, and T. Ikoma, *Gallium Arsenide and Related Compounds, Crete, Greece,* 1987, Inst. Phys. Conf. Ser. No. 91, pp. 431-434.

[100]T. Hiramoto, K. Hirakawa, and T. Ikoma, *4th International Conference on Superlattices, Microstructures, and Microdevices, Trieste, Italy*, 1988.

[101]T. Hiramoto, K. Hirakawa, Y. Iye, and T. Ikoma, to be submitted to Appl. Phys. Lett.

[102]N. W. Ashcroft and N. D. Mermin, *Solid State Physics*, (Holt, Rinehart and Winston, USA, 1976).

[103]M. Kaveh and N. Wiser, Adv. in Phys. **33**, 257 (1984).

[104]B. L. Altshuler, A. G. Aronov, and D. E. Khmelnitsky, J. Phys. **C39**, 7367 (1982).

[105]P. Santhanam, S. Wind, and D. E. Prober, Phys. Rev. Lett. **53**, 1179 (1984).

[106]D. E. Beutler and N. Giordano, Phys. Rev. B**36**, 7705 (1987).

[107]J. J. Lin and N. Giordano, Phys. Rev. B**33**, 1519 (1986).

[108]S. Wind, M. J. Rooks, V. Chandrasekhar, and D. E. Prober, Phys. Rev. Lett. **57**, 633 (1986).

[109]D. Pooke, R. Mottahedeh, M. Pepper, and A. Gundlach, Surf. Sci. **196**, 59 (1988).

[110]Y. Takagaki, K. Ishibashi, S. Ishida, S. Takaoka, K. Gamo, K. Murase, and S. Namba, to be published in Jpn. J. Appl. Phys.

[111]R. P. Taylor, M. L. Leadbeater, G. P. Whittington, P. C. Main, S. P. Beaumont, I. McIntyre, S. Thomas, and C. D. W. Wilkinson, Surf. Sci. **196**, 52 (1988).

[112]H. Sakaki, T. Noda, K. Hirakawa, M. Tanaka, and T. Matsusue, Appl. Phys. Lett. **51**, 1934 (1987).

[113]J. C. Licini, D. J. Bishop, M. A. Kastner, and J. Melngailis, Phys. Rev. Lett. **55**, 2987 (1985).

[114]S. B. Kaplan and A. Hartstein, Phys. Rev. Lett. **56**, 2403 (1986).

[115]S. Y. Chou, D. A. Antoniadis, H. I. Smith, and M. A. Kastner, Solid State Commun. **61**, 571 (1987).

[116]W. J. Skocpol, P. M. Mankiewich, R. E. Howard, L. D. Jackel, D. M. Tennant, and A. D. Stone, Phys. Rev. Lett. **56**, 2865 (1986).

[117]T. J. Thornton, M. Pepper, and H. Ahmed, Phys. Rev. B**36**, 4514 (1987).

[118]K. Ishibashi, H. Kawai, K. Gamo, S. Namba, S. Ishida, K. Murase, Y. Aoyagi, and M. Kawabe, Solid State Commun. **63**, 1169 (1987).

[119]Y. K. Fukai, S. Yamada, H. Asai, S. Ando, and T. Fukui, Extended Abstracts of the 20th International Conference on Solid State Devices and Materials, Tokyo, Japan, 1988, pp. 631-632.

[120]A. D. Stone, Phys. Rev. Lett. **54**, 2692 (1985).

[121]S. Washburn and R. A. Webb, Adv. Phys. **35**, 375 (1986).

[122]T. J. Thornton, M. Pepper, G. J. Davies, and D. Andrews, *in Proc. of 18th International Conference on the Physics of Semiconductors, Stockholm, 1986*, edited by Olof Engstrom (World Scientific Publishing, Singapore, 1987), pp. 1503.

[123]A. Benoit, C. P. Umbach, R. B. Laibowitz, and R. A. Webb, Phys. Rev. Lett. **58**, 2343 (1987).

[124]H. U. Baranger, A. D. Stone, D. P. DiVincenzo, Phys. Rev. B**37**, 6521 (1988).

[125]M. Büttiker, Phys. Rev. B**35**, 4123 (1987).

[126]C. P. Umbach, P. Santhanam, C. van Haesendonck, and R. A. Webb, Appl. Phys. Lett. **50**, 1289 (1987).

[127]K. Ishibashi, *Ph. D. thesis*, Osaka University, 1988.

[128]S. Washburn, C. P. Umbach, R. B. Laibowitz, and R. A. Webb, Phys. Rev. B32, 4789 (1985).

[129]S. Washburn, H. Schmid, D. Kern, and R. A. Webb, Phys. Rev. Lett. **59**, 1791 (1987).

[130]S. Data, M. R. Melloch, S. Bandyopadhyay, R. Noren, M. Vaziri, M. Miller, and R. Reifenberger, Phys. Rev. Lett. **55**, 2344 (1985).

[131]G. Timp, A. M. Chang, J. E. Cunningham, T. Y. Chang, P. Mankiewich, R. Behringer, and R. E. Howard, Phys. Rev. Lett. **58**, 2814 (1987).

[132]K. Ishibashi, Y. Takagaki, K. Gamo, S. Namba, S. Ishida, K. Murase, Y. Aoyagi, and M. Kawabe, Solid State Commun. **64**, 573 (1987).

[133]C. J. B. Ford, T. J. Thornton, R. Newbury, M. Pepper, H. Ahmed, C. T. Foxon, J. J. Harris, and C. Roberts, J. Phys. C**21**, L325 (1988).

[134]N. F. Mott, Rev. Mod. Phys, **50**, 203 (1978).

[135]M. Ya. Azbel and P. Soven, Phys. Rev. B**27**, 831 (1983).

[136]P. A. Lee, Phys. Rev. Lett. **53**, 2042 (1984).

[137]M. Pepper and M. J. Uren, J. Phys. C**15**, L617 (1982).

[138]R. A. Webb, A. Hartstein, J. J. Wainer, and A. B. Fowler, Phys. Rev. Lett. **54**, 1577 (1985).

[139]M. A. Kastner, R. F. Kwasnick, and J. C. Licini, Phys. Rev. B**36**, 8015 (1987).

[140]D. J. Thouless, Phys. Rev. Lett. 39, 1167 (1977).

[141]P. A. Lee and T. V. Ramakrishnan, Rev. Mod. Phys. 57, 287 (1985).

Publication List

1) T. Hiramoto, T. Saito and T. Ikoma:
"Rapid Thermal Annealing of Si^+ Implanted GaAs in the Presence of Arsenic Pressure by GaAs Powder"
Jpn. J. Appl. Phys. **24**, L193 (1985).

2) T. Hiramoto, Y. Mochizuki, T. Saito and T. Ikoma:
"The Role of Gallium Antisite Defect in Activation and Type-Conversion in Si Implanted GaAs"
Jpn. J. Appl. Phys. **24**, L921 (1985).

3) T. Hiramoto, Y. Mochizuki and T. Ikoma:
"Evidence for Creation of Gallium Antisite Defect in Surface Region of Heat-Treated GaAs"
Jpn. J. Appl. Phys. **25**, L830 (1986).

4) T. Hiramoto, T. Odagiri, P. Oldiges, T. Saito and T. Ikoma:
"Submicron Processing of III-V Semiconductors by Focused Ion Beam Technology"
Inst. Phys. Conf. Ser. No.83, 1987, pp. 295.

5) T. Hiramoto, K. Hirakawa, Y. Iye and T. Ikoma:
"One-Dimensional GaAs Wires Fabricated by Focused Ion Beam Implantation"
Appl. Phys. Lett. **51**, 1620 (1987).

6) T. Hiramoto, K. Hirakawa and T. Ikoma:
"Quasi-One-Dimensional, Planar GaAs Wires Fabricated by Focused Ion Beam Implantation"
Inst. Phys. Conf. Ser. No. 91, 1988, pp. 431.

7) T. Hiramoto, K. Hirakawa and T. Ikoma:
"Fabrication of One-Dimensional GaAs Wires by Focused Ion Beam Implantation"
J. Vac. Sci. Technol. **B6**, 1014 (1988).

8) T. Hiramoto and T. Ikoma:
"The Source of Copper Contamination in Commercial Semi-Insulating GaAs Wafers"
Proceedings of the 5th Conference on Semi-Insulating III-V Materials, 1988, pp. 337.

9) T. Hiramoto, K. Hirakawa, Y. Iye, and T. Ikoma:
"Phase Coherent Length and Temperature Independent Dephasing Mechanisms of Electron Waves in GaAs Quantum Wires Fabricated by Focused Ion Beam Implantation"
to be published in Material Research Society Symposia Proceedings.

10) T. Hiramoto, K. Hirakawa, Y. Iye, and T. Ikoma:
"Phase Coherence Length of Electron Waves in Narrow AlGaAs/GaAs Quantum Wires Fabricated by Focused Ion Beam Implantation"
Submitted to Appl. Phys. Lett.

11) T. Hiramoto, K. Hirakawa, Y. Iye, and T. Ikoma:
"Phase Coherence Length and Conductance Fluctuations in Gated AlGaAs/GaAs Quantum Wires"
to be submitted to Appl. Phys. Lett.

12) T. Hiramoto, T. Odagiri, K. Hirakawa, Y. Iye, and T. Ikoma:
"Anomalous Drain Conductance in Quasi-One-Dimensional AlGaAs/GaAs Quantum Wire Transistors Fabricated by Focused Ion Beam Implantation"
Submitted to the Proceedings of International Symposium on Nanostructure Physics and Fabrication, 1989.

Presentations (International)

1) T. Hiramoto, T. Odagiri, P. Oldiges, T. Saito and T. Ikoma:
"Submicron Processing of III-V Semiconductors by Focused Ion Beam Technology"
13th International Symposium on Gallium Arsenide and Related Compounds, Las Vegas, USA, September, 1986.

2) T. Hiramoto, K. Hirakawa and T. Ikoma:
"Quasi-One-Dimensional, Planar GaAs Wires Fabricated by Focused Ion Beam Implantation"
14th International Symposium on Gallium Arsenide and Related Compounds, Crete, Greece, September, 1987.

3) T. Hiramoto, K. Hirakawa and T. Ikoma:
"Fabrication of One-Dimensional GaAs Wires by Focused Ion Beam Implantation"
Japan-US Seminar on Focused Ion Beam Technology and Application, Osaka and Mie, November, 1987.

4) T. Hiramoto and T. Ikoma:
"The Source of Copper Contamination in Commercial Semi-Insulating GaAs Wafers"
5th Conference on Semi-Insulating III-V Materials, Malmö, Sweden, June, 1988.

5) T. Hiramoto, K. Hirakawa, Y. Iye, and T. Ikoma:
"Phase Coherent Length and Temperature Independent Dephasing Mechanisms of Electron Waves in GaAs Quantum Wires Fabricated by Focused Ion Beam Implantation"
First International Conference on Electronic Materials, Tokyo, Japan, June, 1988.

6) T. Hiramoto, K. Hirakawa, and T. Ikoma:
"Phase Coherence Length in GaAs Quantum Wires with Electron Densities Controlled by Gate Electrodes"
4th International Conference on Superlattices, Microstructures, and Microdevices, Trieste, Italy, August, 1988.

7) T. Odagiri, T. Hiramoto, K. Hirakawa, and T. Ikoma:
"GaAs Quantum Wire Transistors Fabricated by Focused Ion Beam Implantation"
International Symposium on Focused Ion Beam Technology, Chicago, USA, October, 1988.

8) T. Hiramoto, K. Hirakawa, and T. Ikoma:
"Electron Transport in Quasi-One-Dimensional AlGaAs/GaAs Wires"
US-Japan Seminar on Alloy Semiconductor Physics and Electronics, Honolulu, USA, October, 1988.

9) T. Hiramoto, T. Odagiri, K. Hirakawa, and T. Ikoma:
"Field Effect Transport in Quasi-1D GaAs/AlGaAs Quantum Wires"
Conference on Advanced Heterostructure Transistors, Hawaii, USA, December, 1988.

10) T. Hiramoto, T. Odagiri, K. Hirakawa, Y. Iye, and T. Ikoma: "Anomalous Drain Conductance in Quasi-One-Dimensional AlGaAs/GaAs Quantum Wire Transistors Fabricated by Focused Ion Beam Implantation" (Invited Talk)
to be presented in International Symposium on Nanostructure Physics and Fabrication, College Station, Texas, USA, March, 1989.